THE UNIVERSITY *of* EDINBURGH

Adaptive Impedance Matching to Compensate Mutual Coupling Effects on Compact MIMO Systems

Reza Mohammadkhani

A thesis submitted for the degree of Doctor of Philosophy.
The University of Edinburgh.
June 2012

Abstract

Multiple-Input Multiple-Output (MIMO) systems promise higher data rates and better quality of service for wireless communications, by using multiple antennas at both the transmitter and receiver. However, applying MIMO technology at small portable wireless devices is faced with the problem of *mutual coupling* between antenna elements due to the limited space to put multiple antennas. It is shown in the literature that the mutual coupling degrades the MIMO performance.

For a given channel matrix and a known mutual coupling model, using *antenna impedance matching network(s)* between the coupled antenna array and its load or source network is proposed by recent studies to counteract the mutual coupling effects and maximise the MIMO performance. There are two issues with the existing matching techniques. First, they employ a model based on open-circuit voltages that separates the channel matrix and the mutual coupling model. This model is not valid except for a limited types of antennas (e.g. half-wavelength dipoles). Secondly, there is no solution among existing approaches that are capable of adapting to variations of the channel matrix.

This thesis focuses on the mutual coupling problem at the receiver. We first examine the most common approaches to model the mutual coupling. For instance, we compare various definitions of *coupling matrix* available in the literature, analyse their relationship and clarify when we can use them. The mutual coupling effects on MIMO performance metrics and impedance matching are also investigated using the conventional open-circuit voltage based model and a new method called *receiving mutual impedances*.

Then we propose the idea of having an *adaptive uncoupled impedance matching* technique which tunes the antenna impedance loads to compensate the effects of the propagation channel and mutual coupling together by directly dealing with the received signals. The mutual coupling model is unknown, but it is included implicitly by using the voltages across the real parts of the antenna load impedances to estimate the total effects. Assuming *identical* impedance loads for all receive antennas, several optimisation techniques such as Gradient-based, Newton-Raphson, and random search methods are investigated to implement such an adaptive impedance match. We found the random search method to be a simple and robust solution in comparison to other approaches.

Finally, we extend this adaptive matching technique to *non-identical* termination case, in which all load impedances are tuned individually. The performance of the adaptive matching networks are compared with the conventional termination scenarios such as: characteristic impedance match, and self-impedance conjugate match. Simulation results for a 3×3 MIMO system under different propagation scenarios show that both *identical* and *non-identical* adaptive impedance matching networks are capable of optimising the performance in the presence of strong mutual coupling and time variations of the channel. The adaptive non-identical match gives a significant improvement in the mean capacity (more than 20% compared to conventional terminations for 0.05λ element separation) at the expense of a longer convergence time compared to the identical match.

Declaration of originality

I hereby declare that the research recorded in this thesis and the thesis itself was composed and originated entirely by myself in the School of Engineering and Electronics at The University of Edinburgh.

Reza Mohammadkhani

Dedication

To my wife
To our parents

Acknowledgements

I would like to thank my supervisor, Prof. John Thompson, for his patient guidance, valuable advice and encouragement during the whole period of my study.

I would also like to thank Dr. Hon Tat Hui from National University of Singapore for his advice and detailed responses to my several questions about the receiving mutual impedance method.

Many thanks go to my friend Dr. Majid Ostadrahimi from the University of Manitoba, Dr. H. Yu from National University of Singapore, and FEKO support team for their help and support during the time I worked with FEKO software.

I would like to express my gratitude to my wife, Neda, for her love, understanding, and encouragement during all of the ups and downs of my research. I am also thankful to our parents for their endless love and support.

And thanks to God , who made all things possible.

Contents

List of figures

List of tables

Acronyms and abbreviations

2D	Two Dimensional
3D	Three Dimensional
AoA	Angle of Arrival
AoD	Angle of Departure
AS	Angular Spectrum
AWGN	Additive White Gaussian Noise
BER	Bit Error Rate
CEM	Computational Electromagnetics
CSI	Channel State Information
EMF	Electromotive Force
FDTD	Finite-Difference Time-Domain
i.i.d	Independent Identically Distributed
MCM	Multiport Conjugate Match
MIMO	Multiple-Input Multiple-Output
MoM	Method of Moment
NFS	Near-Field Scatterers
OC	Open-Circuit method
PAS	Power Azimuth Spectrum
RF	Radio Frequency
RMI	Receiving Mutual Impedance method
RMMSE	Relaxed Minimum Mean Square Error
SISO	Single-Input Single-Output
SINR	Signal to Interference-plus-Noise Ratio
SNR	Signal to Noise Ratio
SVD	Singular Value Decomposition

Nomenclature

B_c	channel coherence bandwidth
C	channel capacity
C_{wf}	waterfilling capacity
$\mathbf{C}_R$	receive array coupling matrix
$\mathbf{C}_T$	transmit array coupling matrix
d	element separation
$\mathbf{e}$	array steering vector
$\mathbf{e}_{mc}$	array steering vector of a coupled array
f_m	maximum Doppler shift
$g_i(\phi)$	antenna pattern of element i over azimuth plane
h	channel impulse response for a SISO system
$\mathbf{H}$	channel matrix of a MIMO system
$\mathbf{H}_w$	i.i.d channel matrix of a MIMO system
$\mathbf{H}_{mc}$	total channel matrix of a compact MIMO system taking the mutual coupling into account
$\hat{\mathbf{H}}_{mc}$	channel estimate of compact MIMO systems
$\mathbf{i}_L$	vector of terminal load currents
$\mathbf{I}$	identity matrix
M	number of receive antennas
N	number of transmit antennas
$\mathbf{n}$	noise vector at the receiver
p	probability density function
P_r	received power
P_t	transmit power
$\mathbf{R}_\mathbf{x}$	covariance matrix of the input signal vector
$\mathbf{S}$	scattering parameter matrix
T_c	channel coherence time
T_s	symbol period
$\mathbf{v}_{oc}$	vector of open-circuit voltages
$\mathbf{v}_L$	vector of terminal voltages

$\mathbf{x}$	vector of transmit signals
$\mathbf{y}$	vector of received signals
z_0	characteristic impedance
z_L	terminal load impedance
z_{in}	input impedance
$\mathbf{Z}$	array antennas impedance matrix
$\mathbf{Z}_L$	terminal load impedance matrix
$\mathbf{Z}_R$	receive array impedance matrix
ϕ	azimuth angle
θ	elevation angle
λ	wavelength
ρ	signal to noise ratio
ρ_{12}	signal correlation coefficient
ρ_e	envelope correlation
τ	spatial delay between array elements
σ	standard deviation of a random variable
σ_n^2	noise power
σ_E^2	estimation error variance
μ	mean-value of a random variable
$\mathbf{\Psi}_R$	receive array covariance matrix
$\mathbf{\Psi}_T$	transmit array covariance matrix
$\mathbb{C}$	set of complex numbers
$\mathbb{R}$	set of real numbers
∂	partial differential operator
C_i	cosine integral
S_i	sine integral
$\det(\cdot)$	determinant operator
$\mathrm{diag}(\cdot)$	diagonal matrix
$E(\cdot)$	expectation operator
$\mathrm{Tr}(\cdot)$	trace of a matrix

Chapter 1
Introduction

1.1 Motivation

In wireless mobile communications, there is an increasing demand for higher data rates and better link quality and coverage. However, there are restrictions of the available bandwidth and limited transmission power. Furthermore, wireless systems communicate through a complex space-time varying channel and they require to overcome channel fading due to multipath propagation.

By the end of the 20th century, Multiple-Input Multiple-Output (MIMO) systems emerged which provide better link quality and higher data-rates for wireless communications by using multiple antennas at both transmit and receive sides of the wireless link [2, 3]. A MIMO system with N transmit and M receive antennas, as shown in Figure 1.1, can mitigate the channel fading by using diversity at both the transmitter and receiver, and can increase data rates up to $\min(N, M)$ times more in comparison to the conventional wireless systems.

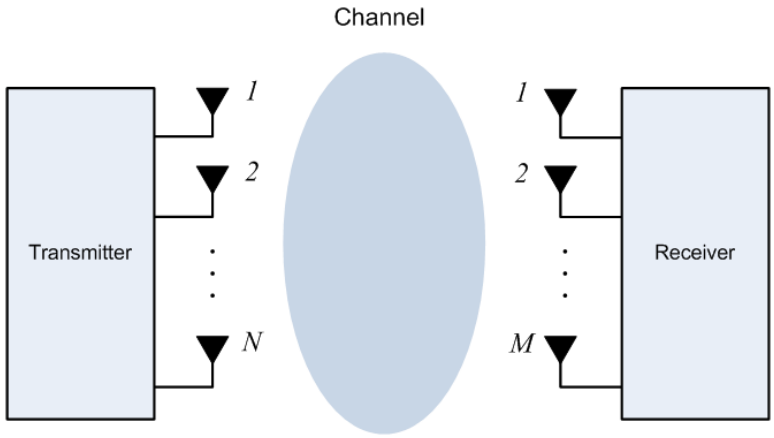

Figure 1.1: *A MIMO system with N transmit and M receive antennas.*

However, applying MIMO wireless technology to small portable devices is restricted with limits on the inter-element separation of antennas. An element spacing less than half a wavelength leads to *mutual coupling*, which describes the electromagnetic interactions between antennas.

This phenomenon can change antenna parameters such as: antenna pattern, and antenna input impedance. Therefore it influences the performance of MIMO systems. According to previous studies, in the presence of mutual coupling, each antenna element is considered as a new scatterer for other elements of the array. Therefore, it can benefit MIMO diversity for some range of element separation. However, mutual coupling effect degrades the received power and the capacity (data rates) due to mismatches between antennas and their termination load impedances. Recent studies have presented antenna impedance matching approaches to improve the MIMO performance in the presence of mutual coupling [4–9]. These studies require prior knowledge of the mutual coupling model and the channel matrix to find a proper impedance match which maximises the compact MIMO performance. The choices of theses impedances are found to be dependent on the proportion of the mutual coupling and the propagation scenario. However, the mutual coupling model used by the existing studies is not accurate in general, and it is only valid for a specific types of antennas such as half-wavelength dipoles. Furthermore, These studies are not able to adapt to changes of the channel matrix.

Therefore, in this thesis it was decided to study the existing mutual coupling model to find a more general approach to search for the optimum impedance matching network corresponding to the propagation channel. It is desired to avoid fitting to explicit mutual coupling model due to the lack of a widely applicable and accurate mathematical model. Therefore, we proposed an *adaptive impedance matching* technique which only relies on the knowledge of the received signals and training sequences. The proposed technique uses the measured channel matrix which includes both the mutual coupling and the propagation scenario effects. It searches for the optimum load impedances iteratively to maximise the compact MIMO performance in the presence of mutual coupling.

1.2 Contributions

The main contributions of this thesis can be summarised as follows:

- Two methods of modelling the mutual coupling are investigated and the electromagnetic simulation software FEKO [10] is used to calculate antenna parameters for an array of two half-wavelength dipoles using both models. The influence of the mutual coupling on compact MIMO performance metrics such as: antenna element pattern, signal correlation, received power, and capacity are examined by using these two models.

- The antenna impedance matching technique is investigated as a solution to mitigate the performance degradation of compact MIMO systems due to the mutual coupling. However, this technique requires knowledge of the mutual coupling model and the channel matrix. In general, there is no simple mathematical approach to model the mutual coupling explicitly. An estimation of the total MIMO channel matrix from the knowledge of the received signals and training sequences, will include the effects of mutual coupling.

- The idea of having an *adaptive impedance matching* network is proposed to counteract the mutual coupling effect on the MIMO performance when there is no knowledge of the mutual coupling model. The channel estimate is used to take account of the mutual coupling effects, and three optimisation techniques including Gradient-based, Newton-Raphson, and random search methods are mathematically and numerically examined to implement such an idea for the identical antenna load impedances. We found the random search method to be a simple and robust technique that provides the best performance.

- The adaptive impedance matching technique is extended to the non-identical load impedances. Simulation results for several propagation scenarios under different conditions such as: slow and fast fading proved the performance of the proposed technique.

1.3 Thesis Structure

The remainder of this thesis is organised as follows:

Chapter 2 provides background information related to this thesis. It reviews some basic characteristics of the wireless propagation channel. Then, a general overview of MIMO wireless systems, followed by descriptions of the MIMO system model and MIMO capacity under different conditions are presented. Antenna matching circuits and the mutual coupling are also discussed briefly at the end of this chapter.

Chapter 3 presents an overview of existing methods of mutual coupling modelling, and discusses the accuracy conditions of such methods. Then, the impact of mutual coupling on MIMO performance metrics such as: antenna pattern, signal correlation, received power, and capacity are evaluated. The antenna impedance matching technique is also investigated as a solution to mitigate the performance degradation due to the mutual coupling effect for two mutual coupling models.

Chapter 4 explains the necessity of having an *adaptive impedance match* for compact MIMO systems. It then proposes the adaptive impedance matching technique, and examines required conditions to implement such an idea. Some estimation methods for the capacity and the received power are addressed and three optimisation techniques: Gradient-based, Newton-Raphson, and random search methods are examined for implementing the adaptive impedance match assuming identical antenna load impedances.

Chapter 5 extends the *adaptive impedance matching* approach to the non-identical load impedances. It then numerically evaluates the performance of the proposed technique for identical and non-identical load impedances, by comparing their results to the conventional terminations such as: the characteristic impedance match and the self-impedance conjugate match. The effect of channel fading (slow and fast fading), and channel estimation error are also considered in the numerical results.

Chapter 6 presents some concluding remarks and suggestions for future research.

Chapter 2
Background

2.1 Introduction

In this chapter, we first describe some basic characteristics of the wireless propagation channel. Then, the advantages of Multiple-Input Multiple-Output (MIMO) wireless systems over conventional systems are reviewed. Next, we introduce the MIMO system model followed by MIMO capacity descriptions under different conditions. Finally, the problem of mutual coupling for small size MIMO systems is addressed. This phenomenon degrades the MIMO performance. Therefore, the rest of this thesis is allocated to find a solution to counteract the mutual coupling in compact MIMO systems.

2.2 Wireless Communications

Wireless communication is one of the fastest growing technologies in our time. However, communication in a wireless channel is faced with a number of challenges including limited power and bandwidth, and a complex space-time varying channel [1, 11–13]. As shown in Figure 2.1, wireless signals pass through multiple paths from the transmitter to the receiver. Each multipath component may experience a change of its amplitude, phase delay and frequency. These signals are added up in the receiver and they interfere with each other in a constructive or destructive way. The amplitude variation of the total signal at the receiver is called *fading* [12]. In general, the variation of the total received signal in terms of different temporal and spatial scales is categorised into: *large-scale* and *small-scale fading* [12, 13].

2.2.1 Large-scale fading

Large-scale fading is the variation of the received power over large distances due to path loss and shadowing. *Path loss* is the propagation loss of the radiated electromagnetic wave in free space which occurs over long distances (100-1000m) between the transmitter and the

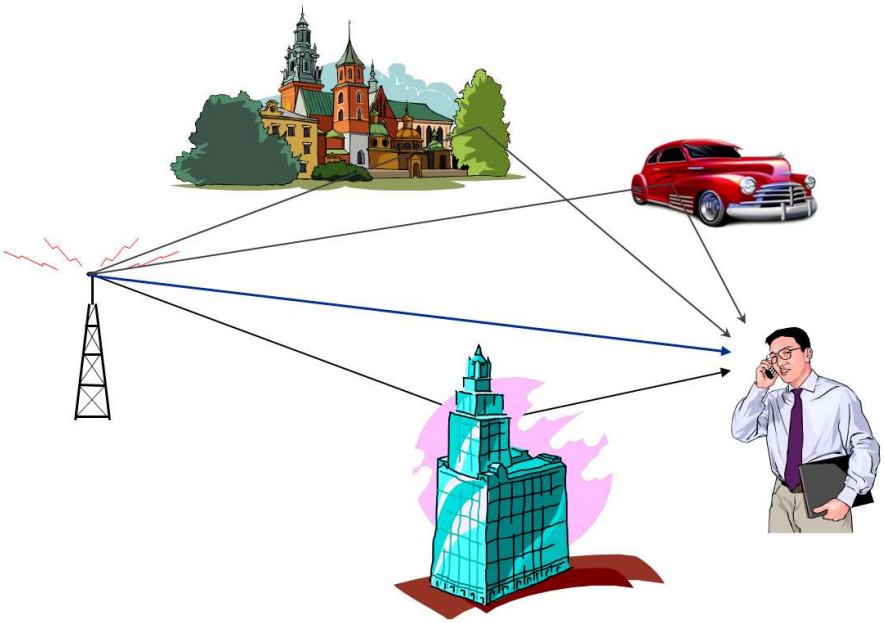

Figure 2.1: *Multipath propagation in wireless communications*

receiver [13]. *Shadowing* is the attenuation of signal power caused by large objects between the transmitter and the receiver. Shadow fading occurs due to different phenomena such as absorption, reflection, diffraction, and scattering on a large scale of few hundred wavelengths (10-100m in outdoor and less for indoor communications) [12, 13].

Path Loss

Consider a transmitter and a receiver separated with a distance of d in free space, and with no objects between them. The ratio of the received power P_r to the transmit power P_t is given by [13]

$$\frac{P_r}{P_t} = \left(\frac{\lambda_c}{4\pi d}\right)^2 G_t G_r \tag{2.1}$$

where λ_c is the carrier frequency wavelength, and G_t and G_r are the transmit and the receive power gains, respectively. However, most of wireless systems communicate through a complex propagation environment. Therefore, unlike the free space, modelling the path loss is not easy and its effect is combined with shadowing and multipath fading. Several empirical models are obtained by averaging the received power at given distances over a few wavelengths [13]. As an example, piecewise linear approximation from measurements is a common approach to model path loss in microcell outdoor and indoor channels [12, 13].

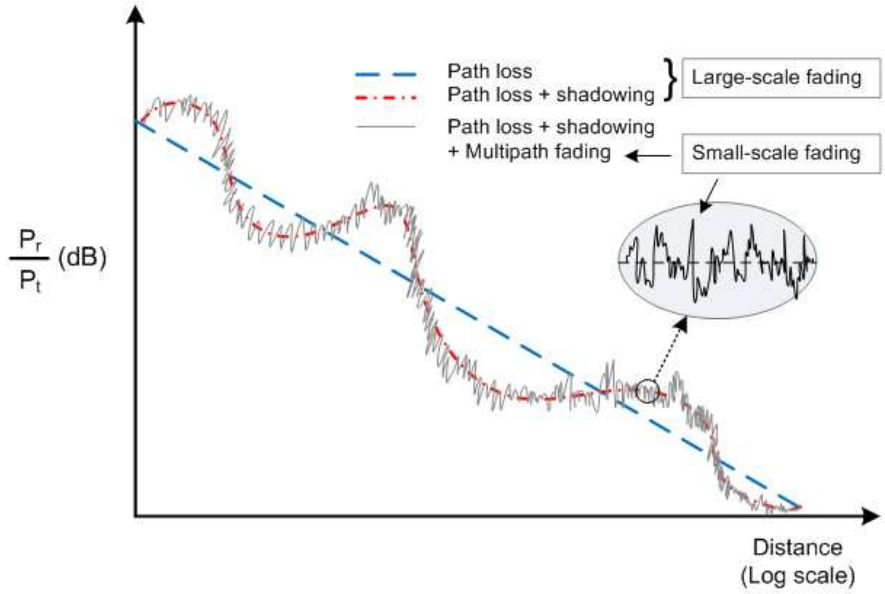

Figure 2.2: *Illustration of channel fading versus distance.*

Shadow Fading

The received signal is attenuated randomly due to blockage from large objects between the transmitter and the receiver, or variation of reflecting surfaces and scatterers [13]. This phenomenon is called *shadow fading* or *shadowing* and it is modelled by assuming the ratio of transmit-to-receive power $\psi = P_t/P_r$ as a random variable with log-normal distribution [12, 13]. However, the distribution of ψ values in dB is converted to a Gaussian distribution given by [13]

$$p(\psi_{dB}) = \frac{1}{\sqrt{2\pi}\sigma_{\psi_{dB}}} \exp\left[-\frac{(\psi_{dB} - \mu_{\psi_{dB}})^2}{2\sigma^2_{\psi_{dB}}}\right]. \tag{2.2}$$

where $\psi_{dB} = 10\log_{10}(P_t/P_r)$ in dB is the random variable, $p(\psi_{dB})$ is the probability density function (pdf) of ψ_{dB}, and $\mu_{\psi_{dB}}$ and $\sigma_{\psi_{dB}}$ are the mean value and the standard deviation of ψ_{dB}, respectively.

2.2.2 Small-scale fading

Fluctuations of the received signal due to the constructive and destructive interference of multipath components is called *small-scale fading*. This fading happens over very short distances on a scale of a few signal wavelength. As an example for a 2GHz carrier frequency, moving from a point by less than 10cm changes a constructive interference to be destructive, or vice

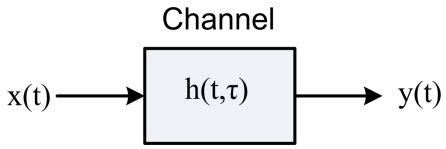

Figure 2.3: *Sketch of a wireless communication system.*

versa [12]. Figure 2.2 illustrates path loss, shadowing, and multipath fading versus distance. As can be seen from the figure, for multipath fading, the signal amplitude fluctuates around a local mean value, which is determined by path-loss and shadowing.

As shown in Figure 2.3, the total effect of multipath propagation is modelled by defining a channel coefficient $h(t, \tau)$ which relates the received signal $y(t)$ to the transmitted signal $x(t)$ as follows:

$$y(t) = \int_0^{\tau_{max}} h(t, \tau)x(t - \tau)d\tau + n(t) \tag{2.3}$$

where $h(t, \tau)$ is the channel response at time t to a transmitted impulse at time $(t - \tau)$, τ_{max} is the maximum length of the channel response, and $n(t)$ is the receiver noise. With a large number of independent multipath components and no dominant line-of-sight (LOS) signal component, the channel coefficient is modelled as a complex random variable with a uniform distribution for its phase, and a Rayleigh distribution for its amplitude $r = |h|$ given by [13]

$$p(r) = \frac{r}{\sigma^2} \exp\left[-\frac{r^2}{2\sigma^2}\right]. \tag{2.4}$$

2.2.3 Slow versus fast fading

Time-varying multipath channels are categorised as *slow* or *fast fading* channels. For the latter case, the channel impulse response changes rapidly within the symbol period [14]. This can happen due to movement of the transmitter or the receiver. Assuming f_m to be the maximum Doppler shift, the channel *coherence time* T_c is related to f_m as follows [14]:

$$T_c \approx \frac{1}{f_m} \tag{2.5}$$

Denoting the symbol/frame period by T, the fast fading condition for a channel with the coherence time of T_c is described by $(T > T_c)$. On the other hand, for slow fading the channel response does not change over the period of T, and $(T \ll T_c)$.

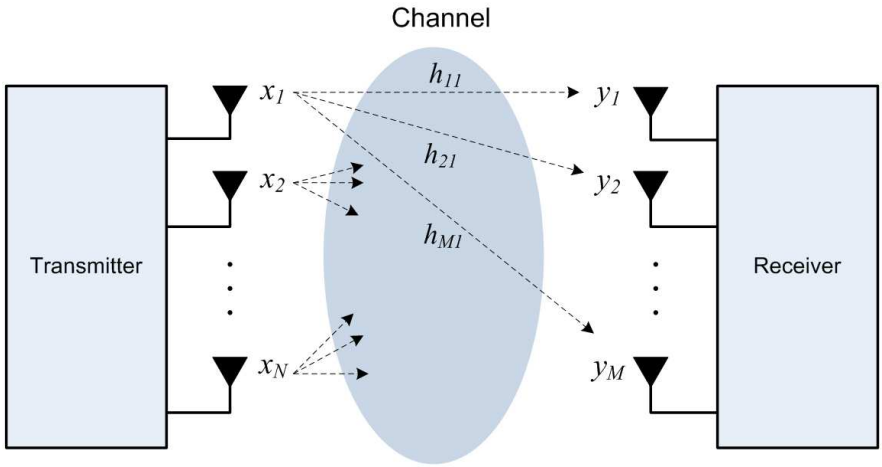

Figure 2.4: *Schematic diagram of a $N \times M$ MIMO wireless system.*

2.2.4 Flat versus frequency-selective fading

For a time-varying multipath channel in the frequency domain, the *channel coherence bandwidth* B_c is defined as the frequency difference in which two frequency components are correlated [12]. For a narrowband signal with a bandwidth of $W \ll B_c$, all the signal components are highly correlated, which means the fading over all signal components is equal. This case is called *flat-fading*. On the other hand, if the signal bandwidth $W \gg B_c$, then the channel behaves differently for different frequencies and we have *frequency-selective fading*.

2.3 MIMO Systems

Over the last decade, the use of multiple antennas at both transmit and receive end, popularly known as MIMO systems, have been one of the most active research areas in the field of wireless communication. Figure 2.4 shows a schematic diagram of a MIMO system with N transmit and M receive antennas. MIMO technology can increase the data rate and/or improve the quality (bit-error rate) of communication by exploiting spatial properties as a new dimension to enhance the performance [1–3, 15, 16].

2.4 MIMO benefits

MIMO technology can provide significant performance gains such as *array gain*, *interference reduction*, *spatial diversity gain* and *spatial multiplexing gain* [1, 11]. In the following, we

briefly describe these gains and how they can be exploited.

2.4.1 Array gain

Array gain is the increasing of signal-to-noise ratio (SNR) at the receiver due to the coherent combination of the wireless signals at the receiver or transmitter or both [1, 11]. Arriving signals at the receive antennas, which have different amplitudes and phases, can be coherently combined to obtain an enhanced signal quality. The average increase in the SNR at the receiver is related to the number of the receive antennas [13].

2.4.2 Interference reduction

Interference in wireless channels arises from the sharing of time and frequency resources for multiple users. In array antennas, the spatial properties of the desired signal and interference are usually not the same. So we can reduce the interference by exploiting these differences. However, interference reduction methods usually need channel knowledge for the desired signal. By the use of array gain and interference reduction techniques, we can improve signal-to-noise-plus-interference ratio (SINR). Figure 2.5.(a) shows an array that forms the beampattern by coherent combination of array elements output to maximize in the direction of the desired signal (array gain) and place a null in the direction of interference (interference reduction) [17].

2.4.3 Spatial diversity gain

The signal level at the receiver in a wireless system fluctuates or fades. Spatial diversity mitigates fading (distortion and attenuation of wireless signal) by providing the receiver with multiple (ideally independent) copies of the transmitted signal in space, frequency or time. So the probability that at least one of these copies does not experience a deep fade increases dramatically. In a MIMO system both transmit and receive array antennas can be used to obtain diversity gain [1, 13]. Figure 2.5.(b) illustrates the spatial diversity principle, where statistically independent copies of each signal received by different antennas are added together to mitigate fading.

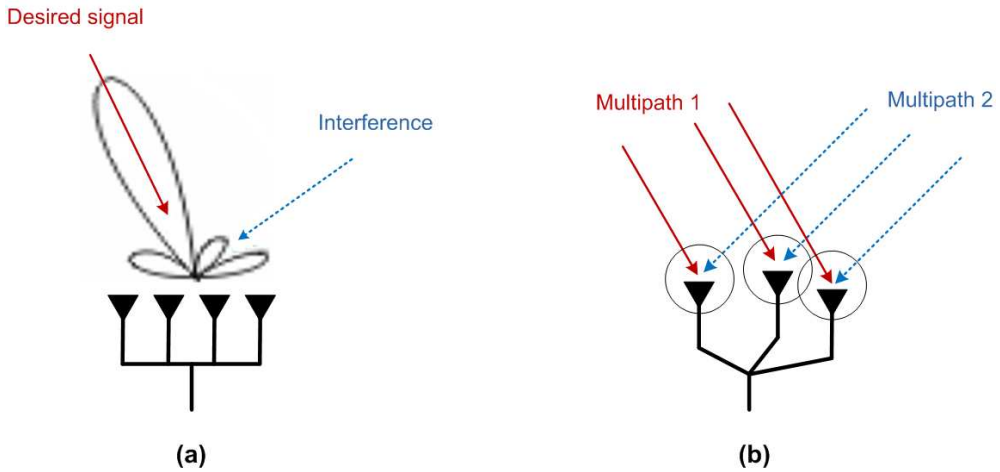

Figure 2.5: *A comparison of (a) array beamforming with (b) spatial diversity.*

2.4.4 Spatial multiplexing gain

Spatial multiplexing is a specific concept for MIMO systems which allows the transmitter to increase the transmission rate (or channel capacity) by sending parallel independent data-streams simultaneously on the same radio frequency. Under suitable conditions related to the number of receive antennas and the channel conditions, the receiver can successfully separate and decode the transmitted information [1–3, 15, 16].

2.5 MIMO System Model

In order to understand the performance limits of MIMO systems, we should understand the nature of the MIMO channel. Consider a MIMO system with N transmit and M receive antennas, as shown in Figure 2.4. A linear time-variant MIMO channel response can be represented by the $M \times N$ matrix $\mathbf{H}(\tau, t)$ as:

$$\mathbf{H}(\tau,t) = \begin{bmatrix} h_{1,1}(\tau,t) & h_{1,2}(\tau,t) & \dots & h_{1,N}(\tau,t) \\ h_{2,1}(\tau,t) & h_{2,2}(\tau,t) & \dots & h_{2,N}(\tau,t) \\ \vdots & \vdots & \ddots & \vdots \\ h_{M,1}(\tau,t) & h_{M,2}(\tau,t) & \dots & h_{M,N}(\tau,t) \end{bmatrix} \tag{2.6}$$

where $h_{i,j}(\tau, t)$ is the time-variant channel response between the jth transmit antenna and the ith receive antenna, which is the response at time t to an impulse applied at time $(t-\tau)$. The jth column of the $\mathbf{H}(\tau, t)$ is often referred to as the spatio-temporal signature of the jth transmit

antenna across the receive array. The relation of the N spatial signatures determines the ability to separate the signals sent from the transmitter to a receiver [1, 11].

We note that in the channel matrix description of (2.6), the effects of antenna array configuration and frequency filtering (bandwidth-dependent) are included. The MIMO channel input-output relationship between the $N \times 1$ transmit signal vector $\mathbf{x}(t)$ and the $M \times 1$ receive signal vector $\mathbf{y}(t)$ can be written as [18]:

$$\mathbf{y}(t) = \int_{\tau} \mathbf{H}(t, \tau)\mathbf{x}(t - \tau)d\tau + \mathbf{n}(t) \tag{2.7}$$

where $\mathbf{n}(t)$ is the additive noise (interference and noise) in the receiver.

Throughout this thesis, we assume two options for the time variation of the channel: (a) *block fading* model, where the channel matrix is constant over the interval of a transmission block, and (b) *fast fading* model where the channel matrix may change over a few symbol periods. Furthermore, we consider *narrowband* communication, which is valid when the channel response is constant over the system bandwidth (*frequency-flat fading*) or when signals are divided into narrowband bins and processed separately [1, 16]. In this case, (2.7) can be simplified to

$$\mathbf{y}(t) = \mathbf{H}(t)\ \mathbf{x}(t) + \mathbf{n}(t) \tag{2.8}$$

where $E\{\mathbf{x}\} = \mathbf{0}$ ($E\{\cdot\}$ is the expectation operator), and $E\{\mathbf{n}\mathbf{n}^H\} = \sigma_n^2\mathbf{I}_M$ for additive white Gaussian noise $\mathbf{n}(t)$ [1]. This is the case we consider in this thesis, unless otherwise specified.

A variety of channel models have been proposed for MIMO systems in the literature, some of which are based on measurements [19, 20]. Generally, MIMO channel models can be classified into (i) *physical* and (ii) *analytical* models [18]. The physical channel model can be constructed by specifying angle-of-departure (AoD) at transmitter, angle of arrival (AoA) at receiver, path attenuation, antenna spacing at both ends and other realistic parameters [7]. Analytical models are statistical-based models which are used to describe the MIMO channel in simulations and theoretical analysis. We have considered two popular models which characterise the MIMO channel matrix statistically in terms of the correlation between the matrix entries: classical independent, identically distributed (i.i.d.) Rayleigh fading, and Kronecker channel models [18].

2.5.1 Classical i.i.d. Rayleigh fading channel model

Assuming suitable array element spacing and a rich scattering environment, the entries of $\mathbf{H}$ can be assumed to be independent, zero-mean, unit-variance, circularly symmetric complex Gaussian random variables [1–3], i.e., the entries are defined as

$$h_{m,n} = \mathcal{N}(0, \frac{1}{2}) + j\,\mathcal{N}(0, \frac{1}{2}) \tag{2.9}$$

where $j = \sqrt{-1}$ and $\mathcal{N}(\mu, \sigma^2)$ denotes a Gaussian random variable with mean μ and variance σ^2. We get $\mathbf{H} = \mathbf{H}_w$ as the i.i.d. Rayleigh fading channel model.

2.5.2 Kronecker model

In practice, a low level of scattering in the environment and/or close antenna element spacing leads to correlation between the entries of channel matrix $\mathbf{H}$ [21–23]. Considering the correlation structure, a correlation matrix needs to be constructed upon the correlation model or measured data [24]. In the case of independent fading statistics for the transmitter and receiver, this correlation matrix can be created by the Kronecker product of two separated matrices [19]. A common way to include the correlation among the channel matrix entries is to use Kronecker model as [19, 25–27]

$$\mathbf{H} = \mathbf{\Psi}_R^{1/2} \mathbf{H}_w \mathbf{\Psi}_T^{1/2} \tag{2.10}$$

where $\mathbf{\Psi}_T$ and $\mathbf{\Psi}_R$ are the correlation matrices at the transmit and receive ends, respectively. This model has been validated by comparing with measured data for small size MIMO systems such as 2×2 and 3×3 [19, 28, 29].

2.6 MIMO Capacity

Transmission rate and bit-error rate (BER) are two significant performance metrics for any communication system. In this section, we briefly review the Shannon capacity, which shows the theoretical upper bound of the maximum data rate [13], and the outage probability for narrowband MIMO systems. Generally, the capacity depends on our knowledge of the channel gain matrix $\mathbf{H}$ or its distributions at the receiver and/or transmitter [30].

2.6.1 Deterministic MIMO Channel Capacity

For a 1×1 (SISO[1]) wireless system, the Shannon capacity is given by:

$$C = \log_2(1 + \rho|h|^2) \qquad \text{bits/s/Hz} \tag{2.11}$$

where ρ is the SNR at the RX antenna, and h is the normalised complex gain for the wireless channel. Here we assume the fading is frequency-flat, therefore the channel gain is just a scalar number. As we see from (2.11) the capacity only increases logarithmically with the SNR.

Now we consider the capacity for the MIMO wireless channel. Assume that the MIMO channel $\mathbf{H}$ is deterministic and perfectly known at the receiver (this knowledge can be obtained via transmitting training sequences and tracking these at the receiver). Then the capacity for the system described by (2.8) is given by [13, 15]

$$C = \max_{\mathbf{R_x}:\, \mathrm{Tr}(\mathbf{R_x})=P_T} \log_2 \left[\det(\mathbf{I}_M + \frac{1}{\sigma_n^2} \mathbf{H}\mathbf{R_x}\mathbf{H}^H) \right] \qquad \text{bits/s/Hz} \tag{2.12}$$

where $\mathbf{I}_M$ is the $M \times M$ identity matrix, $\mathrm{Tr}(\cdot)$ is the trace, P_T is the total transmit power, σ_n^2 is the noise power at the receiver, and $\mathbf{R_x} = \mathrm{E}\{\mathbf{x}\mathbf{x}^H\}$ is the covariance matrix of the transmitted signal $\mathbf{x}$. The diagonal elements of $\mathbf{R_x}$ represents the transmit power by each antenna, and therefore the inequality $\mathrm{Tr}(\mathbf{R_x}) \leq P_T$ defines the total transmit power constraint. Referring to (2.12), it is clear that the optimisation subject to $\mathbf{R_x}$ depends on the transmitter's knowledge of $\mathbf{H}$. In the following, we consider different cases of channel knowledge at the transmitter.

Channel Known at Transmitter: Water-filling

Let us consider a case that the $M \times N$ channel gain matrix $\mathbf{H}$ is known for both the transmitter and the receiver. By using the singular-value-decomposition (SVD) for the matrix $\mathbf{H}$ we have

$$\mathbf{H} = \mathbf{U}\mathbf{\Sigma}\mathbf{V}^H \tag{2.13}$$

where the $M \times M$ matrix $\mathbf{U}$ and $N \times N$ matrix $\mathbf{V}$ are unitary matrices[2], and $\mathbf{\Sigma}$ is an $M \times N$ diagonal matrix with non-negative entries [11]. The diagonal elements of the matrix $\mathbf{\Sigma}$, denoted by σ_i, are singular values of $\mathbf{H}$ so that $\sigma_i = \sqrt{\lambda_i}$ where λ_i is the ith eigenvalue of $\mathbf{H}\mathbf{H}^H$

[1] single-input single-output

[2] If $N \times N$ matrix $\mathbf{A}$ is unitary, then $\mathbf{A}\mathbf{A}^H = \mathbf{A}\mathbf{A}^H = \mathbf{I}_N$

[13]. The matrix $\mathbf{H}$ has $R_{\mathbf{H}}$ nonzero singular values σ_i, which $R_{\mathbf{H}}$ is the rank of $\mathbf{H}$, and $R_{\mathbf{H}} \leq \min(N, M)$.

The MIMO channel can be transformed into $R_{\mathbf{H}}$ independent parallel channels by pre-multiplying the transmit vector by the matrix $\mathbf{V}$, and post-multiplying the receive vector by the matrix $\mathbf{U}^H$. In other words, the channel input $\mathbf{x}$ is created by $\mathbf{x} = \mathbf{V}\widetilde{\mathbf{x}}$, which $\widetilde{\mathbf{x}}$ is the data stream vector, and the channel output $\mathbf{y}$ is multiplied by $\mathbf{U}^H$, so we have

$$\begin{aligned} \widetilde{\mathbf{y}} &= \mathbf{U}^H(\overbrace{\mathbf{H}\mathbf{x} + \mathbf{n}}^{\mathbf{y}}) \\ &= \mathbf{U}^H(\mathbf{U}\mathbf{\Sigma}\mathbf{V}^H(\mathbf{V}\widetilde{\mathbf{x}}) + \mathbf{n}) \\ &= \mathbf{\Sigma}\widetilde{\mathbf{x}} + \mathbf{U}^H\mathbf{n} \\ &= \mathbf{\Sigma}\widetilde{\mathbf{x}} + \widetilde{\mathbf{n}} \end{aligned} \tag{2.14}$$

where $\widetilde{\mathbf{n}} = \mathbf{U}^H\mathbf{n}$. Since $\mathbf{\Sigma}$ is a diagonal matrix, we have $\widetilde{\mathbf{y}} = \sigma_i\widetilde{\mathbf{x}} + \widetilde{\mathbf{n}}$ for $i = 1, 2, \cdots, R_{\mathbf{H}}$. Now, there are $R_{\mathbf{H}}$ orthogonal parallel channels so that the transmitter can use the waterfilling algorithm to allocate power to these channels as an optimum way. The power allocation can be expressed as

$$P_i = (\mu - \frac{1}{\sigma_i^2})^+, \qquad 1 \leq i \leq R_{\mathbf{H}} \tag{2.15}$$

where P_i is the power of $\widetilde{\mathbf{x}}_i$, x^+ is equal to $\max(x, 0)$, and the waterfilling level μ is chosen to satisfy $\sum_{i=1}^{R_{\mathbf{H}}} P_i = P_T$. The channel capacity can be obtained by choosing an appropriate power P_i for each $\widetilde{\mathbf{x}}$. The covariance matrix for $\mathbf{x}$ which maximises (2.12) is $\mathbf{R}_{\mathbf{x}} = \mathbf{V}\mathbf{P}\mathbf{V}^H$, where the $N \times N$ matrix $\mathbf{P}$ is a diagonal matrix. If we assume the singular values of $\mathbf{H}$ are in descending order, then $\mathbf{P} = \mathrm{diag}(P_1, \cdots, P_{R_{\mathbf{H}}}, 0, \cdots, 0)$. Substitution of $\mathbf{R}_{\mathbf{x}}$ into (2.12) yields the waterfilling capacity as [11–13]

$$C_{wf} = \sum_{i=1}^{R_{\mathbf{H}}} \log_2 \left[1 + \frac{P_i}{\sigma_n^2}\sigma_i^2\right] \tag{2.16}$$

It can be seen that the capacity in (2.16) is obtained from the sum of the capacities of subchannels.

Channel Unknown at Transmitter: Equal Power Allocation

When the channel matrix $\mathbf{H}$ is known to the receiver, but unknown to the transmitter, the power is equally allocated among the transmit antennas to form N independent streams, or $\mathbf{R_x} = (P_T/N)\mathbf{I}_N$. It results in the equal power capacity given by

$$C_{ep} = \log_2 \left[\det(\mathbf{I}_M + \frac{\rho}{N}\mathbf{H}\mathbf{H}^H) \right] \tag{2.17}$$

where $\rho = P_T/\sigma_n^2$ is the average SNR at the receiver.

2.6.2 Capacity of fading MIMO Channels

In the previous section, the MIMO capacity for one realisation of the channel matrix $\mathbf{H}$ is considered. Wireless communication system analysis should always include the effect of the channel fading. In this case, the entries of the channel matrix $\mathbf{H}$ are random variables. There are two different definitions to characterise the fading channel capacity: *ergodic capacity* and *outage capacity*. The channel matrix is known at the receiver, but it may be known or unknown to the transmitter.

Ergodic Capacity

The ergodic capacity is an expected value of the capacity over all realisations of the channel matrix [12]. Consider a time-varying channel with random matrix $\mathbf{H}$ that is known at the receiver but not at the transmitter. Ergodic capacity defines the maximum rate, averaged over all realisations of the channel, which can be realised based on a fixed transmission strategy (rate and/or power) [11, 13]. In other words, the problem is to find the optimum $\mathbf{R_x}$ to maximise

$$C = \max_{\mathbf{R_x}:\, \mathrm{Tr}(\mathbf{R_x})=P_T} E_{\mathbf{H}} \left\{ \log_2 \left[\det(\mathbf{I}_M + \frac{1}{\sigma_n^2}\,\mathbf{H}\mathbf{R_x}\mathbf{H}^H) \right] \right\} \tag{2.18}$$

where $E_{\mathbf{H}}\{\cdot\}$ is the expectation over the distribution of the channel matrix $\mathbf{H}$. For the i.i.d. zero-mean circularly symmetric and unit-variance channel model, $\mathbf{H} = \mathbf{H}_w$, the optimum input covariance to maximise (2.18) is $\mathbf{R_x} = (\frac{P_T}{N})\mathbf{I}_N$. In this case, the ergodic capacity becomes [13]

$$C = E_{\mathbf{H}} \left\{ \log_2 \left[\det(\mathbf{I}_M + \frac{\rho}{N}\mathbf{H}\mathbf{H}^H) \right] \right\}. \tag{2.19}$$

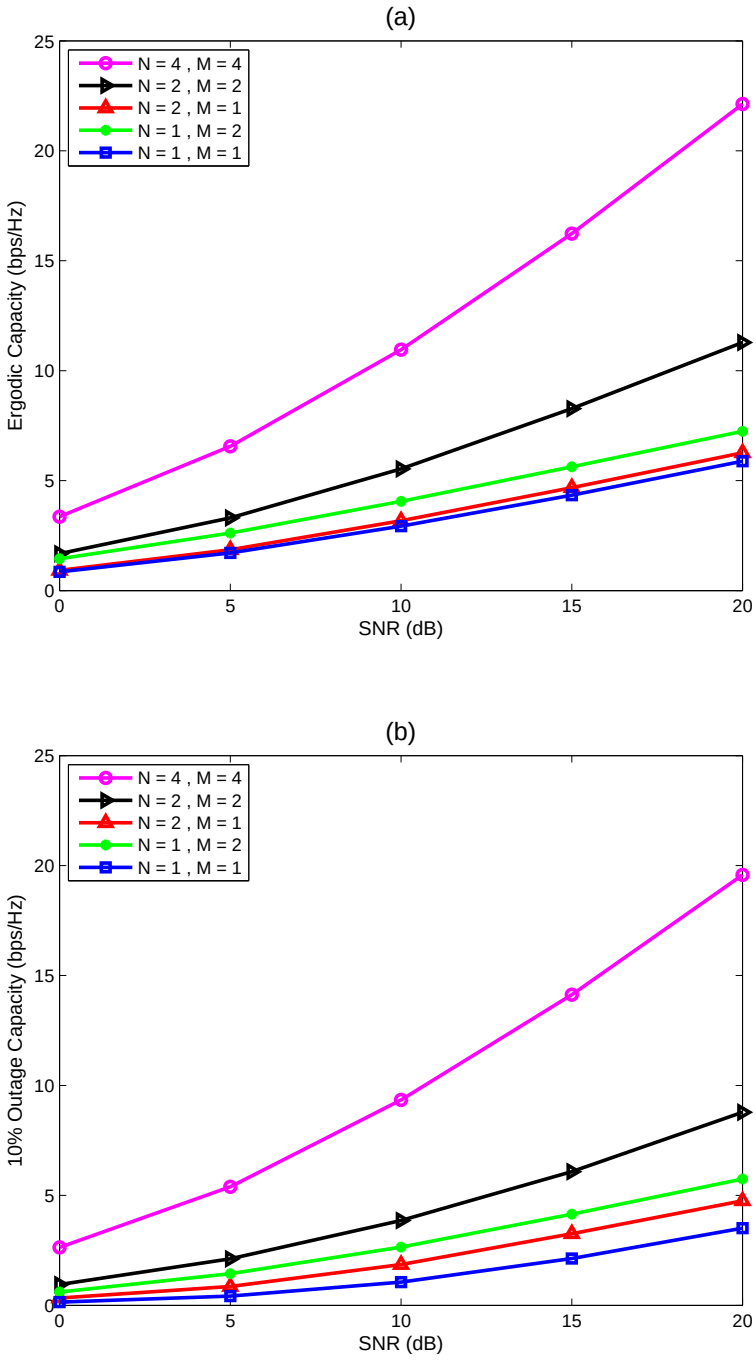

Figure 2.6: *(a) Ergodic capacity, and (b) 10% outage capacity versus average received SNR for different MIMO configurations with N transmit and M receive antennas, under the assumption of i.i.d. Rayleigh-fading channel model and equal power allocation at the transmitter. These results match Fig.5 and Fig.6 from [1].*

Outage Capacity

The outage capacity is defined over slowly time-varying channels, where the data is transmitted over a time period that is much shorter than the channel coherence time (i.e., $\mathbf{H}$ is constant over a relatively long transmission time) [11–13]. Thus, we can compute the (Shannon) capacity for each realization of $\mathbf{H}$, and capacity becomes a random variable with an associated cumulative distribution function (CDF) [12]. Now, we define the $q\%$ outage capacity $C_{out,q}$ as the transmission rate that is guaranteed for $(100-q)\%$ of the channel realisations [1]. In other words, the outage capacity $C_{out,q}$ can be obtained from the follow relation

$$P(C \leq C_{out,q}) = q\% \tag{2.20}$$

where C is the instantaneous channel capacity, and for the case where the channel is only known at receiver, can be obtained from (2.17).

Figure 2.6 shows the ergodic capacity and 10% outage capacity for different MIMO configurations. We assumed that the channel is known for the receiver but not for the transmitter, and i.i.d. channel model is applied, i.e. $\mathbf{H} = \mathbf{H}_w$. The 10% outage capacity shows the minimum transmission rate which is achieved over 90% of the time. Therefore, it is expected to be lower than the ergodic capacity which is an averaged value of the capacity over all the channel realisations. We also observe that MIMO systems with a larger number of antennas can achieve higher data rates. Furthermore, comparing 2×1 and 1×2 MIMO configurations reveals that having more receive antennas is more effective than using more transmit antennas. This is due to the restriction of equal power allocation at the transmitter.

2.7 Antenna Matching Circuit

The antenna is the interface between the transmitter or the receiver and the wireless propagation environment which affects the performance of the communication system. Such an effect is even more for MIMO systems that use multiple antennas at both sides of the wireless link.

An antenna is a device which convert the radio-frequency (RF) signal into the electromagnetic wave at the transmitter, and vice versa at the receiver. The performance of an antenna system is not only dependent on the antenna characteristics, but also it is influenced by the transmission line characteristics. In practice, these characteristics are not the same [31]. For instance, the

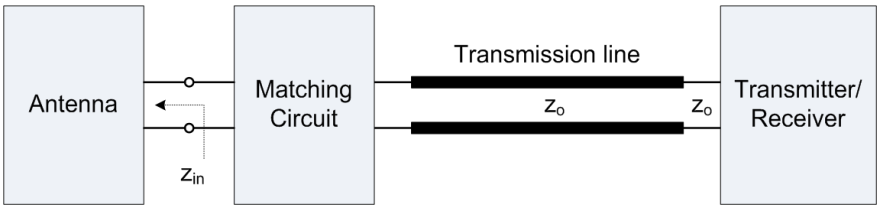

Figure 2.7: *Block diagram of a transmitter or receiver.*

characteristic impedance of the transmission line is real (resistive) whereas for the antenna element it is complex. Therefore, a matching circuit is used between the antenna and the transmitter or the receiver. This is shown in Figure 2.7 for a typical transmitter or receiver with a single antenna. Usually, impedance of the transmitter or receiver is equal to the characteristic impedance z_0 of the transmission line [32]. Using Thevenin equivalent circuits, the above configuration can be simplified as shown in Figure 2.8 for the transmitter or the receiver. As an example for the receiver, when we have no matching circuit, the load impedance z_L is equal to the transmission line characteristic impedance z_0. However, in practice, the matching circuit is matched to the conjugate of the antenna impedance in order to have maximum power transfer [31, 32].

In practice, matching networks are used to have either no reflections, or maximum power transfer. In order to explain the concept of matching circuit, we consider a simple electric circuit with a load impedance z_L connected to a source v_s in Figure 2.9. Without a matching circuit, according to the circuit theory, maximum power is transferred from the source to the load z_L when $z_L = z_s^*$. This condition is called the *conjugate match*. However, for some applications we can not change the load. Therefore, a matching circuit is used between the load and the source with an input impedance z_M toward the source, as shown in part (b) of Figure 2.9. Reflection coefficient of the matching circuit is given by

$$\Gamma_M = \frac{z_M - z_0}{z_M + z_0} \tag{2.21}$$

And the conjugate match for this circuit means that $z_M = z_s^*$, and consequently $\Gamma_M = \Gamma_s^*$.

2.8 Mutual Coupling

When two or more antennas are placed close together, whether each one is transmitting or receiving, they interact electromagnetically in a complicated way. This phenomenon is called

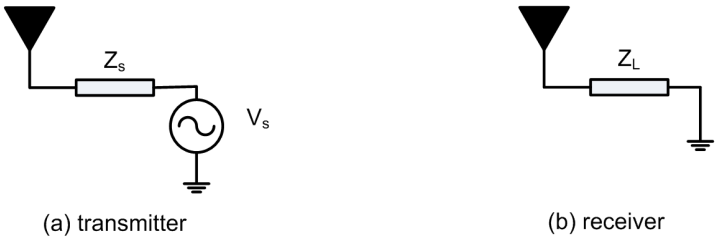

Figure 2.8: *Simple model of a (a) transmitter, or (b) receiver with a single antenna.*

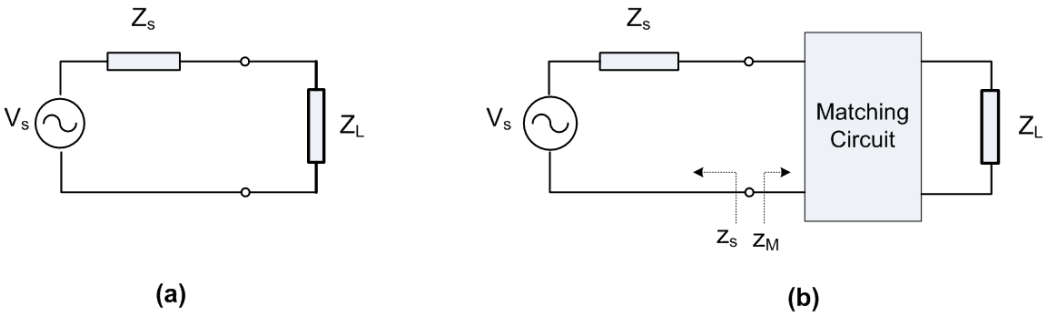

Figure 2.9: *A load connected to a source voltage (a) without, (b) with a matching circuit.*

mutual coupling [31, 32] and it may change the parameters of each antenna such as: antenna gain, beamwidth, pattern, resonance frequency, and input impedance [31–33]. The mutual coupling mechanism for a receive array of two antennas can be explained as shown in Figure 2.10. A plane wave (0) is incident at antenna 1 and induces current at the antenna. One part of the incident wave energy is absorbed and it goes through the antenna feed. The other part is re-radiated into all directions around the antenna as (2). A portion of the re-scattered energy goes toward antenna 2, shown by (3) in the figure, and adds up to the incident wave energy (0). Some part of the energy received by antenna 2 is re-radiated again and this process is repeated infinitely. The amount of the absorbed and re-radiated energy is dependent on the termination impedances of the antenna elements [31]. The effect of such interactions depends on the location of the antenna in the array. Figure 2.11 illustrates the coupling paths between antenna elements for a linear array of three identical antennas with element spacing of d. For such an array structure, the proportion of mutual coupling for the middle antenna would be larger than the other antennas. The first and the third antennas are influenced by the mutual coupling similarly.

In general, the proportion of the mutual coupling for each array-element depends on different parameters including: inter-element spacing, antenna element pattern, array geometry, relative positioning of the antenna element in the array, operational frequency, and near field scatter-

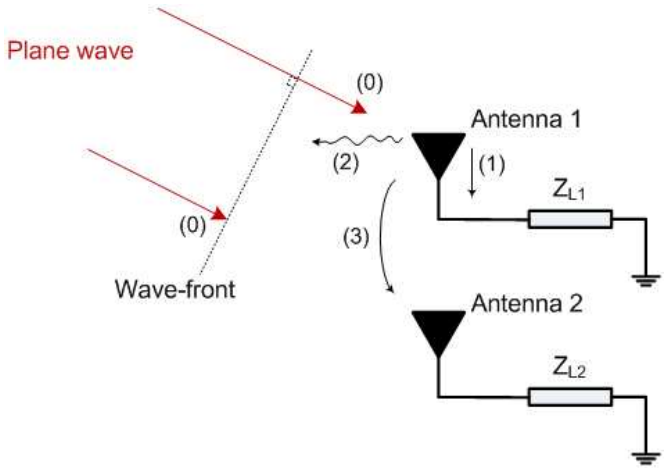

Figure 2.10: *Mutual coupling mechanism between two receive antennas.*

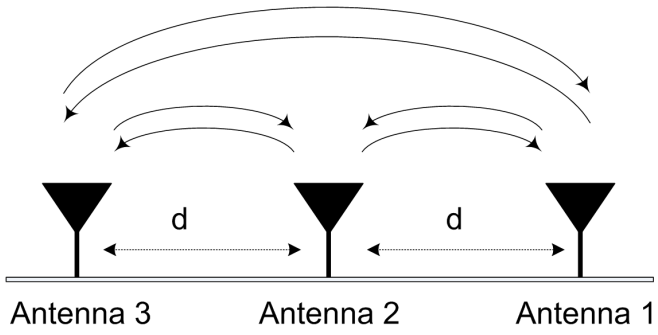

Figure 2.11: *Mutual coupling between antennas.*

ers [31, 33]. Most of these parameters can be measured or estimated except near field scatterers which are random in nature, and can increase the mutual coupling between antennas [33]. From now on, we use the term *coupled array* for closely spaced antennas, which are affected by mutual coupling.

Implementation of MIMO technology on small personal communication devices require to place multiple antennas close together. Therefore the mutual coupling affects the MIMO communication performance. Many studies have investigated the effect of mutual coupling on MIMO systems. Although it benefits the MIMO diversity gain for a specific range of antenna separation by reducing the signal correlation [21, 23, 34–36], it degrades the MIMO received power and the capacity due to mismatch between antennas and their termination loads [5, 22, 37, 38]. We further investigate this effect on MIMO performance in the following chapter and then propose an adaptive impedance matching technique which counteract the mutual coupling effect by tuning the antenna termination loads.

2.9 Summary

In this chapter we reviewed different types of fading for wireless channels, followed by an overview of MIMO technology benefits over traditional wireless systems. After that we described how a MIMO system can be modelled and the MIMO capacity under different channel propagation conditions is defined. Then we mentioned the mutual coupling problem which degrades the MIMO performance in small size wireless devices. In the following chapters we examine the existing mutual coupling models and propose an adaptive antenna impedance matching technique in order to mitigate the mutual coupling effect.

Chapter 3
Mutual Coupling

3.1 Introduction

It is shown in the literature that mutual coupling between closely spaced antennas mostly has undesired effects on the performance of compact MIMO systems. For instance, it changes the input impedance of each array element and therefore the received power will be reduced due to the increased mismatch between the antennas and their loads or sources [35]. However, mutual coupling may also have some beneficial effects such as diminishing spatial channel correlation, which is desired to be reduced in order to optimise the performance of MIMO communications [21, 23, 33, 36].

This chapter investigates the impact of mutual coupling on the performance of compact MIMO systems. First, an overview of existing methods of mutual coupling modelling, and the required conditions for the accuracy of such models are presented. Then, the influence of mutual coupling on common performance metrics such as: *signal correlation, antenna pattern, received power*, and *capacity* would be evaluated.

Next, antenna impedance matching is used as an interesting solution to mitigate mutual coupling effects. There are two kinds of impedance matching network introduced in the literature. One is a coupled matching network [39] which is also called a *multi-port conjugate match* (MCM) [4]. The other one is an uncoupled (or individual-port) impedance match [5–7, 38]. Although the former one is claimed to provide optimal solutions and significant performance improvement [21], it can only operate effectively over a narrow-bandwidth [9, 37]. It also has a complicated structure with interconnections between matching network ports, which makes it difficult to construct practically [37]. The latter one, in comparison, is much easier to construct and it can achieve sub-optimum matching solutions with a wider bandwidth [37, 38]. Therefore, throughout this thesis, uncoupled matching networks are used to counteract the mutual coupling. Finally, we examine the receiving mutual impedance method of mutual coupling modelling for uncoupled matching networks.

3.2 Mutual Coupling Effects

Many studies have investigated the impact of mutual coupling on MIMO performance metrics such as: signal correlation and diversity gain [4, 5, 21, 23, 33, 35–37, 40], element pattern and radiation efficiency [23, 35], received power [4, 5, 21, 40], and capacity [4, 6, 21, 36, 40].

It is shown that the mutual coupling can benefit coupled arrays by reducing the spatial correlation between antennas for some range of element separation [23, 36], and consequently improve the diversity gain [21, 35]. However, the mutual coupling distorts the antenna element pattern [4, 23] which in turn degrades the radiation efficiency [35]. Furthermore, it reduces the received power due to the increased mismatch between the receive antennas and their termination loads [6].

There are some disagreement in the literature about the effect of mutual coupling on the MIMO capacity. Some studies claim an improvement in the capacity due to the mutual coupling for some range of element separation [36], while some others show a capacity degradation in the presence of mutual coupling [22]. This is mainly due to ignoring the effect of the received power on the capacity by the former studies. It has been revealed that the received power and the correlation both affect the capacity [23, 41]. However, the received power has a stronger effect on the capacity [40].

The effect of different types of antenna terminations on the correlation coefficient, the diversity gain, and the received power in the presence of mutual coupling is investigated in [21, 35]. Such an issue is studied in more details in [5, 40] by changing the real and imaginary parts of antenna termination loads for the correlation, the received power, and the capacity. Interestingly, it is found that a proper choice of antenna load impedances can mitigate the mutual coupling effect and improve the performance.

Modelling the mutual coupling is also an important concern in the literature. Most of previous studies use a method suggested by Gupta and Ksienski [42] to model the mutual coupling using impedance parameters or the equivalent scattering parameters [43] of the antenna array. In this method, *antennas with open-circuited terminals* are considered to have no effect on other close proximity antennas. In other words, open-circuited antennas are assumed to have no influence on other antennas. Consequently, *open-circuit terminal voltages* of antennas, while all are open-circuited, *are assumed free of mutual coupling*. This is not true in general and the incident wave can induce currents on the open-circuited antennas which in turn, they affect

other antennas [44]. However, for a few cases such as an array of *half-wavelength dipole antennas*, induced currents under open-circuit condition are so small such that the method in [42] gives a valid approximation of the mutual coupling [23, 44]. We call the above method as the *open-circuit model* and describe it in the following section.

Despite the simplicity of the open-circuit approach, the accuracy of such a model for coupled arrays is questioned by several studies [44–49], and alternative approaches are suggested. In some studies [50–52], the relation between the isolated and coupled element patterns is used to model the mutual coupling. Such methods are complicated in general and they fail to model the mutual coupling for unusual array geometries [44]. Some others use the method of moment (MoM) to analyse the mutual coupling [45, 46, 53]. However, such methods require the knowledge of array quantities such as voltages and currents of the elements [54]. In [48, 55], a new concept of *receiving mutual impedance*, based on the relation of isolated and coupled terminal voltages, is introduced to model the mutual coupling for receive arrays. The advantage of this method over other methods is that, like the open-circuit approach, it deals with the terminal voltages and currents rather than the element pattern or current distribution. It also includes the effect of loading and external source to calculate the receiving mutual impedances.

This chapter is organised as follows. In Section 3.3, we review the open-circuit and the receiving mutual impedance methods to model the mutual coupling. Section 3.4 examines the impact of mutual coupling on MIMO performance metrics such as: the antenna pattern, the signal correlation, the received power, and the capacity by employing both the open-circuit and the receiving mutual impedance models. In Section 3.5, the antenna impedance matching is used to mitigate the performance degradation due to the mutual coupling. Finally, this chapter is concluded in Section 3.6.

3.3 Mutual Coupling Modelling

In this section, we first review the circuit equivalent of an isolated (stand-alone) antenna. It is followed by a circuit model for an antenna element of a coupled array. Then, the coupling matrix is introduced as the most common approach to take the effect of mutual coupling into account.

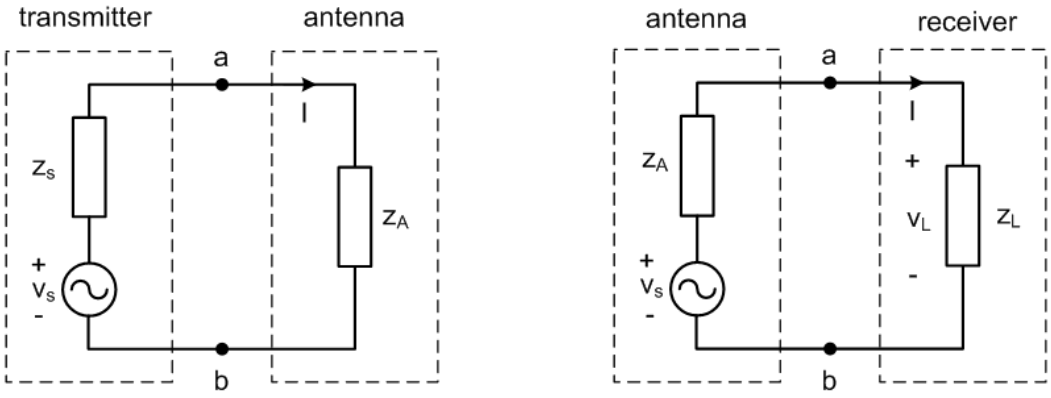

(a) transmit mode (b) receive mode

Figure 3.1: *Equivalent circuits of a stand-alone antenna for the transmit and receive modes.*

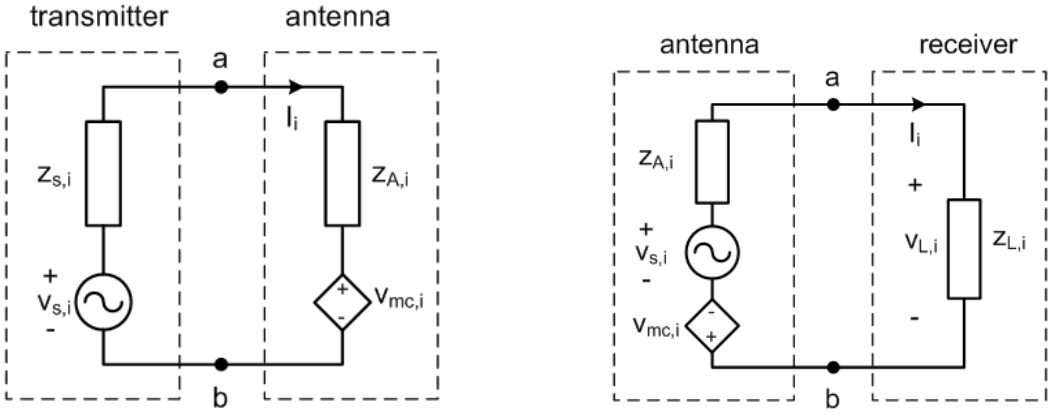

(a) transmit mode (b) receive mode

Figure 3.2: *Equivalent circuits of an array element for the transmit and receive coupled arrays.*

3.3.1 Antenna Equivalent Circuit

The *Input impedance* of an antenna is defined as the impedance presented by the antenna at its terminals, or the ratio of the voltage to the current at a pair of its terminals [31, 32]. This can be written as follows:

$$Z_{in} = R_{in} + jX_{in} \tag{3.1}$$

where R_{in} is the input resistance of the antenna comprising two components: radiation and ohmic loss resistances . The term X_{in} denotes the input reactance which represents the power stored in the near field. For a stand-alone antenna, the input impedance is also called the *self-impedance*. The equivalent circuit for such an antenna, connected to the corresponding transmitter/receiver through its terminals, is shown in Figure 3.1. For the transmit mode, the feeding transmit circuit is simply modelled by a voltage source V_s and an internal impedance z_s, and the antenna is represented by its self-impedance z_A [56]. In the receive mode, V_s denotes the induced voltage at the antenna due to the incident wave, and z_L is the terminal load impedance. As a result of the reciprocity theorem [31], z_A is the same for both transmitting and receiving modes. The symbol I is the terminal current for both cases.

Assume that we have a transmit/receive array of M closely separated antennas. Each antenna element i for ($i = 1, 2, \cdots, M$) with its corresponding transmit/receive circuit can be simply modelled by the equivalent circuits shown in Figure 3.2. The controlled source $V_{mc,i}$ is the voltage induced at the antenna due to the mutual coupling. For the transmit mode shown in Figure 3.2(a), the parameters of the transmitter block at the left hand side of the antenna terminal port, are assumed to be known or measurable. But the coupling voltage $V_{mc,i}$ is unknown and we need to formulate it in terms of known parameters.

Having the transmit and the receive arrays separated far away from each other, the incident wave at the receiver can be considered as a (far-field) plane-wave. Referring to the receive mode in Figure 3.2(b), the total induced voltage in the ith antenna due to the plane wave and the mutual coupling effects of the other antennas, can be expressed as [57]

$$V_{ind,i} = V_{s,i} - V_{mc,i} \tag{3.2}$$

where $V_{s,i}$ represents the voltage induced by the incident plane wave which is free from the mutual coupling, and $V_{mc,i}$ is due to mutual coupling effects. In practice, the terminal voltage and current of each antenna i, are the only parameters which can be measured at the receiver.

3.3.2 Open-circuit Model

For this model, the impedance parameters of the array antennas are defined as follows. The *self impedance* of each array-element is defined as the ratio of the voltage to the current of its terminals while the rest of antennas are open-circuited. The *mutual impedances* between each pair of coupled antennas are defined as the ratio of the open-circuit voltage across the terminals of one antenna to the current flowing through the terminals of the other one while it is excited or loaded, and the rest of antennas are open-circuited [31, 32, 56].

Now we can describe the impedance matrix of a coupled array of M antennas as follows:

$$\mathbf{Z} = \begin{pmatrix} z_{11} & z_{12} & \cdots & z_{1M} \\ z_{21} & z_{22} & \cdots & z_{2M} \\ \vdots & \vdots & \ddots & \vdots \\ z_{M1} & z_{M2} & \cdots & z_{MM} \end{pmatrix}. \tag{3.3}$$

where z_{ii} is the self-impedance of the ith antenna for ($i = 1, 2, \cdots, M$), and z_{ij} is the mutual impedance between the ith and jth antennas for ($i \neq j$, and $i, j = 1, 2, \cdots, M$). The self- and the mutual-impedances of the elements of a coupled array can be calculated using either the classical induced electromotive force (EMF) method [31, 56], or numerical methods in computational electromagnetics (CEM) such as: the method of moments (MoM), and finite-difference time-domain (FDTD) [38]. Calculation of the mutual impedance matrix using EMF method for several structures of an array of two dipole antennas is described in detail in appendix B.

By using the impedance parameters of the array, and neglecting the scattering effects of open-circuited antennas [58], we can rewrite equation (3.2) as follows [42, 57]:

$$V_{ind,i} = V_{oc,i} - \sum_{j \neq i, j=1}^{M} I_j z_{ij} \tag{3.4}$$

where $V_{oc,i}$ is the terminal voltage for ith element while all antennas (including the element i) are in the open-circuit condition, and it represents the share of incident plane wave without any mutual coupling effect. The term I_j is the terminal current for jth element, and z_{ij} denotes the *mutual impedance* between ith and jth elements for ($i \neq j$, and $i, j = 1, 2, \cdots, M$) defined as the ratio of the open-circuit voltage across the terminals of ith antenna (only induced by the radiated field of jth antenna) to the current flowing through the terminals of jth antenna while

it is excited or loaded, and the rest of antennas are open-circuited. Referring to Figure 3.2(b), and using the relationship between the terminal current and voltage, we have

$$V_{ind,i} = I_i(z_{A,i} + z_{L,i}). \tag{3.5}$$

If we substitute (3.5) into (3.4), then we can get the following expression

$$I_i\left(z_{A,i} + z_{L,i}\right) + \sum_{j\neq i, j=1}^{M} I_j\left(z_{ij}\right) = V_{oc,i} \tag{3.6}$$

or

$$\begin{bmatrix} z_{A,1}+z_{L,1} & z_{12} & \cdots & z_{1M} \\ z_{21} & z_{A,2}+z_{L,2} & \cdots & z_{2M} \\ \vdots & \vdots & \ddots & \vdots \\ z_{M1} & z_{M2} & \cdots & z_{A,M}+z_{L,M} \end{bmatrix} \begin{bmatrix} I_1 \\ I_2 \\ \vdots \\ I_M \end{bmatrix} = \begin{bmatrix} V_{oc,1} \\ V_{oc,2} \\ \vdots \\ V_{oc,M} \end{bmatrix} \tag{3.7}$$

The above equation can be rewritten as

$$\mathbf{i}_L = (\mathbf{Z}_R + \mathbf{Z}_L)^{-1}\mathbf{v}_{oc} \tag{3.8}$$

where $\mathbf{Z}_R$ is the mutual impedance matrix of the array, $\mathbf{i}_L$ is the vector of terminal currents, and $\mathbf{Z}_L$ is the diagonal matrix of antenna terminal loads, given by

$$\mathbf{Z}_L = \begin{pmatrix} z_{L1} & 0 & \cdots & 0 \\ 0 & z_{L2} & \cdots & 0 \\ \vdots & \vdots & \ddots & \vdots \\ 0 & 0 & \cdots & z_{LM} \end{pmatrix}. \tag{3.9}$$

Using the relationship between the terminal voltages and currents, terminal voltages can be expressed in terms of the open-circuit voltages as follows:

$$\mathbf{v}_L = \mathbf{Z}_L(\mathbf{Z}_R + \mathbf{Z}_L)^{-1}\mathbf{v}_{oc} \tag{3.10}$$

Assuming identical antenna elements which are terminated with the same load impedance z_L,

the above equation is simplified to

$$\begin{aligned} \mathbf{v}_L &= \left[z_L(\mathbf{Z}_R + z_L\mathbf{I}_M)^{-1}\right]\mathbf{v}_{oc} \\ &= \mathbf{C}_R\mathbf{v}_{oc} \end{aligned} \tag{3.11}$$

where $\mathbf{C}_R$ is a $M \times M$ matrix and is called the *coupling matrix*. This matrix relates and converts the term $\mathbf{v}_{oc}$, which is free of mutual coupling, to the term $\mathbf{v}_L$ which includes the mutual coupling effects. Applying such coupling matrices, is one of the most popular approaches to model the mutual coupling in antenna array and MIMO applications.

Example

Let us consider a simple array of two identical centre-driven z-directed half-wavelength ($\lambda/2$) wire dipoles, as shown in Figure 3.3, with the wire radius of $\lambda/300$, and the element separation of d at the frequency of 1800MHz. Figure 3.4 illustrates the equivalent circuits of the array elements using the open-circuit model. Using the theoretical EMF method (refer to appendix B) and FEKO electromagnetic simulation software [10], self and mutual impedance values of the array elements are calculated and shown in parts (a) and (b) of Figure 3.5 for different element separations d. FEKO software provides the numerical values of impedance parameters which are closer to experimental data [38]. As can be seen from Figure 3.5(b) at the right-hand-side, the self impedance values calculated using FEKO are dependent on the element separation d. This confirms the results in [38, Chapter 2] and [4], and it means even for half-wavelength dipoles, the open-circuited antennas can affect other antennas for small inter-element spacing d. We further investigate this issue using FEKO software. Let antenna 2 be open-circuited and antenna 1 be terminated in a load impedance z_{L1}. Both antennas are assumed to be excited by a far field plane-wave coming from the azimuth angle $\phi = 45^\circ$ and the elevation angle $\theta = 90^\circ$. Now, we try different values of the load impedance z_{L1}, and calculate V_{oc1} from the following expression

$$V_{oc1} = I_1(z_{L1} + z_{11}). \tag{3.12}$$

This equation is obtained from Figure 3.4 assuming $I_2 = 0$ for the open-circuited antenna 2. As we can see from Figures 3.6 and 3.7, for a specific element separation, the variation of the antenna termination load does not change the open-circuit voltage. However, the value of V_{oc1} depends on the element separation. This means the open-circuited antenna 2 has a constant effect on the antenna 1 which is independent of the condition of antenna 1.

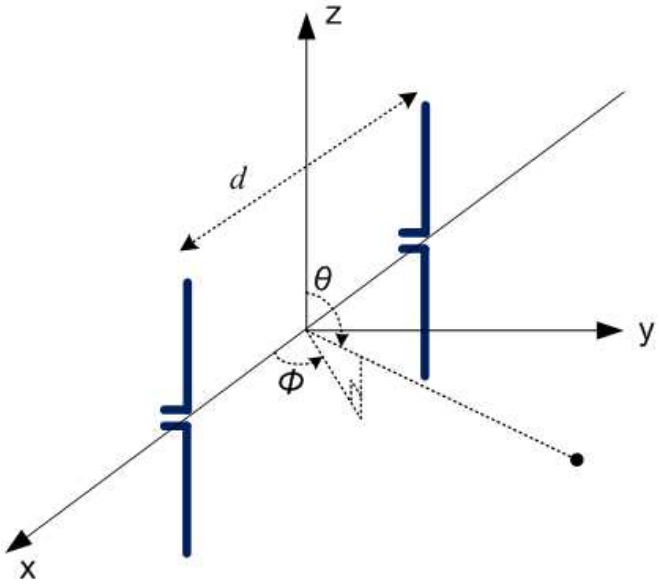

Figure 3.3: *Linear array of two side-by-side half-wavelength dipoles.*

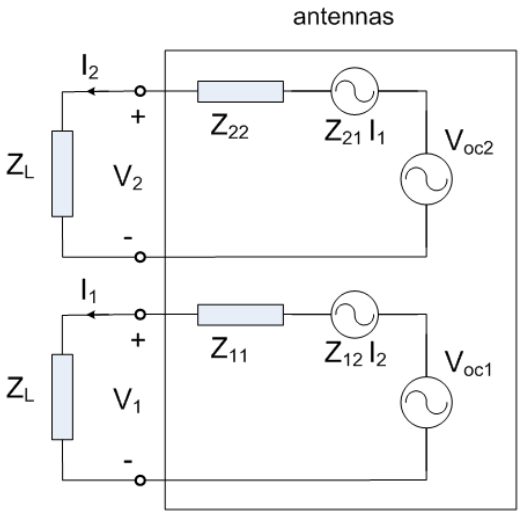

Figure 3.4: *Equivalent circuit of an array of two antennas, using open-circuit model.*

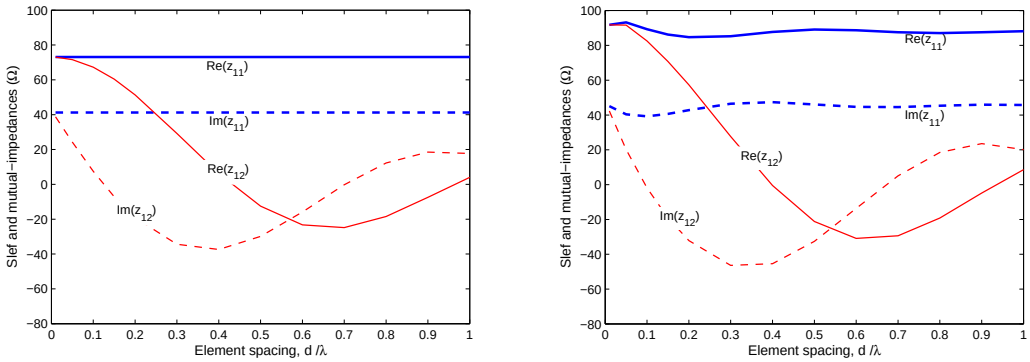

(a) EMF (b) FEKO

Figure 3.5: *Self and mutual impedances of an array of two $\lambda/2$ dipoles with the separation d (a) using EMF method, (b) using FEKO software.*

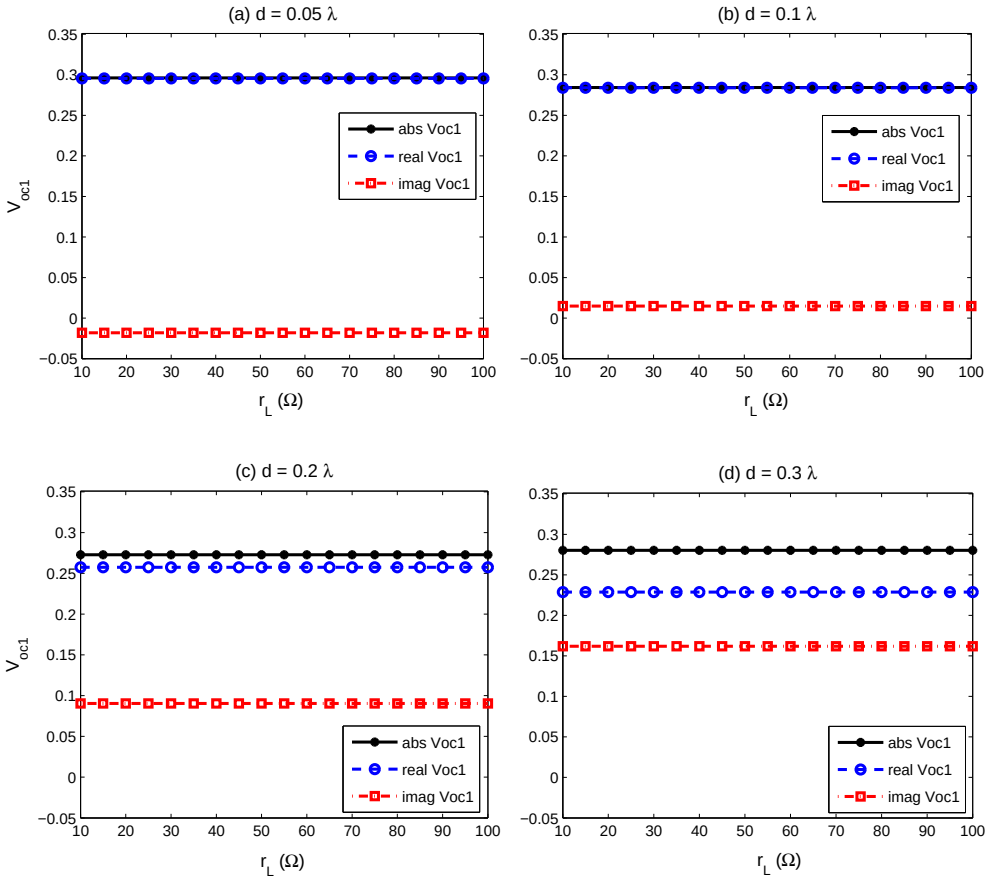

Figure 3.6: *Calculated value of V_{oc1} from (3.12) when antenna 2 is open-circuited and antenna 1 is terminated in a resistive load $z_{L1} = (r_L + j0)\Omega$, for the element separation of (a) 0.05λ, (b) 0.1λ, (c) 0.2λ, and (d) 0.3λ.*

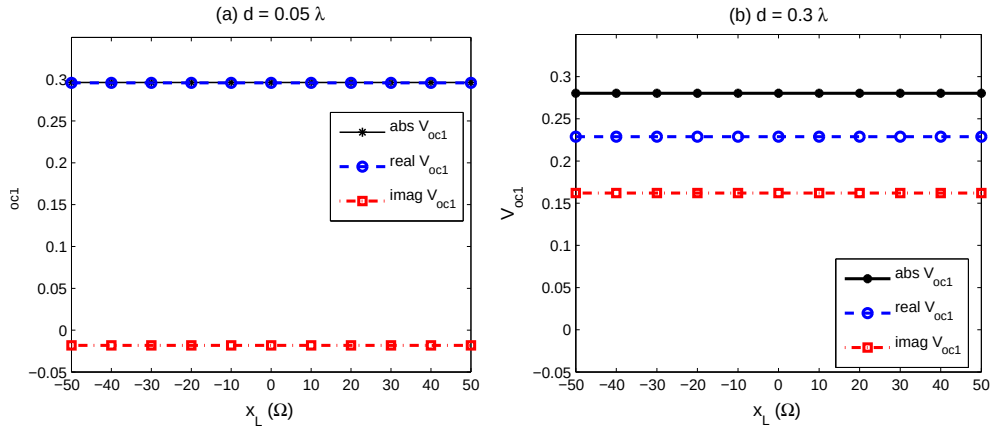

Figure 3.7: *Calculated values of V_{oc1} from (3.12) when antenna 2 is open-circuited and antenna 1 is terminated in a complex load $z_{L1} = (50 + jx_L)\Omega$, for the element separation of (a) 0.05λ, (b) 0.3λ.*

3.3.3 Receiving Mutual Impedance method

As stated earlier, the open-circuit model uses the mutual impedances between each pair of antennas, while one antenna is connected to a source and the other one is in the receiving mode and open-circuited, to extract the mutual coupling model. The following issues are associated with the application of such mutual impedances for the receive arrays. First, the antenna behaviour may not be the same for the transmit and receive modes [48, 49]. Second, the effect of terminal loads is not taken into account [48]. An interesting method is introduced by Hui [55, 59] to overcome the above issues by defining a new mutual impedance called the *receiving mutual impedance*. In the following we describe this method in detail.

Let us consider an array of two dipoles as shown in Figure 3.3, both terminated in a load impedance z_L. The voltage across the terminal load of any of these antennas consists of two components [48]: the voltage due to the arrived signal alone, and the induced voltage due to the current distribution of the other antenna (i.e. mutual coupling). The relationship between the terminal voltages V_1 and V_2, and the voltages due to the signal alone, U_1 and U_2, can be written as

$$V_1 = U_1 - z_{12}^R I_2 \tag{3.13a}$$

$$V_2 = U_2 - z_{21}^R I_1 \tag{3.13b}$$

where z_{12}^R and z_{21}^R are the mutual impedances between the antennas, and I_1 and I_2 are the

terminal currents flowing through the terminal loads z_L of the antennas. The terminal voltages and currents are related by

$$V_1 = z_L I_1 \tag{3.14a}$$

$$V_2 = z_L I_2. \tag{3.14b}$$

We note that in this new method, equations (3.13a) and (3.13b) are different from the conventional concept in the open-circuit model, and they do not use the open-circuit voltages which require knowledge of the self-impedances of antennas. Here, the new mutual impedance z_{12}^R is defined as the ratio of the induced voltage across the terminal load of antenna 1, due to the terminal current I_2 flowing through the terminal load of antenna 2, to this terminal current, i.e.,

$$z_{12}^R = \frac{U_1 - V_1}{I_2}. \tag{3.15}$$

It is called *receiving mutual impedance*, and it is distinguished by the superscript $(\cdot)^R$ from the conventional definition in this thesis. Similarly, z_{21}^R can be defined by changing the position of antenna 1 and antenna 2 in the previous expression for z_{12}^R.

In this method, instead of having one antenna in transmitting mode and exciting the others by the field of this antenna, a plane wave excitation from the horizontal direction in the far field is used to obtain an estimated current distribution over all the antennas. This approximation is accurate for the signals with low elevation angles relative to the horizon due to the isotropic pattern of z-directed $\lambda/2$ dipole antenna over horizontal plane [59, 60]. Substituting (3.14a)-(3.14b) into (3.13a)-(3.13b) results in

$$\begin{bmatrix} V_1 \\ \\ V_2 \end{bmatrix} = \begin{bmatrix} 1 & \frac{z_{12}^R}{z_L} \\ \frac{z_{21}^R}{z_L} & 1 \end{bmatrix}^{-1} \begin{bmatrix} U_1 \\ \\ U_2 \end{bmatrix} \tag{3.16}$$

This is an equivalent relationship to equation (3.11), which relates the coupled terminal voltages V_i, to uncoupled terminal voltages U_i for ($i = 1, 2$). This means that with knowledge of the receiving mutual impedances, and the coupled terminal voltages, the uncoupled terminal voltages U_i can be obtained.

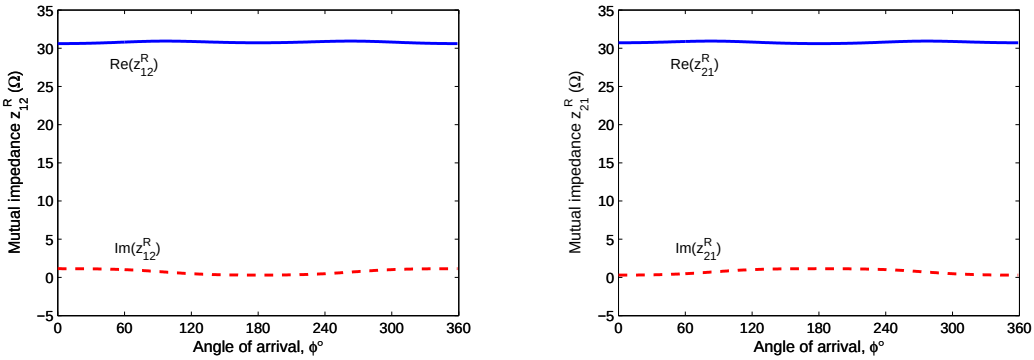

(a) z_{12}^R (b) z_{21}^R

Figure 3.8: *Real and imaginary parts of the receiving mutual impedances between elements of an array of two $\lambda/2$ dipoles with the separation $d = 0.05\lambda$, and an incident plane wave excitation coming from the horizontal angle ϕ. Antennas are identically loaded with load impedance $z_L = 50\Omega$.*

Example

To investigate the characteristics of receiving mutual impedance, we consider an array of two dipoles, as described in the example of section 3.3.2. Both antennas are identically terminated with a load impedance z_L, and excited by an incident far-field plane wave from the azimuth angle of ϕ. Figure 3.8 shows the real and imaginary parts of the receiving mutual impedances z_{12}^R and z_{21}^R versus the plane wave arrival angle $\phi \in [0°, 360°]$, for $z_L = 50\Omega$. It is observed from the figure that the values of z_{12}^R and z_{21}^R are similar for identical dipoles, although they may not be the same in general. These values are also roughly independent of the arrival angle of the plane wave due to the omnidirectional pattern of z-directed dipoles in horizontal (xy) plane [55]. The real and imaginary parts of the receiving mutual impedance z_{12}^R, and the conventional mutual impedance z_{12} using open-circuit model, versus the element separation in wavelength (d/λ) are shown in Figure 3.9.

The effect of termination load is also depicted in Figure 3.10. It can be seen that the receiving mutual impedance is significantly influenced by the variation of antenna terminal load z_L. This is an interesting idea which some studies applied to counteract the effect of mutual coupling in MIMO systems by finding a proper terminal load which optimises the performance metric in the presence of mutual coupling [5, 21, 37, 40, 61].

Equation (3.16) can be extended to an array of M antennas. Assume $\mathbf{v} = [V_1, V_2, \ldots, V_M]^T$ is the vector of terminal voltages including the mutual coupling, and $\mathbf{u} = [U_1, U_2, \ldots, U_M]^T$

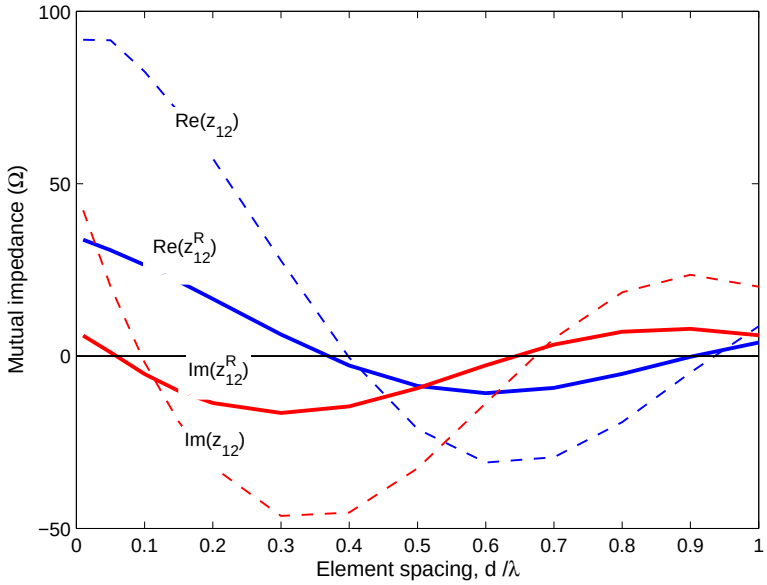

Figure 3.9: *Receiving mutual impedance in comparison to the conventional mutual impedance (open-circuit voltages) for an array of two $\lambda/2$ dipoles with the separation d. For the latter case, the antennas are excited by a plane wave from the horizontal angle $\phi = 45°$, and identically loaded with load impedance $z_L = 50\Omega$.*

represents the terminal voltages at the receive array without the mutual coupling effect. Using the new concept of receiving mutual impedances, the relation between $\mathbf{v}$ and $\mathbf{u}$ can be written as

$$\mathbf{v} = (\mathbf{Z}^R)^{-1}\mathbf{u} \tag{3.17}$$

where

$$\mathbf{Z}^R = \begin{bmatrix} 1 & \frac{z_{12}^R}{z_L} & \dots & \frac{z_{1M}^R}{z_L} \\ \frac{z_{21}^R}{z_L} & 1 & \dots & \frac{z_{2M}^R}{z_L} \\ \vdots & \vdots & \ddots & \vdots \\ \frac{z_{M1}^R}{z_L} & \frac{z_{M2}^R}{z_L} & \dots & 1 \end{bmatrix}, \tag{3.18}$$

and z_{ij}^R $(i, j = 1, 2, \dots, M)$ is the receiving mutual impedance between the ith and jth receiving antennas, as defined in (3.15).

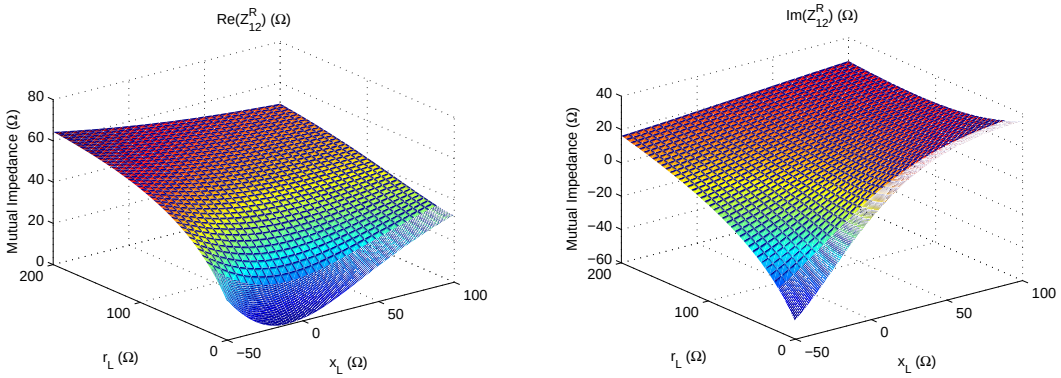

(a) Real part

(b) Imaginary part

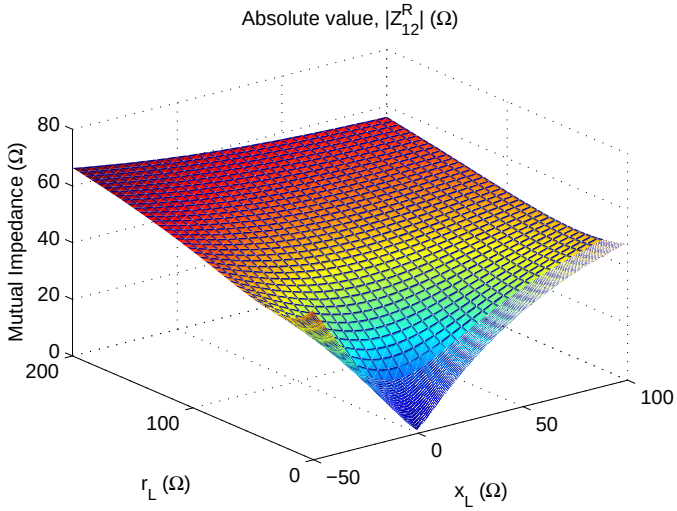

(c) absolute value

Figure 3.10: *Absolute value, real and imaginary parts of the receiving mutual impedance z_{12}^R versus the real and imaginary parts of the antenna terminal loads $z_L = r_L + jx_L$. Antennas are separated at $d = 0.05\lambda$, and excited by a plane wave from the azimuth angle $\phi = 45^\circ$ and the elevation angle $\theta = 90^\circ$.*

3.3.4 Coupling Matrix

Most of previous studies take account of the mutual coupling by defining a coupling matrix $\mathbf{C}$ to relate the coupled and uncoupled quantities using either impedance parameters (Z-parameters), or the equivalent scattering parameters (S-parameters) of the coupled array. Such definition is briefly introduced earlier in (3.11) of section 3.3.2. Before describing the coupling matrix in details, we note that the Z-parameter or S-parameter representations of a multi-port network are related as follows[56, eq. (13.3.4)]:

$$\mathbf{S} = (\mathbf{Z} - z_0\mathbf{I})(\mathbf{Z} + z_0\mathbf{I})^{-1} \tag{3.19a}$$

$$\mathbf{Z} = (\mathbf{I} - \mathbf{S})^{-1}(\mathbf{I} + \mathbf{S})z_0 \tag{3.19b}$$

where $\mathbf{Z}$ is the impedance matrix, $\mathbf{S}$ is the scattering matrix of the network, and z_0 is a chosen characteristic/reference impedance. In other words, having one of the impedance or scattering representations of a network, the other one can be obtained from the above equations.

Open-circuit Model

There are two different and contradictory ways to define the coupling matrix $\mathbf{C}$ using open-circuit model in the literature. Assuming the receive mode, the first expression is given by [23, 36]

$$\mathbf{C}_R = (z_A + z_L)(\mathbf{Z}_R + z_L\mathbf{I}_M)^{-1} \tag{3.20}$$

where z_A is the self-impedance, and z_L is the terminal load impedance for each antenna element. The term $\mathbf{Z}_R$ represents the mutual impedance matrix of the receive array as defined in (3.3) , and $\mathbf{I}$ is an identity matrix. The Second definition is given by [6, 22, 38, 40]

$$\mathbf{C}_R = z_L(\mathbf{Z}_R + z_L\mathbf{I}_M)^{-1} \tag{3.21}$$

which is taken from (3.11), where $\mathbf{v}_L$ is the vector of antenna terminal voltages when each antenna is terminated in z_L, and $\mathbf{v}_{oc}$ is the vector of open-circuited antenna terminal voltages. Referring to Figure 3.2, we can use the above definitions for a coupled transmit array by replacing z_L with z_s, and $\mathbf{Z}_R$ with the corresponding impedance matrix of the array denoted by $\mathbf{Z}_T$.

Having two different definitions is potentially confusing for researchers working on coupled

arrays. Some have considered both models in their analysis [62], and some others tried to realise which model is right [38], or they ignored the coupling matrix definitions and considered the whole system to find the input-output relationship in their studies [7, 38, 40]. Here we present an explanation of the link between these definitions and clarify when we can use which one.

Referring to Figure 3.1(b), we can express the terminal voltage vector of the receive array in the absence of mutual coupling, in terms of $\mathbf{v}_{oc}$ as follows:

$$\mathbf{v}_{L,nc} = \frac{z_L}{z_A + z_L}\mathbf{v}_{oc}. \tag{3.22}$$

Getting back to equation (3.11), and substituting the above equation, the relation between the terminal voltage vectors with and without mutual coupling effects, can be written as

$$\begin{aligned} \mathbf{v}_{L,mc} &= \left[(z_A + z_L)(z_L\mathbf{I}_M + \mathbf{Z}_R)^{-1}\right]\mathbf{v}_{L,nc} \\ &= \mathbf{C}_R\mathbf{v}_{L,nc} \end{aligned} \tag{3.23}$$

where $\mathbf{v}_{L,mc}$ denotes the terminal voltage vector, taking the mutual coupling into account. This gives us the first expression for the coupling matrix.

Therefore, it depends which coupled and uncoupled quantities are desired to be related. For instance, whenever we need to express the terminal voltage vector $\mathbf{v}_L$ in the presence of mutual coupling (the coupled quantity), in terms of impedance parameters of the array and the open-circuited terminal voltages (uncoupled quantity), we use the second definition of $\mathbf{C}_R$ in (3.21). On the other hand, the first definition in (3.20) relates the coupled terminal voltage vector $\mathbf{v}_L$ to the virtual uncoupled terminal voltages which are assumed to be free of the mutual coupling.

In order to take the mutual coupling into account for MIMO systems, the input-output relationship described in (2.8), can be modified by using the coupling matrix concept as follows [23]

$$\mathbf{y}(t) = \underbrace{\mathbf{C}_R\mathbf{H}\mathbf{C}_T}_{\mathbf{H}_{mc}}\mathbf{x}(t) + \mathbf{n}(t) \tag{3.24}$$

where $\mathbf{C}_T$ and $\mathbf{C}_R$ are the coupling matrices for the transmit and the receive array antennas, and $\mathbf{H}_{mc}$ is the modified channel matrix including the mutual coupling effects. For such an application, normalisation of the coupling matrix has been of interest by previous studies.

Normalisation. Now we examine the limiting value of both coupling matrix definitions for

large element-separation (e.g. $d \gg \lambda$), when there is no mutual coupling. For such a case, the array impedance matrix $\mathbf{Z}_R$ is diagonal and for identical antennas it would be $\mathbf{Z}_R = z_A\mathbf{I}_M$. Therefore, we have

- First definition: $\mathbf{C}_R = \mathbf{I}_M$
- Second definition: $\mathbf{C}_R = \left(\dfrac{z_L}{z_A + z_L}\right)\mathbf{I}_M$

This issue has been considered in [22] by dividing the coupling matrix, the second definition in (3.21), by a normalisation factor $C_R = z_A^*/(z_A + z_A^*)$ for identical antennas. Therefore, [22] suggests a modified coupling matrix as

$$\mathbf{C}_R = \left(\frac{2\Re(z_A)}{z_A^*}\right) z_L(\mathbf{Z}_R + z_L\mathbf{I}_M)^{-1}. \tag{3.25}$$

This is similar to the normalisation of the received power of coupled arrays in [5] to the received power of a single antenna matched to its self-impedance conjugate.

There is another point from previous studies [7, 40] that in practical MIMO applications the voltage across the real part of the terminal load z_L is considered as the received signal rather than the voltage across the complex z_L. Therefore, we need to modify the existing coupling matrix expressions to include such an issue.

Receiving Mutual Impedance Method

Similar to the open-circuit based model, we can define a coupling matrix for the receiving mutual method. Referring to the relation between the terminal voltage vector $\mathbf{v}$ in the presence of mutual coupling, and the terminal voltage vector $\mathbf{u}$ in the absence of mutual coupling in (3.17), the coupling matrix can be expressed as

$$\mathbf{C}_R = (\mathbf{Z}^R)^{-1} = z_L \begin{bmatrix} z_L & z_{12}^R & \dots & z_{1M}^R \\ z_{21}^R & z_L & \dots & z_{2M}^R \\ \vdots & \vdots & \ddots & \vdots \\ z_{M1}^R & z_{M2}^R & \dots & z_L \end{bmatrix}^{-1} \tag{3.26}$$

where $\mathbf{Z}^R$ is defined in (3.18). In order to relate the voltage across the resistive part of z_L to the uncoupled voltage vector $\mathbf{u}$, the above equation has to be multiplied by a factor of r_L/z_L,

where r_L is the real part of z_L.

3.4 Impact of Mutual Coupling

Now that the coupling matrix is introduced, we can investigate the influence of mutual coupling on the MIMO performance metrics such as: antenna patterns, signal correlation, received power, and capacity.

3.4.1 Antenna Pattern

In this section, we use the coupling matrix to take account of mutual coupling effects on the antenna element pattern for coupled arrays. Let us consider a linear receive array of M with the element separation of d as shown in Figure 3.11. The array steering vector (under narrowband assumption) in the absence of mutual coupling is given by [63]

$$\mathbf{e}(\phi) = \begin{bmatrix} g_1(\phi) \\ g_2(\phi)e^{j\tau} \\ \vdots \\ g_M(\phi)e^{j(M-1)\tau} \end{bmatrix} \tag{3.27}$$

where $\tau = \frac{2\pi d}{\lambda}\sin(\phi)$ is the delay between the received signals, ϕ is the angle between the direction of arrival and the array broadside, and $g_i(\phi)$ is the *i*th antenna pattern for ($i = 1, 2, \ldots, M$). Taking the mutual coupling effects into account, the received array steering vector is written as [34]

$$\mathbf{e}_{mc}(\phi) = \mathbf{C}_R\,\mathbf{e}(\phi). \tag{3.28}$$

The array impedance matrix for the open-circuit model is shown to be symmetric Toeplitz [64] for identical antennas. Therefore the coupling matrix for an array of two identical antennas could be expressed as

$$\mathbf{C}_R = \begin{bmatrix} a & b \\ b & a \end{bmatrix} \tag{3.29}$$

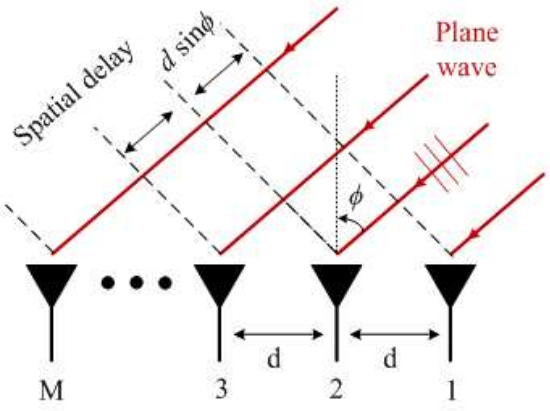

Figure 3.11: *A linear array of M antennas with the element separaion of d.*

and consequently,

$$\mathbf{e}_{mc}(\phi) = \begin{bmatrix} e_{1,mc}(\phi) \\ e_{2,mc}(\phi) \end{bmatrix} = \begin{bmatrix} ag_1(\phi) + bg_2(\phi)e^{j\tau} \\ bg_1(\phi) + ag_2(\phi)e^{j\tau} \end{bmatrix} \tag{3.30}$$

where $\mathbf{e}_{mc}(\phi)$ is the array steering vector in the presence of mutual coupling. Comparing (3.27) and (3.30) results in the received antenna pattern vector in the presence of mutual coupling as

$$\mathbf{g}_{mc}(\phi) = \begin{bmatrix} g_{1,mc}(\phi) \\ g_{2,mc}(\phi) \end{bmatrix} = \begin{bmatrix} ag_1(\phi) + bg_2(\phi)e^{j\tau} \\ bg_1(\phi)e^{-j\tau} + ag_2(\phi) \end{bmatrix}. \tag{3.31}$$

The above equation describes the complex element patterns of the array in the presence of mutual coupling. Absolute values of $\mathbf{e}_{mc}(\phi)$ and $\mathbf{g}_{mc}(\phi)$ are equal. Their corresponding entries may differ in phase due to spatial delay between reference point and antenna elements.

Example. Now we consider an array of two identical wire dipole antennas with the separation of $d = 0.05\lambda$, wire radius of $\lambda/300$, and a length of $\lambda/2$. Figure 3.12 shows the element pattern of antenna 1 in the presence of mutual coupling, calculated by the receiving mutual impedance (RMI) method, and the open circuit method using $\mathbf{C}_{R1}$ in (3.20) and $\mathbf{C}_{R2}$ in (3.21) denoted by OC1 and OC2 in the legend of the figure, respectively. These results are compared to the antenna pattern simulated by FEKO software [10] when both antennas are identically terminated with a load impedance of $z_L = 50\Omega$ and excited by a far-field plane-wave from the azimuth angle of ϕ from 0° to 360° with the step size of 1°, in addition to the pattern of stand-alone antenna 1 terminated with $z_L = 50\Omega$ and excited by the same plane-wave. As can be seen, both the RMI and the open-circuit (using $\mathbf{C}_{R1}$) approaches model the mutual coupling for

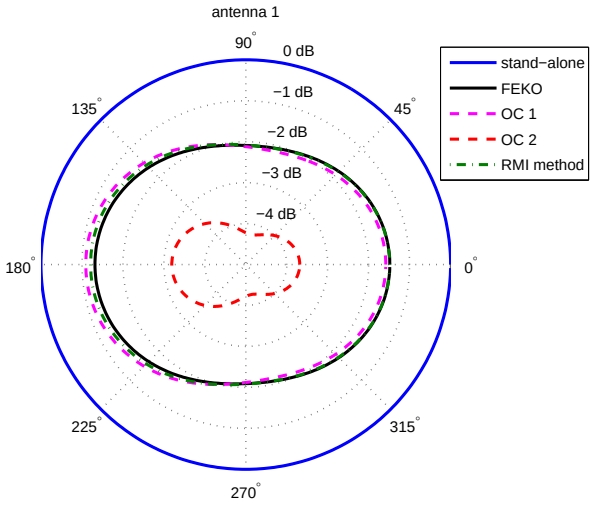

Figure 3.12: *Element pattern of antenna 1 for an array of two identical half-wavelength dipoles with the separation of* 0.05λ.

$\lambda/2$ dipoles accurately. However, for the open-circuit model using the coupling matrix defined in (3.21), the result is quite different. Here, we should use $\mathbf{C}_{R1}$ which relates quantities in the same kind such as: coupled terminal currents to uncoupled terminal currents, or coupled terminal voltages to uncoupled terminal voltages. Therefore, care has to be taken when the coupling matrix is used for modelling the mutual coupling.

3.4.2 Signal Correlation

The diversity gain of MIMO systems employing coupled arrays is affected by the mutual coupling effect. The signal correlation coefficient is a metric to investigate such effects. There are three approaches in the literature to compute the correlation between received signals of two antennas. One approach defines the correlation coefficient in terms of the far-field antenna pattern and the nature of the incident field at the place of antennas [35]. The former term can implicitly include the effects of mutual coupling into the definition of the correlation coefficient [33, 65]. Another approach is based on the scattering parameters of the array antenna [66, 67]. The third and the most practical approach directly defines the correlation based on the received signals [65].

Using the Antenna Pattern

For this approach, the correlation coefficient can be expressed as [33]

$$\rho_{12} = \frac{\int_{-\pi}^{\pi}\int_{0}^{\pi} e_1(\theta,\phi)e_2^*(\theta,\phi)p(\theta,\phi)\sin\theta d\theta d\phi}{\sqrt{\int_{-\pi}^{\pi}\int_{0}^{\pi}|e_1(\theta,\phi)|^2 p(\theta,\phi)\sin\theta d\theta d\phi}\sqrt{\int_{-\pi}^{\pi}\int_{0}^{\pi}|e_2(\theta,\phi)|^2 p(\theta,\phi)\sin\theta d\theta d\phi}} \tag{3.32}$$

where $e_i(\theta,\phi)$ is the electric field pattern for ith antenna, and $p(\theta,\phi)$ is the joint probability density function of the angle of arrival in terms of the both azimuth ϕ and elevation θ angles. Envelope correlation is more useful for practical measurements [33] and it is related to the correlation coefficient by

$$\rho_e = |\rho_{12}|^2. \tag{3.33}$$

Equation (3.32) represents a three-dimensional (3D) correlation coefficient. However, channel measurements have shown that most part of the energy is in the azimuth plane [68]. Therefore, we can simplify (3.32) into a two-dimensional (2D) version given by [35, 40]

$$\rho_{12} = \frac{\int_{-\pi}^{\pi} e_1(\phi)e_2^*(\phi)p(\phi)d\phi}{\sqrt{\int_{-\pi}^{\pi}|e_1(\phi)|^2 p(\phi)\,d\phi}\sqrt{\int_{-\pi}^{\pi}|e_2(\phi)|^2 p(\phi)\,d\phi}} \tag{3.34}$$

where ϕ is the arrival angle in the azimuth plane, $p(\phi)$ is the power azimuth spectrum (PAS) of the incident field, and $e_i(\phi)$ for ($i = 1, 2$) is in fact the entries of the array steering vector in (3.27). There are three common functions to model the PAS for wireless communications [26, 69, 70]: a truncated Laplacian function, a truncated Gaussian function, and a uniform distribution, given by

$$p(\phi) = \begin{cases} \dfrac{1}{2\Delta\phi} & \text{Uniform} \\ c_1 \exp\left(-\frac{(\phi-\phi_0)^2}{2\sigma^2}\right) & \text{Gaussian} \\ c_2 \exp\left(-\sqrt{2}\frac{|\phi-\phi_0|}{\sigma}\right) & \text{Laplacian} \end{cases} \tag{3.35}$$

where c_1 and c_2 are scalars, and for both Laplacian and Gaussian functions σ is the angular spread (AS) and ϕ_0 is the mean angle of arrival for the interval $\phi \in [-\Delta\phi + \phi_0, \Delta\phi + \phi_0]$. For the uniform distribution, we have AS $= \frac{\Delta\phi}{\sqrt{3}}$ [69]. The scalar values c_1 and c_2 are calculated such that the integral of $p(\phi)$ with respect to the angle of arrival ϕ over the azimuth plane, i.e. $\phi \in [-\pi, \pi)$, is equal to one. The probability density function of the uniform, Gaussian and Laplacian distributions with $\Delta\phi = 60^\circ$, and AS = 30° are shown in Figure 3.13.

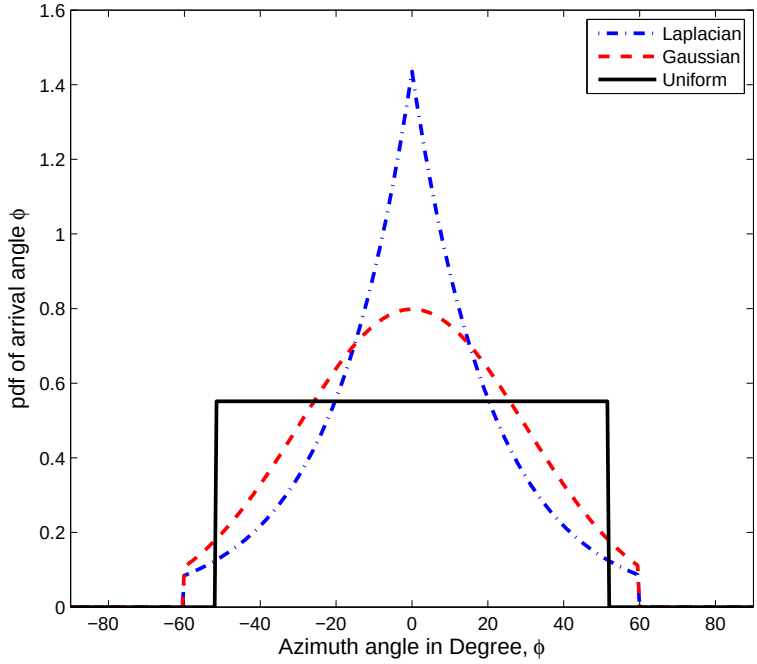

Figure 3.13: *The probability density function of the uniform, Gaussian and Laplacian distributions with* $\Delta\phi = 60°$*, and AS* = $30°$.

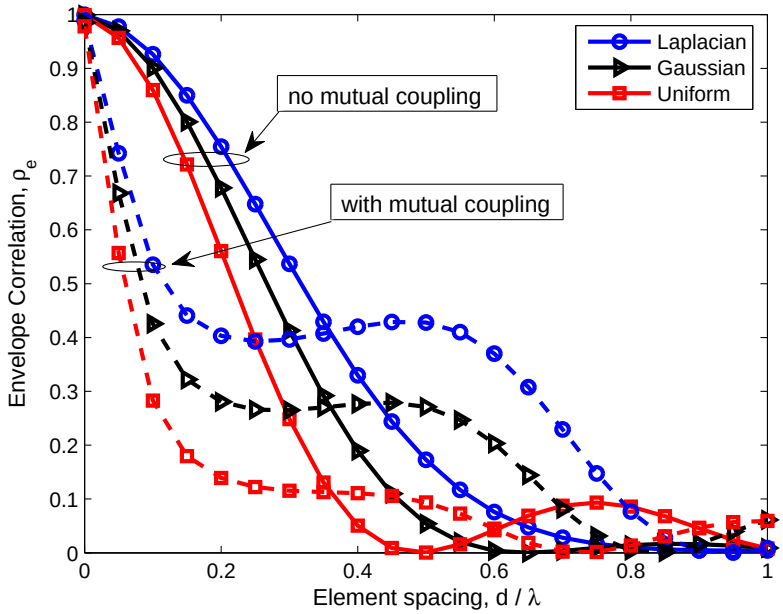

Figure 3.14: *Envelope correlation coefficient vs. antenna spacing for different scatterer distributions at* $\phi_0 = 0°$*, and* $AS = 30°$.

Taking mutual coupling effects into account and referring to (3.28) and (3.34), the 2D correlation between two coupled antennas can be obtained from (3.34) by substituting the coupled steering vector entries in the place of $e_i(\phi)$. As an example, some simulations are performed for the three PAS functions in (3.35): uniform, truncated Laplacian, and truncated Gaussian. Figure 3.14 shows the result for given PAS functions with $AS = 30°$, the mean angle of arrival $\phi_0 = 0°$, and $\Delta\phi = 30°\sqrt{3}$. It can be seen that in all types of PAS models, mutual coupling in a specific range of antenna spacing $d < 0.4\lambda$, has a positive effect on diversity gain and decreases the correlation.

Using the Scattering-parameters

Assuming $\mathbf{S}$ to be the scattering matrix of two antennas terminated with a reference load z_0, the envelope correlation can be expressed as follows [66]

$$\rho_e = \frac{|S_{11}^* S_{12} + S_{21}^* S_{22}|^2}{(1 - (|S_{11}|^2 + |S_{21}|^2))(1 - (|S_{22}|^2 + |S_{12}|^2))} \tag{3.36}$$

Signal-based Approach

The most common expression for the correlation coefficient is given by [5, 60]

$$\rho_{12} = \frac{E\{V_1 V_2^*\}}{\sqrt{E\{V_1 V_1^*\} E\{V_2 V_2^*\}}} \tag{3.37}$$

where V_i for ($i = 1, 2$) is the received signal at ith antenna, $E\{\}$ denotes expectation over the symbol time, and the superscript $(\cdot)^*$ denotes the complex conjugate.

Using the open-circuit model, the open-circuit terminal voltages are assumed to be free of mutual coupling, and they are related to the coupled terminal voltages across the impedance loads by (3.11). The correlation coefficients of the coupled terminal voltages can be calculated from (3.37) in terms of the correlation coefficient of the open-circuit voltages. Assuming ρ_0 as the complex correlation between the open-circuit terminal voltages of two identical antennas, a

closed form expression of ρ_{12} is calculated in [5] as follows

$$\begin{aligned}\rho_{12} &= \frac{1}{\sqrt{|z_A+z_L|^2+|z_{12}|^2-2\Re\{\rho_0(z_A+z_L)z_{12}^*\}}} \\ &\times \frac{\rho_0|z_A+z_L|^2+\rho_0^*|z_{12}|^2-2\Re\{(z_A+z_L)z_{12}^*\}}{\sqrt{|z_A+z_L|^2+|z_{12}|^2-2\Re\{\rho_0^*(z_A+z_L)z_{12}^*\}}}.\end{aligned} \tag{3.38}$$

In general, such expression can be obtained from the following equation [21]

$$\rho_{12} = \frac{R_{L,12}}{\sqrt{R_{L,11}R_{L,22}}} \tag{3.39}$$

where $\mathbf{Q}_L$ is the covariance matrix of the coupled terminal voltage vector $\mathbf{v}_L$, written by

$$\begin{aligned}\mathbf{Q}_L &= E\{\mathbf{v}\mathbf{v}^H\} \\ &= \mathbf{C}_R \underbrace{E\{\mathbf{v}_{oc}\mathbf{v}_{oc}^H\}}_{\mathbf{R}_{oc}} \mathbf{C}_R^H.\end{aligned} \tag{3.40}$$

On the other hand, for the receiving mutual impedance method, the terminal voltages across the load impedance of isolated antennas are considered to be the uncoupled signals, related to the coupled terminal voltages by (3.17)-(3.18). Therefore, the correlation coefficients of the coupled terminal voltages could be obtained from equations (3.37) or (3.39). A closed-form expression for the correlation coefficient is presented in [60, 71] assuming a real correlation coefficient ρ_0 for uncoupled terminal voltages, i.e. $E\{U_1U_2^*\} = E\{U_1^*U_2\}$. We can expand this expression to the complex form of ρ_0 as follows

$$\begin{aligned}\rho_{12} &= \frac{1}{\sqrt{|z_L|^2+|z_{12}^R|^2-2\Re\{\rho_0 z_L(z_{12}^R)^*\}}} \\ &\times \frac{\rho_0|z_L|^2+\rho_0^* z_{12}^R(z_{21}^R)^*-z_L(z_{21}^R)^*-z_L^* z_{12}^R}{\sqrt{|z_L|^2+|z_{21}^R|^2-2\Re\{\rho_0^* z_L(z_{21}^R)^*\}}}.\end{aligned} \tag{3.41}$$

We also recall that for identical passive antenna elements, we have $z_{12}^R = z_{21}^R$. It is similar to the conventional mutual coupling for the open-circuit model.

3.4.3 Received Power

The received power for each element of a coupled array is investigated in [5, 22, 34]. It is shown that the mutual coupling for small element separation degrades the received power due to the mismatch between the antenna elements and their terminal loads [37]. Similar to the signal correlation, the received power can be calculated using antenna patterns, or directly from the received signals. Using the antenna pattern approach, the mean received power at antenna i of the array denoted by P_i, can be written as [34]

$$P_i = \int_{-\pi}^{\pi} |e_i(\phi)|^2 \, p(\phi) \, d\phi. \tag{3.42}$$

The mutual coupling effects can be taken into account by employing coupled antenna pattern from (3.28).

The other method defines the mean power as the expected value of the terminal voltage [22, 72]. Therefore, P_i for each antenna i is written by

$$P_i = E\{V_i V_i^*\}. \tag{3.43}$$

Using (3.11) or (3.17) we can express the coupled received power in terms of uncoupled received power, or the correlation coefficient of the received signals [5, 22]. However, it is worth noting that in [5], the received power P_i is defined as

$$P_i = \frac{E\{\Re\{z_L\}|I_i|^2\}}{P_0} = \frac{E\{\Re\{z_L\}|I_i|^2\}}{E\{\Re\{z_A^*\}|I_0|^2\}} \tag{3.44}$$

where I_i is the terminal current of ith antenna, and P_0 is a normalisation factor defined as the received power by a single conjugate-matched antenna. The term I_0 denotes the terminal current of the single antenna. Such a definition is due to the fact that in practical MIMO applications, *the voltage across the real part of the terminal load* z_L is considered as the received signal rather than the voltage across the complex load z_L [38, 40, 73]. This concern is discussed for defining the coupling matrix in section 3.3.4. Using the open-circuit model and considering an array of two identical half-wavelength dipoles terminated identically with a load impedance z_L,

Andersen and Lau [5] express the element received power as follows

$$P_1 = \frac{4r_A r_L}{|(z_A+z_L)^2 - z_{12}^2|^2}\left(|z_A+z_L|^2 + |z_{12}|^2 - 2\Re\{\rho_0(z_A+z_L)z_{12}^*\}\right) \tag{3.45}$$

$$P_2 = \frac{4r_A r_L}{|(z_A+z_L)^2 - z_{12}^2|^2}\left(|z_A+z_L|^2 + |z_{12}|^2 - 2\Re\{\rho_0^*(z_A+z_L)z_{12}^*\}\right) \tag{3.46}$$

where r_A and r_L are the real parts of z_A and z_L, respectively.

Using the receiving mutual impedance method, we derive the expression of the received power for the above scenario of identical antennas. From equations (3.16) and (3.43), it follows that

$$P_1 = \frac{|z_L|^2}{|z_L^2 - (z_{12}^R)^2|^2}\left(|z_L|^2 + |z_{12}^R|^2 - 2\Re\{\rho_0 z_L (z_{12}^R)^*\}\right) \tag{3.47}$$

$$P_2 = \frac{|z_L|^2}{|z_L^2 - (z_{21}^R)^2|^2}\left(|z_L|^2 + |z_{21}^R|^2 - 2\Re\{\rho_0^* z_L (z_{21}^R)^*\}\right). \tag{3.48}$$

If we assume the received power defined for the voltage across the resistant part of the terminal load, the above expressions would be multiplied by a factor of $(|z_A|^2|r_L|^2)/(|r_A|^2|z_L|^2)$. Therefore,

$$P_1 = \frac{(|z_A|^2|r_L|^2)/|r_A|^2}{|z_L^2 - (z_{12}^R)^2|^2}\left(|z_L|^2 + |z_{12}^R|^2 - 2\Re\{\rho_0 z_L (z_{12}^R)^*\}\right) \tag{3.49}$$

$$P_2 = \frac{(|z_A|^2|r_L|^2)/|r_A|^2}{|z_L^2 - (z_{21}^R)^2|^2}\left(|z_L|^2 + |z_{21}^R|^2 - 2\Re\{\rho_0^* z_L (z_{21}^R)^*\}\right). \tag{3.50}$$

3.4.4 Capacity

Consider a narrowband MIMO system of N transmit and M receive antennas, with a $M \times N$ channel matrix $\mathbf{H}$ as shown in Figure 3.15. Assuming a Rayleigh-fading propagation channel and using the popular Kronecker structure, the channel matrix can be expressed as [12]

$$\mathbf{H} = \mathbf{\Psi}_R^{1/2}\mathbf{H}_w\mathbf{\Psi}_T^{1/2} \tag{3.51}$$

where $\mathbf{H}_w$ is a $M \times N$ matrix with independent identically distributed (iid) and zero-mean unit-variance complex Gaussian entries, and $\mathbf{\Psi}_T$ and $\mathbf{\Psi}_R$ are the transmit and receive spatial

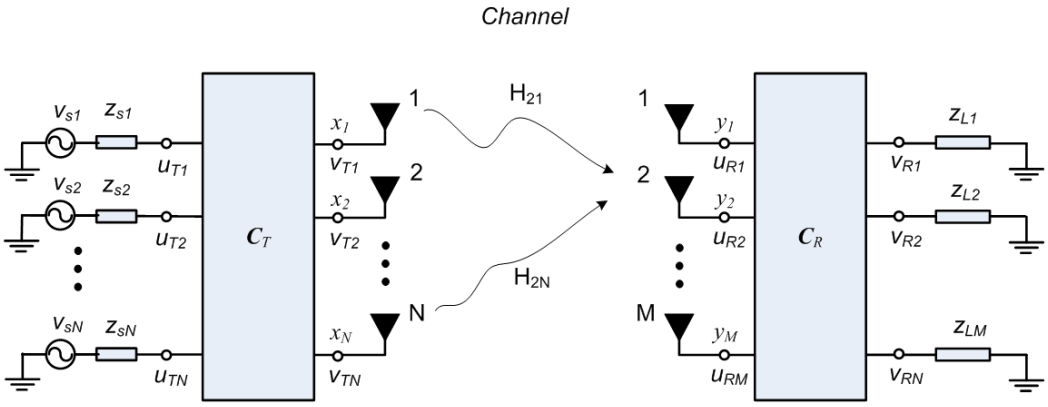

Figure 3.15: *Block diagram of a $N \times M$ MIMO system including the mutual coupling effects between antennas, represented by the coupling matrices $\mathbf{C}_T$ and $\mathbf{C}_R$ at the transmitter and receiver, respectively.*

channel correlation matrices, respectively. These covariances are defined as

$$\mathbf{\Psi}_R = (1/M)E\{\mathbf{H}\mathbf{H}^H\}, \tag{3.52}$$

$$\mathbf{\Psi}_T = (1/N)E\{\mathbf{H}^H\mathbf{H}\}. \tag{3.53}$$

Entries of such matrices can be calculated using the approaches introduced in Section 3.4.2. We note that the Kronecker model has deficiencies for large number of antennas [28]. However it is still valid for 2×2 and 3×3 MIMO systems which are used in this thesis. The ergodic capacity (mean capacity) for a MIMO system with a random channel matrix $\mathbf{H}$ is given by [12, 13]

$$C = \max_{\mathbf{R_x}:\, \mathrm{Tr}(\mathbf{R_x})=\rho} E_{\mathbf{H}} \left\{ \log_2 \left[\det(\mathbf{I}_M + \frac{1}{\sigma_n^2}\, \mathbf{H}\mathbf{R_x}\mathbf{H}^H) \right] \right\} \tag{3.54}$$

where $E_{\mathbf{H}}\{\cdot\}$ is the expectation over the distribution of the channel matrix $\mathbf{H}$, σ_n^2 is the noise power, and $\mathbf{R_x} = E\{\mathbf{x}\mathbf{x}^H\}$ is the covariance matrix of the input vector $\mathbf{x}$. We assume the channel matrix $\mathbf{H}$ is known to the receiver, but the transmitter has no knowledge of the channel. So the transmit power will be divided equally among all the transmit antennas, i.e. $\mathbf{R_x} = (P_t/N)\mathbf{I}_N$ [2], where P_t is the total transmit power. Thus, the resulting ergodic capacity can be written as

$$C = E_{\mathbf{H}} \left\{ \log_2 \det \left(\mathbf{I}_M + \frac{\rho}{N}\mathbf{H}\mathbf{H}^H \right) \right\} \tag{3.55}$$

where $\rho = P_t/\sigma_n^2$ is the average signal-to-noise ratio at the receiver. In order to take the mutual coupling into account, a modified channel matrix $\mathbf{H}_{mc}$ is created as follows [22, 23]

$$\mathbf{H}_{mc} = \mathbf{C}_R \mathbf{H} \mathbf{C}_T = \mathbf{C}_R (\mathbf{\Psi}_R^{1/2} \mathbf{H}_w \mathbf{\Psi}_T^{1/2}) \mathbf{C}_T \tag{3.56}$$

where $\mathbf{C}_T$ and $\mathbf{C}_R$ are the transmit and receive coupling matrices, respectively. Assuming the voltages across the resistive parts of antenna impedance load z_L as the receive signals, and considering identical half-wavelength dipole antennas for transmit and receive arrays, with sufficiently separated transmit antennas, an equivalent to the above equation is represented as [7]

$$\mathbf{H}_{mc} = 2 r_{11} \mathbf{R}_L^{1/2} (\mathbf{Z}_R + \mathbf{Z}_L)^{-1} \underbrace{\mathbf{\Psi}_R^{1/2} \mathbf{H}_w \mathbf{\Psi}_T^{1/2}}_{\mathbf{H}_{nc}} \mathbf{R}_T^{-1/2} \tag{3.57}$$

where $\mathbf{Z}_R$ and $\mathbf{Z}_T$ are the receive and transmit array impedance matrices, respectively with diagonal entries $Z_{R,ii}, Z_{T,ii}$ being the self impedances and the off-diagonal entries $Z_{R,ij}, Z_{T,ij}$, $(i \neq j)$ denoting the mutual impedances. The real parts of $\mathbf{Z}_L$ and $\mathbf{Z}_T$ are denoted by $\mathbf{R}_L$ and $\mathbf{R}_T$, respectively and $r_{11} = R_{T,11}$. For the special case of no mutual coupling ($Z_{R,ij} = Z_{T,ij} = 0$) with matching of all the transmit and receive antennas to their self-impedances, the channel matrix simplifies to the term represented by $\mathbf{H}_{nc}$. Throughout this thesis, we assume that the transmit antennas are separated sufficiently, self-impedance matched and that $\mathbf{\Psi}_T = \mathbf{I}_M$. Thus the channel matrix $\mathbf{H}_{mc}$ from (3.57) can be simplified as [7]

$$\mathbf{H}_{mc} = 2\sqrt{r_{11}} \mathbf{R}_L^{1/2} (\mathbf{Z}_R + \mathbf{Z}_L)^{-1} \underbrace{\mathbf{\Psi}_R^{1/2} \mathbf{H}_w}_{\mathbf{H}_{nc}}. \tag{3.58}$$

From now on, we use this expression of the channel matrix taking the mutual coupling into account for the open-circuit model.

Now we substitute $\mathbf{H}_{mc}$ into (3.55) at the place of $\mathbf{H}$. Therefore, we have

$$C = E \left\{ \log_2 \det \left(\mathbf{I}_M + \frac{\rho}{N} \mathbf{H}_{mc} \mathbf{H}_{mc}^H \right) \right\}. \tag{3.59}$$

To calculate the capacity using the receiving mutual impedance method, we need to define a coupling matrix for the transmit side as well. Referring to Figure 3.15, the relationship between the terminal voltages at the transmit antennas with and without the mutual coupling, denoting

by $\mathbf{v}_T$ and $\mathbf{U}_T$ respectively, is written as [72]

$$\mathbf{v}_T = (\mathbf{Z}^T)^{-1}\mathbf{U}_T \tag{3.60}$$

where $\mathbf{Z}^T$ similar to (3.18) is defined by

$$\mathbf{Z}^T = \begin{bmatrix} 1 & \frac{z_{12}^R}{z_A} & \dots & \frac{z_{1N}^T}{z_A} \\ \frac{z_{21}^T}{z_A} & 1 & \dots & \frac{z_{2N}^T}{z_A} \\ \vdots & \vdots & \ddots & \vdots \\ \frac{z_{N1}^T}{z_A} & \frac{z_{N2}^T}{z_A} & \dots & 1 \end{bmatrix}, \tag{3.61}$$

where z_A is the input impedance of the antennas, and z_{ij}^T $(i, j = 1, 2, \dots, N_T)$ is the transmitting mutual impedance between the ith and jth transmitting antennas. As an example, z_{12}^T is defined as [72]

$$z_{12}^T = \left.\frac{V_{T1}}{I_2}\right|_{V_{s1}=0} \tag{3.62}$$

It should be noted that the coupled voltage $V_{T1}\big|_{V_{s1}=0}$ is the voltage across the antenna input impedance rather than the open-circuit voltage as in the conventional method [72]. Considering (3.17) and (3.60), the transmit and receive correlation matrices (including spatial correlation and mutual coupling) can be expressed as

$$\mathbf{Q}_T = E\{\mathbf{v}_T\mathbf{v}_T^H\} = (\mathbf{Z}^T)^{-1}E\{\mathbf{U}_T\mathbf{U}_T^H\}(\mathbf{Z}^T)^{-H} \tag{3.63a}$$

$$\mathbf{Q}_R = E\{\mathbf{v}_R\mathbf{v}_R^H\} = (\mathbf{Z}^R)^{-1}E\{\mathbf{U}_R\mathbf{U}_R^H\}(\mathbf{Z}^R)^{-H} \tag{3.63b}$$

where $E\{\cdot\}$ is the expectation operator over all multipath scattering directions. We note that by the correlation matrices of the uncoupled terminal voltages at the transmit and receive sides, denoted by $E\{\mathbf{U}_T\mathbf{U}_T^H\}$ and $E\{\mathbf{U}_R\mathbf{U}_R^H\}$ respectively, only the spatial correlation is taken into account, whereas $\mathbf{Q}_T$ and $\mathbf{Q}_R$ include the mutual coupling as well. Comparing to the spatial correlation matrices in (3.52) and (3.53), we have

$$\mathbf{\Psi}_R = E\{\mathbf{U}_R\mathbf{U}_R^H\}, \tag{3.64}$$

$$\mathbf{\Psi}_T = E\{\mathbf{U}_T\mathbf{U}_T^H\}. \tag{3.65}$$

Using the Kronecker channel model and taking the mutual coupling into account, the channel matrix $\mathbf{H}_{mc}$ can be expressed as follows

$$\begin{aligned}\mathbf{H}_{mc} &= \mathbf{Q}_R^{1/2}\mathbf{H}_w\mathbf{Q}_T^{1/2} \\ &= \left(\mathbf{C}_R\mathbf{\Psi}_R\mathbf{C}_R^H\right)^{1/2}\mathbf{H}_w\left(\mathbf{C}_T\mathbf{\Psi}_T\mathbf{C}_T^H\right)^{1/2}\end{aligned} \tag{3.66}$$

where $\mathbf{C}_R = (\mathbf{Z}^R)^{-1}$ and $\mathbf{C}_T = (\mathbf{Z}^T)^{-1}$ are the receive and transmit coupling matrices.

Several studies have investigated the effects of mutual coupling on the capacity of MIMO systems [22, 23, 40, 41, 58]. The capacity is an important performance criterion which is affected by both efficiency and correlation of the system [40]. Two different types of channel normalisations are used in some studies [23, 41] to investigate such effects. Normalisation of $\mathbf{H}_{mc}$ in (3.56) is one way to remove the effect of the received power changes due to the mutual coupling, and to provide an opportunity to reveal the effects of the correlation or richness of multipath channel on the capacity. The other approach is to normalise $\mathbf{H}$ in (3.51) which includes the variation of instantaneous received power into the calculation of the capacity. It is shown that normalising $\mathbf{H}$ results in the capacity degradation for the element separation less than $d = 0.4\lambda$, while the former normalisation shows an improvement for the capacity in the same region of d [23, 41]. However, [40] shows that the received power has a stronger effect on the capacity in comparison with the correlation, and a stronger received power results in a better capacity performance.

3.5 Antenna Impedance Matching

Antenna impedance matching is introduced by many studies as an interesting solution to counteract the effect of mutual coupling. Applying a complex coupled matching network [39] known as the Multiport-Conjugate Match (MCM) [4] is introduced as a decoupling network which may decouple the signals from closely spaced antennas completely. Using network analysis, a matching network can be placed between the coupled array and antenna loads (receive mode) or excitation sources (transmit mode) such that it can be conjugate-matched from one side to the antenna array and from the other side to the loads/sources. This is shown in Figure 3.16. However, constructing such a network due to the required interconnections between all ports of the matching network is complicated and it also offers only narrowband matching performance [37].

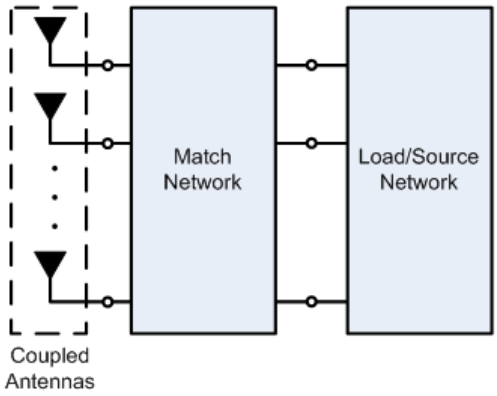

Figure 3.16: *Block diagram of a coupled receive/transmit array employing an impedance matching network.*

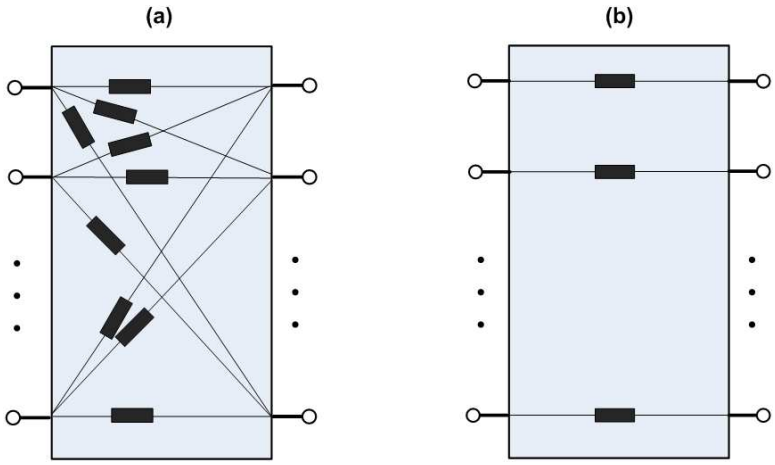

Figure 3.17: *Schematic diagram of (a) coupled (MCM), and (b) uncoupled matching networks.*

These problems motivate researchers to work on simpler uncoupled termination approaches [5–9] which are easier to implement and can achieve near-optimal performance with a wider bandwidth [9, 37]. A schematic diagram of both coupled (MCM) and uncoupled matching networks are shown in Figure 3.17. For uncoupled matching approaches, we assume the mutual coupling model and the random channel matrix are given. Then we can find an optimum terminal load for each antenna element such that the performance metric (such as diversity gain, received power, and capacity) will be maximised. This is the method we are interested in to mitigate the mutual coupling.

However, existing studies use the open-circuit approach to model the mutual coupling in their investigations. As discussed in section 3.3, this model is not accurate in general, except for specific types of antennas such as half-wavelength dipoles. Therefore, we examine the receiving mutual impedance method, described in section 3.3.3, to model the mutual coupling. This model has not been used for uncoupled impedance matching except in [60] in which the envelope correlation is investigated when antennas are identically terminated with a variable real load impedance.

In this section, we investigate the effect of uncoupled impedance matching on MIMO performance metrics (signal correlation, received power, and capacity) in the presence of mutual coupling. We use both open-circuit and receiving mutual impedance approaches to model the mutual coupling. Consider a 2×2 MIMO system of identical half-wavelength dipole antennas as shown in Figure 3.15, with identical source and terminal load impedances, i.e. $z_{s1} = z_{s2} = z_s$ and $z_{L1} = z_{L2} = z_L$. For the sake of simplicity, we assume that the transmit antennas are sufficiently separated to ignore the mutual coupling at the transmit side, i.e. $\mathbf{v}_T = \mathbf{u}_T$, and $\mathbf{\Psi}_T = \mathbf{I}_2$ is considered.

Antennas are considered as wire dipoles with a wire radius of $\lambda/400$, and element spacing $d = 0.05\lambda$ at a frequency of 1800 MHz. The receiving mutual impedances for different values of the terminal load impedance $z_L = r_L + jx_L$ are obtained from FEKO software [10] based on the method described in section 3.3.3.

We calculate the performance metrics for both mutual coupling models (open-circuit and receiving mutual impedance methods) over different complex values of z_L. Assume that ρ_0 is the

uncoupled terminal voltage correlation defined by

$$\rho_0 = \frac{E\{U_{R1}U_{R2}^H\}}{\sqrt{E\{U_{R1}U_{R1}^H\}E\{U_{R2}U_{R2}^H\}}} \tag{3.67}$$

For both mutual coupling models in our simulation, the following scenarios are considered for ρ_0: uniform distribution, and two Laplacian distribution cases with $(\phi_0 = 0^\circ, \sigma = 40^\circ)$ and $(\phi_0 = 45^\circ, \sigma = 40^\circ)$. In the case of the uniform distribution, $\rho_0 = J_0(2\pi d/\lambda)$, where $J_0(\cdot)$ is the zeroth-order Bessel function of the first kind. A reference SNR of 20 dB is assumed for all scattering distribution scenarios.

Figure 3.18 shows the 3D plot of the absolute value of the correlation in the presence of the mutual coupling under different scattering distribution at the receiver with the right-hand-side sub-figures (b),(d),(f) for the the open-circuit model, and the left-hand-side sub-figures (a),(c),(e) for the receiving mutual impedance model. It can be seen that the results from both models have the same trend, and for each propagation scenario we can find a z_L (or a range of z_L) which minimises the signal correlation. However, these impedance choices depend on the scattering scenario.

Similarly, the total received power for all receive antennas in dB is shown in Figure 3.19. We see that the optimum load impedance z_L which maximises the received power is different for the open-circuit and the receiving mutual impedance models under the same propagation scenario. Using the open-circuit model, the optimum z_L is $(2 - j20)\Omega$ at (b), $(175 - j50)\Omega$ at (d), and $(2 - j20)\Omega$ at (f). On the other hand, the receiving mutual impedance model gives a $z_L = 1\Omega$ as the optimum load for all propagation scenarios at (a),(c),(e). However, there is a local maximum at $(2 - j20)\Omega$ as well. Referring back to Figure 3.10, we see that the absolute value of the mutual impedance for the receiving mutual impedance method has a minimum at $z_L = 1\Omega$. Such an effect makes a maximum peak for the received power at the corresponding load impedance value, independent of the propagation scenario.

To further the investigation, the mean capacity calculated from (3.59) by averaging over 1000 channel realisations, is shown in Figure 3.20. Similar to the total received power, the mean capacity is maximised at different load impedances corresponding to the propagation environment for the open-circuit mutual coupling model. These z_L values are $(11 - j20)\Omega$ at (b), $(18 - j25)\Omega$ at (d), and $(11 - j20)\Omega$ at (f). Using the receiving mutual impedance model, the

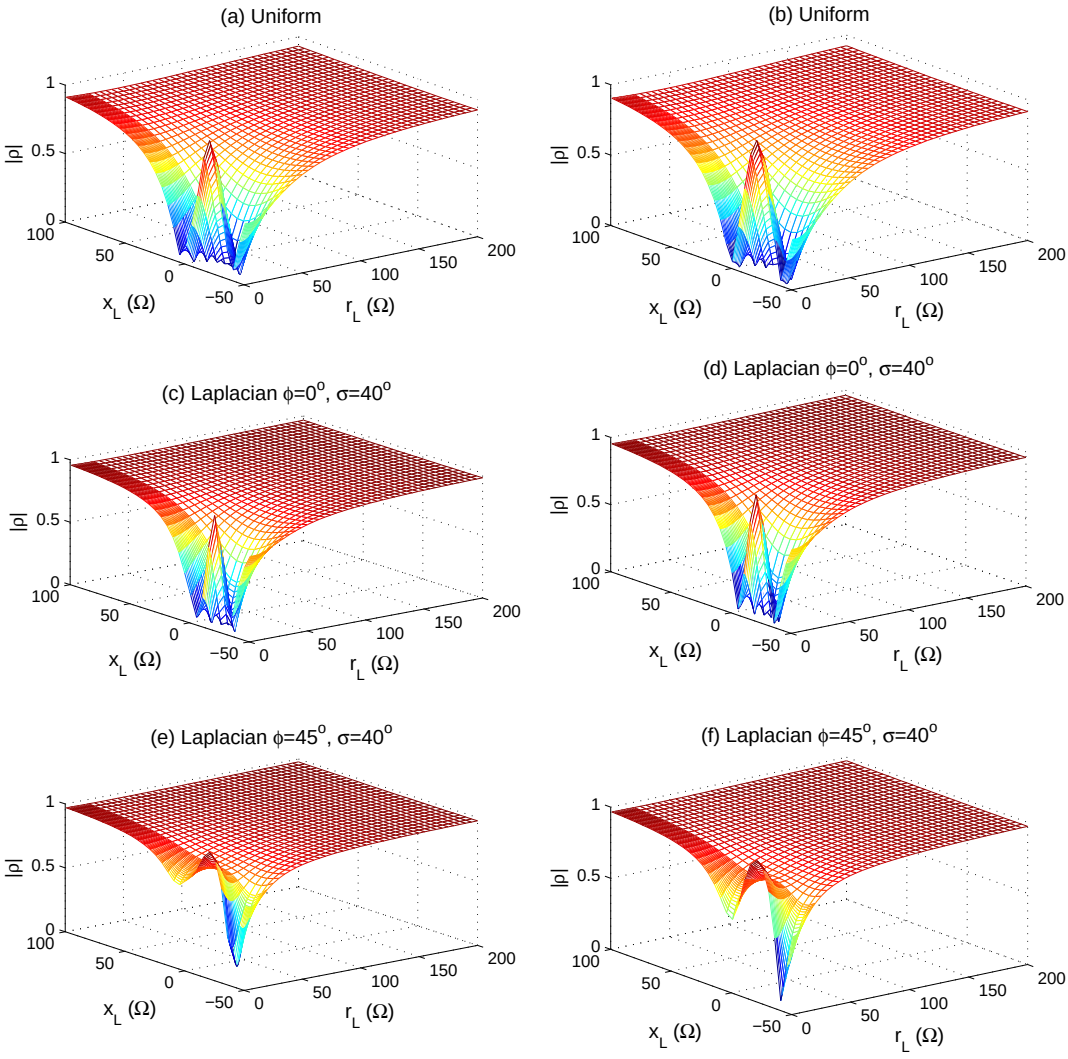

Figure 3.18: *Absolute value of the correlation versus the real and imaginary parts of terminal load $z_L = r_L + jx_L$ for the receiving mutual impedance method at (a),(c),(e), and the open-circuit model at (b),(d),(f).*

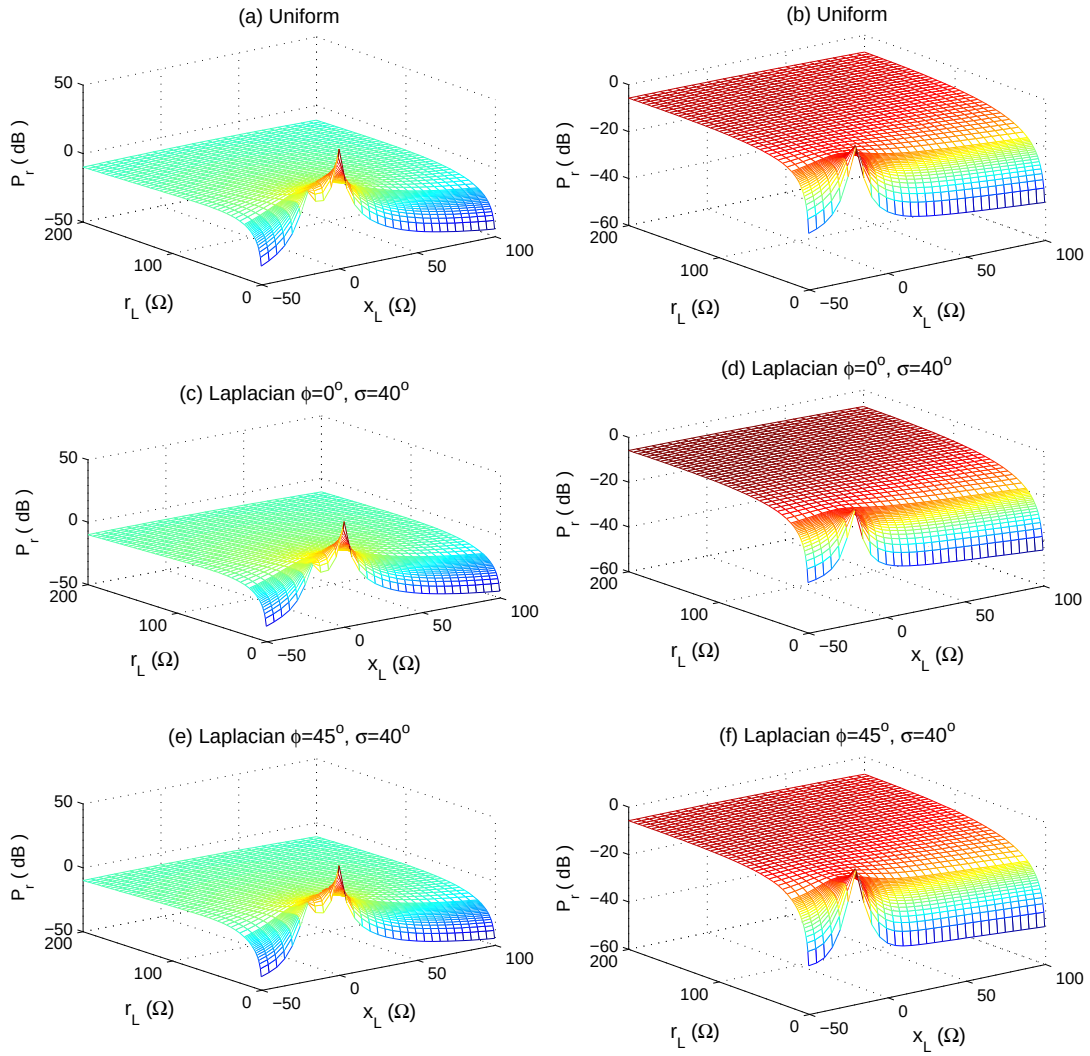

Figure 3.19: *The total received power versus the real and imaginary parts of terminal load* $z_L = r_L + jx_L$ *for the receiving mutual impedance method at (a),(c),(e), and the open-circuit model at (b),(d),(f).*

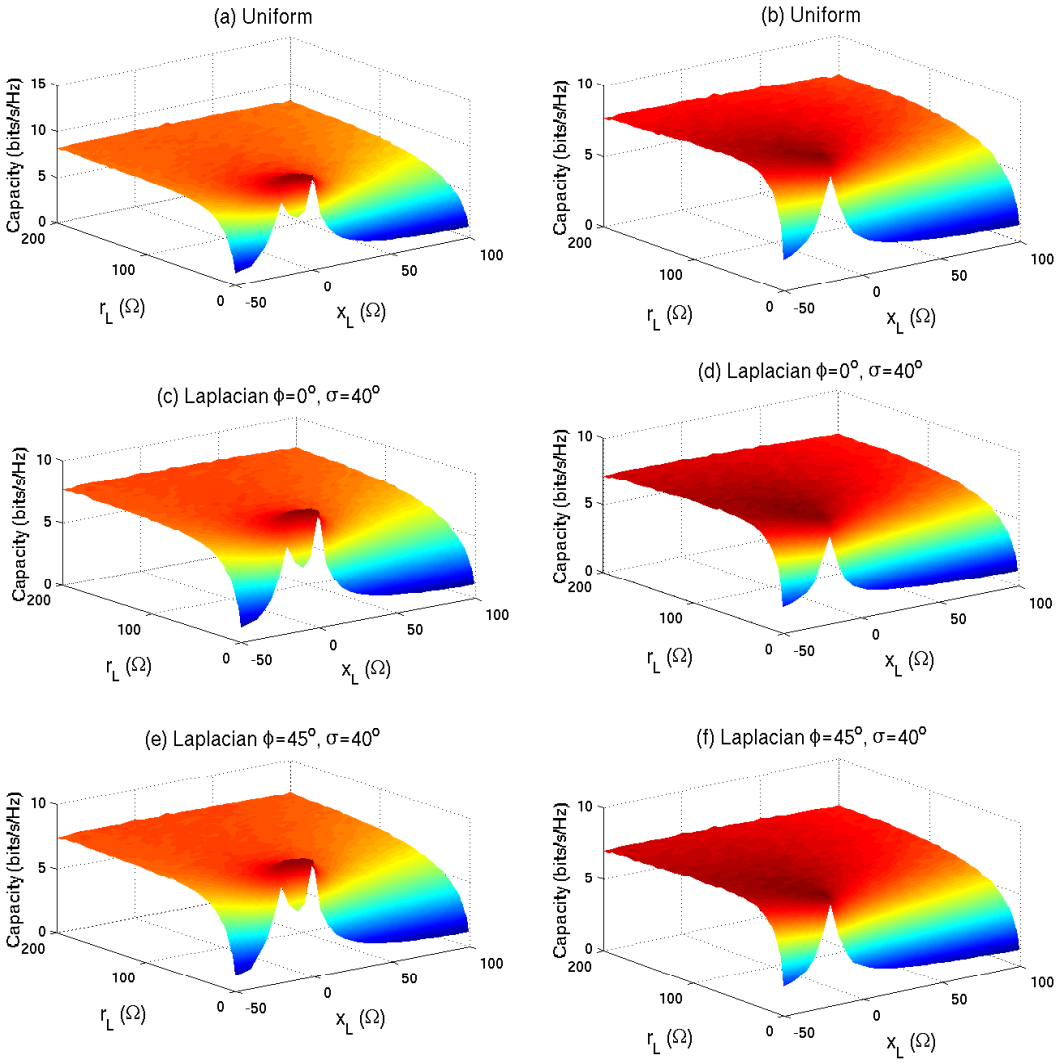

Figure 3.20: *The ergodic capacity versus the real and imaginary parts of terminal load* $z_L = r_L + jx_L$ *for the receiving mutual impedance method at (a),(c),(e), and the open-circuit model at (b),(d),(f).*

mean capacity always has a global maximum at $z_L = 1\Omega$ for all propagation scenarios, and a local maximum at a load impedance corresponding to the propagation environment.

Since the open-circuit model is only valid for specific types of antennas such as $\frac{\lambda}{2}$ dipole antennas, we examined the receiving mutual impedance method as an alternative model for the use of antenna impedance matching technique. The above simulation results for a 2×2 MIMO system of $\frac{\lambda}{2}$ dipole antennas show that the receiving mutual impedance method yields apparently erroneous results at 1Ω, so it is not clear that this method can be used with confidence.

Therefore, in the following chapters we look for adaptive impedance matching techniques which use no mathematical mutual coupling model, but its effects is taken into account by estimating the performance of compact MIMO systems from the receiving signals. We investigate the performance of such algorithms for half-wavelength dipole antennas in which open-circuit model is valid and the system can be simulated in our numerical studies.

3.6 Conclusion

In this chapter, we addressed the problem of mutual coupling for compact MIMO systems. We reviewed the open-circuit and the receiving mutual impedance methods to model the mutual coupling. The open-circuit model is a simple and popular model in the literature to investigate the mutual coupling effect. However, it is only valid for specific types of antennas such as half-wavelength dipoles. Therefore, we studied the receiving mutual impedance method as an alternative model. Then, we examined the influence of the mutual coupling on MIMO performance metrics using both the open-circuit and the receiving mutual impedance methods. After that we investigated the antenna impedance matching approach to counteract the performance degradation of MIMO systems due to the mutual coupling. Simulation results for a 2×2 MIMO system of half-wavelength dipole antennas show that the receiving mutual impedance method is not useful for finding the optimum load which maximises the capacity or the received power.

Chapter 4
Adaptive Impedance Matching Network

4.1 Introduction

As stated in chapter 3, in previous studies antenna impedance matching is presented as a solution for compensating the performance degradation of compact MIMO systems due to the mutual coupling. For a given channel matrix and a known mutual coupling model, an impedance load network can be found which can maximise the desired performance metric. However the channel matrix and the mutual coupling may vary with time, and the impedance match should be adapted accordingly. There is no solution in the literature to track such issue and find an optimum load network corresponding to these changes.

In this chapter we present an uncoupled *adaptive impedance match* to counteract the effect of mutual coupling on the performance of compact MIMO systems.

This chapter is organised as follows. We first explain why we need an adaptive impedance match for compact MIMO systems in Section 4.2. Then, Section 4.3 briefly reviews the system model. Next, the idea of adaptive impedance match is introduced in Section 4.4 and required conditions to implement such an idea are examined . It follows by introducing some estimation methods for the received power and the capacity in Section 4.5. After that, the following optimisation techniques: Gradient-based, Newton-Raphson, and random-search methods are examined for implementing the proposed adaptive match network in Section 4.6. Finally, we conclude the chapter in Section 4.7.

4.2 Necessity of Adaptive Impedance Match

Previous studies examined the effect of antenna terminal load impedances on the signal correlation [5, 6], the received power [5, 6], and the capacity [6, 7] for identical load impedances. Then, [74, 75] extended the concept to non-identical load impedances. It is found that an impedance

matching network can be applied to a compact MIMO system in order to compensate the impact of mutual coupling, and to maximise the performance metric, for a given random channel matrix taking the mutual coupling into account. However, such methods require a *priori* knowledge of the propagation channel and an accurate model of the mutual coupling.

As pointed out earlier in chapter 3, modelling of mutual coupling is a challenging issue for coupled array applications. Existing matching approaches use the open-circuit model or the equivalent scattering model which is not accurate in general, except for specific types of antennas such as half-wavelength dipoles. In addition, it is shown that near-field scatterers (NFS) around antennas can increase the mutual coupling between array elements [33, 76]. As an example, conductive objects within a quarter wavelength proximity of antenna elements can have the NFS effects. Since the occurrences of NFS are unknown and uncontrollable to array applications, the mutual coupling model has to be estimated or modified frequently [76]. Fortunately, although NFS are occurring randomly, the variation rate of NFS is appeared to be much slower than the channel itself, even for fast-fading channels [33].

Furthermore, existing matching solutions are not designed to track the time variations of the propagation channel. Therefore, we propose an *adaptive uncoupled matching* solution in this thesis which includes the changes of the channel matrix and the mutual coupling, by dealing with the received signals at antenna terminals. The received signals are assumed to be the currents flowing through the impedance loads of the antenna terminals, or the voltages across the real (resistive) parts of the impedance loads for array applications. In this thesis, we consider the latter case which is the most common case for MIMO applications [40].

This chapter presents the possible approaches to have an adaptive uncoupled matching network for identical terminal loads. It will be extended to non-identical loads in the next chapter. This method starts from an initial value of the load impedance network and calculates the corresponding value of the desired performance metric (the received power or the capacity). Then, it changes the load impedance network according to an iterative optimisation technique to find a value which maximises the performance metric. However, the mutual coupling model in general is either unknown or it is not separable from the channel matrix. Therefore, the total channel matrix has to be estimated from the received signal (for example by using training sequences) to obtain a value of the performance metric corresponding to each change of the load impedance network.

4.3 System Model

Consider a MIMO system of N transmit and M receive antennas, communicating through a frequency-flat fading channel. Using a discrete-time baseband model, the input-output relationship at time instant k is given by

$$\mathbf{y}[k] = \mathbf{H}_{mc}[k]\mathbf{x}[k] + \mathbf{n}[k] \tag{4.1}$$

where $\mathbf{x}[k] \in \mathbb{C}^N$ is the transmit signal vector, $\mathbf{y}[k] \in \mathbb{C}^M$ is the receive signal vector, $\mathbf{H}_{mc}[k] \in \mathbb{C}^{M\times N}$ denotes the channel matrix including the mutual coupling effect, and $\mathbf{n}[k] \in \mathbb{C}^M$ represents a vector of additive white Gaussian noise (AWGN) at the receiver, which is assumed to be complex Gaussian noise with zero-mean and covariance matrix $\sigma_n^2\mathbf{I}_M$ at the terminal loads.

As stated in the previous chapter, the channel matrix $\mathbf{H}_{mc}[k]$ can be written as

$$\mathbf{H}_{mc} = \mathbf{C}_R\mathbf{H}\mathbf{C}_T \tag{4.2}$$

where $\mathbf{H}$ is the channel matrix without taking the mutual coupling effects into account. $\mathbf{C}_R$ and $\mathbf{C}_T$ are the coupling matrices at the receive and transmit sides, respectively. When there is no coupling at the transmit side, $\mathbf{C}_T = \mathbf{I}_N$. It is shown in chapter 3 that for a given $\mathbf{H}$ and a known mutual coupling model $\mathbf{C}_R$, an impedance load network $\mathbf{Z}_L$ can be found which maximises the performance metric (diversity gain, received power, or capacity). However, the channel matrix $\mathbf{H}$ and the mutual coupling model may vary with time. Therefore, the choice of the impedance network $\mathbf{Z}_L$ should be updated accordingly.

In this thesis, we propose the idea of having an *adaptive impedance match* which tunes the terminal load network $\mathbf{Z}_L$ in order to compensate the effect of $\mathbf{H}_{mc}[k]$ and maximise the desired performance metric. We perform such an idea by changing the load impedance network $\mathbf{Z}_L$, and obtaining feedback due to this change in load network by estimating the corresponding value of the performance metric (the received power or the capacity) from the received signals. By comparing the current metric value and the previously optimum one (the maximum value over previous steps), the algorithm selects the better impedance network as the optimum termination until that step. It then changes the terminal impedances according to an optimisation technique for the next step. This process will be repeated until the algorithm converges to an optimum termination network, in terms of received power or capacity.

In order to model the effect of load impedance variations, we use the channel model in (3.58) for the open-circuit mutual coupling model. As stated in the previous chapter, this model may not be exact for the coupled receive array in general. However, it is still valid for a limited types of antennas such as half-wavelength dipoles, and it is validated by empirical studies [38] for half-wavelength dipoles. Therefore, it can reveal the total behaviour of the system and the impact of terminations on the compact MIMO performance. We also note that the adaptive algorithm is blind to the system model, and it has only a knowledge of the received signals and the training sequences.

4.4 Adaptive Impedance Match

In this section, we examine the adaptive impedance match approach for a $N \times M$ MIMO system described by (4.1). We assume there is only mutual coupling in the receive array, and the transmit antennas are spaced sufficiently such that there is no mutual coupling at the transmitter.

As stated earlier, the desired performance metric, either the received power or the capacity, is a function of received signals, i.e.,

$$f(\mathbf{y}) = f(\mathbf{H}_{mc}\mathbf{x} + \mathbf{n}) \tag{4.3}$$

For simplicity of notation, we drop the time index k. According to the previous results on impedance matching solutions [4–8, 35, 40], the total channel matrix $\mathbf{H}_{mc}$ which includes the mutual coupling effects, and therefore influences $f(\mathbf{y})$, depends on the termination impedance matrix $\mathbf{Z}_L$ of the coupled array. Denoting the channel matrix with no mutual coupling by $\mathbf{H}$, we can write our optimisation problem as below

$$\max_{\mathbf{Z}_L} f(\mathbf{H}, \mathbf{C}_R) \tag{4.4}$$

where the second argument, $\mathbf{C}_R$, is dependent on $\mathbf{Z}_L$. In other words, we would like to find a terminal impedance network $\mathbf{Z}_L$ which compensates any performance degradation due to the *mutual coupling* and/or changes in the *channel matrix*. Here, we are interested in uncoupled

terminations where $\mathbf{Z}_L$ is a diagonal matrix written as

$$\mathbf{Z}_L = \begin{pmatrix} z_{L1} & 0 & \cdots & 0 \\ 0 & z_{L2} & \cdots & 0 \\ \vdots & \vdots & \ddots & \vdots \\ 0 & 0 & \cdots & z_{LM} \end{pmatrix}. \tag{4.5}$$

During the period of optimisation, the channel matrix $\mathbf{H}$ is assumed to be fixed or varying slowly so that the channel can be estimated at the receiver. The mutual coupling model is also assumed to be changed only by the variation of $\mathbf{Z}_L$. Then, the optimisation problem (4.4) can be simplified as

$$\max_{z_{L1},\cdots,z_{LM}} f(z_{L1},\cdots,z_{LM}) \tag{4.6}$$

where $z_{Li} = r_{Li} + jx_{Li}$ for $i = 1,\cdots,M$ with $r_{Li} \in \mathbb{R}^+$ and $x_{Li} \in \mathbb{R}$ denoting the real (resistance) and imaginary (reactance) parts of z_{Li}, respectively. We consider two different kinds of uncoupled terminations: (i) *identical* loading, which all diagonal entries are equal to a load $z_L = r_L + jx_L$, and (ii) *non-identical* loading in which terminal loads $z_{L1}, z_{L2}, \cdots, z_{LM}$ are individually tuned to optimise the compact MIMO performance.

We let $\mathbf{z} = [r_{L1}, x_{L1}, \cdots, r_{LM}, x_{LM}]^T$ be the vector of *optimisation variables*. Then, we try to find an optimal $\mathbf{z}_{opt}$ in which $f(\mathbf{z}_{opt})$ has the maximum possible value of f. This could be obtained by producing a maximising sequence $\mathbf{z}^{(m)}, (m = 1,\cdots)$ where $f(\mathbf{z}^{(m+1)}) > f(\mathbf{z}^{(m)})$, from the following iterative equation [77]

$$\mathbf{z}^{(m+1)} = \mathbf{z}^{(m)} + \alpha^{(m)} \Delta\mathbf{z}^{(m)} \tag{4.7}$$

where m denotes the iteration number, the scalar $\alpha^{(m)} \geq 0$ is the scale factor, and the vector $\Delta\mathbf{z}^{(m)}$ determines the *direction of optimisation* at iteration m.

In order to implement such an adaptive impedance match, we need to:

1. Estimate or measure the performance metric value per iteration, i.e. $f(\mathbf{z}^{(m)})$
2. Specify $\Delta\mathbf{z}$ according to an optimisation technique.

We further investigate using *Gradient-ascent*, *Newton-Raphson*, and *random search* techniques to determine the vector $\Delta\mathbf{z}$ in order to find the choice of $\mathbf{z}$ which maximises the received power

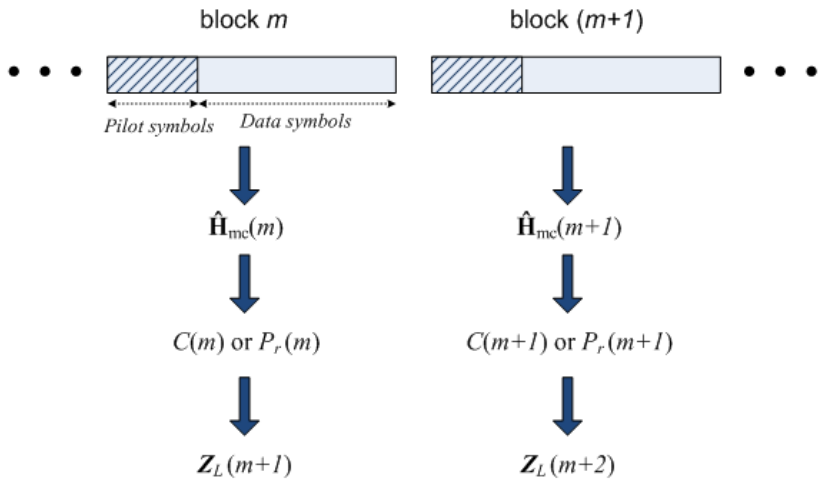

Figure 4.1: *An overview of the adaptive impedance matching algorithm.*

or the capacity. We explain these methods in the following sections. In this chapter, we examine the received power and the capacity of MIMO systems for *identical* terminal impedances. It will be extended to the *non-identical* loading case in the next chapter.

4.5 MIMO Capacity and Received Power Estimation

As stated in the previous sections of this chapter, the adaptive algorithm has no knowledge of the system except the receiving signals and the termination load network $\mathbf{Z}_L$ which is controlled by the algorithm. Figure 4.1 shows an overview of the proposed idea of the adaptive impedance matching technique. The algorithm starts from an initial termination load such as characteristic impedance load, and then estimates the total channel matrix $\mathbf{H}_{mc}$ from the knowledge of training/pilot symbols. Then the performance metric, the capacity or the received power, is calculated to predict the optimal load network $\mathbf{Z}_L$ for the next symbol block. This process continues until it converges to an optimal load network which maximises the performance metric.

In this section, we review some channel estimation approaches. We further consider a time averaging estimation of the received signals covariance matrix to approximate the capacity or the received power of MIMO systems. However, using channel estimates are more practical to implement the adaptive impedance matching algorithm.

The ergodic capacity of a MIMO system described in (4.1), with the channel matrix $\mathbf{H}_{mc}$ taking

the mutual coupling into account, is given by [12, 13]

$$C = \max_{\mathbf{R_x}} E\left\{\log_2\left[\det(\mathbf{I}_M + \frac{1}{\sigma_n^2}\mathbf{H}_{mc}\mathbf{R}_x\mathbf{H}_{mc}^H)\right]\right\}. \tag{4.8}$$

As mentioned in Section 3.4.4, when there is no channel information at the transmitter, equal power is allocated to each transmit antenna, and the above equation can be simplified as

$$C = E\left\{\log_2\left[\det(\mathbf{I}_M + \frac{\rho}{N}\mathbf{H}_{mc}\mathbf{H}_{mc}^H)\right]\right\} \tag{4.9}$$

where $\rho = P_T/\sigma_n^2$ is the average signal-to-noise ratio at the receiver.

To exploit the capacity benefits of MIMO technology, accurate channel knowledge at the receiver and/or transmitter is usually required. One of the most popular channel estimation approaches is the training-based estimator [78, 79] which can directly estimate the channel matrix including antenna mutual coupling effects, from knowledge of the received signals and (transmitted) training signals.

In this chapter, we examine two methods which estimate the channel matrix $\mathbf{H}_{mc}$ using training-sequences. We assume symbols are transmitted in blocks with a length of L data symbols in total, and each block contains L_p training/pilot symbols. Rewriting the input-output relation for the transmitted *training vector* $\mathbf{p}_k$ at time instant k, we have

$$\mathbf{y}_{p,k} = \mathbf{H}_{mc}\mathbf{p}_k + \mathbf{n}_k, \qquad k = 1, 2, \ldots, L_p \tag{4.10}$$

For the first approach which is a least-square (LS) estimator, the channel estimate is expressed as follows [78]

$$\hat{\mathbf{H}}_{mc} = \mathbf{Y}_p\left(\mathbf{P}^H(\mathbf{P}\mathbf{P}^H)^{-1}\right) \tag{4.11}$$

where $\mathbf{P} = [\mathbf{p}_1, \mathbf{p}_2, \ldots, \mathbf{p}_{L_p}]$ is the $N \times L_p$ *training matrix*, and $\mathbf{Y}_p = [\mathbf{y}_{p1}, \mathbf{y}_{p2}, \ldots, \mathbf{y}_{pL_p}]$ is the $N \times L_p$ corresponding received signal matrix. The channel estimation error for this method subject to a power constraint $||\mathbf{P}||^2 = P$ for a given maximum transmit power P , is expressed by [79]

$$\min_{\mathbf{P}} J_{LS} = \min_{\mathbf{P}} E\left\{||\mathbf{H}_{mc} - \hat{\mathbf{H}}_{mc,LS}||^2\right\} = \frac{\sigma_n^2 N^2 M}{P}, \tag{4.12}$$

where $||\cdot||$ is a Frobenius matrix norm. It is obtained under the following condition

$$\mathbf{P}\mathbf{P}^H = \frac{P}{N}\mathbf{I}. \tag{4.13}$$

We use a discrete Fourier transform (DFT) matrix to satisfy the above equation in our simulations. From the above discussion, we can express the relationship between the channel matrix $\mathbf{H}_{mc}$ and its estimate $\hat{\mathbf{H}}_{mc}$ as follows:

$$\mathbf{H}_{mc} = \hat{\mathbf{H}}_{mc} + \Delta\mathbf{H} \tag{4.14}$$

where $\Delta\mathbf{H}$ is the estimation error matrix.

The second estimation approach, which is called the *relaxed minimum mean-square-error* (RMMSE) approach [79], is a modified version of the former estimator which reduces the estimation error. Using this method and having an orthogonal training matrix satisfying (4.13), the channel estimate is given by [79]

$$\hat{\mathbf{H}}_{mc} = \frac{N \operatorname{Tr}\left\{\mathbf{Y}_p \mathbf{Y}_p^H\right\}}{P\left(\operatorname{Tr}\left\{\mathbf{Y}_p \mathbf{Y}_p^H\right\} + \sigma_n^2 NM\right)} \mathbf{Y}_p \mathbf{P}^H. \tag{4.15}$$

The mean capacity of a 3×3 MIMO system versus the real and imaginary parts of the terminal impedance load for 200 channel realisations, assuming a known channel matrix $\mathbf{H}_{mc}$ and estimated channel matrices using the above methods, are shown in Figure 4.2. The capacity value for each case is normalised to its maximum and plotted in the right-hand-side sub-figures (b),(d),(f). The channel model in (3.58) is used with element spacing $d = 0.05\lambda$, signal-to-noise-ratios (SNR) of 5 dB, and uniform scattering distribution at the receiver.

The mean capacity is maximised for $z_L = 13 - j34$ with the maximum value of $C_{max} = 2.53$ (bits/s/Hz). While the first estimator in (4.11) gives $\hat{C}_{max} = 2.81$ (bits/s/Hz) at $z_L = 9 - j36$, and the second estimator gives $\hat{C}_{max} = 2.72$ (bits/s/Hz) at $z_L = 9 - j36$. As we see from the capacity values and the left hand side contours, the second estimator has a smaller error estimation in comparison to the first one. Although both estimators give an optimum impedance load different from the actual value, but the normalised capacity contours for both approaches have a very similar trend to the actual case with known channel matrix.

In addition to the above estimation methods, we further use a simple time averaging method in this chapter to estimate the capacity corresponding to each choice of $\mathbf{Z}_L$. Let $\mathbf{R}_{\mathbf{x}}$ denote the covariance matrix of the input vector $\mathbf{x}$. Then the output covariance matrix $\mathbf{R}_{\mathbf{y}}$ associated with

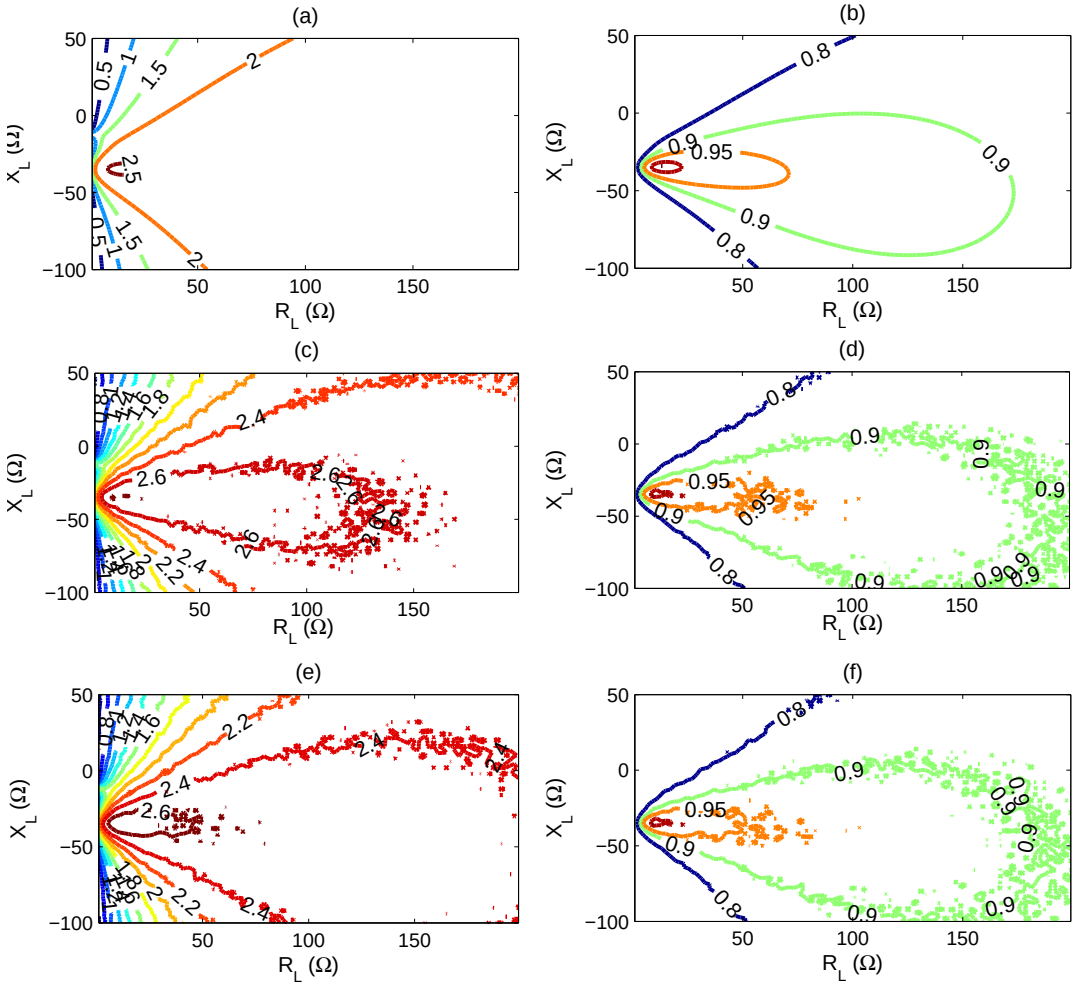

Figure 4.2: *Mean capacity of a 3×3 MIMO system versus the real and imaginary parts of the terminal impedance load for: (a) known channel matrix $\mathbf{H}_{mc}$, (c) channel estimate $\hat{\mathbf{H}}_{mc}$ in (4.11), and (e) channel estimate $\hat{\mathbf{H}}_{mc}$ in (4.15). Contour plots of the capacity values normalised to the corresponding maximum values are shown in the right-hand-side sub-figures (b),(d),(f).*

the received signal vector $\mathbf{y}$ can be written as:

$$\begin{aligned}\mathbf{R}_{\mathbf{y}} &= E\{\mathbf{y}\mathbf{y}^H\} \\ &= \mathbf{H}_{mc}E\{\mathbf{x}\mathbf{x}^H\}\mathbf{H}_{mc}^H + E\{\mathbf{n}\mathbf{n}^H\} \\ &= \mathbf{H}_{mc}\mathbf{R}_{\mathbf{x}}\mathbf{H}_{mc}^H + \sigma_n^2\mathbf{I}_M \end{aligned} \tag{4.16}$$

where $(\cdot)^H$ is conjugate-transpose operator, and $\mathbf{x}$ and $\mathbf{n}$ are assumed to be uncorrelated. In other words, $E\{\mathbf{x}\mathbf{n}^H\} = E\{\mathbf{n}\mathbf{x}^H\} = \mathbf{0}$. From the above equation and (4.8) it can be seen that we could use (an estimation of) the covariance matrix of the received signals to calculate the capacity, rather than estimating a channel model including the mutual coupling effect[1]. One way of implementing this idea is substituting a time averaged estimation of $\mathbf{R}_{\mathbf{y}}$ given by

$$\mathbf{R}_{\mathbf{y}} = E\{\mathbf{y}\mathbf{y}^H\} \approx \frac{1}{L}\sum_{k=k_0}^{k_0+L-1}\mathbf{y}[k]\mathbf{y}^H[k] \tag{4.17}$$

into the argument of $\log_2 \det$ function at (4.8) as follows

$$\hat{C} = \log_2 \det\left(\frac{1}{\sigma_n^2 L}\sum_{k=k_0}^{k_0+L-1}\mathbf{y}[k]\mathbf{y}^H[k]\right) \tag{4.18}$$

where k_0 is the starting sample time, L is the data-block length, and k is the time index for discrete-time samples. We further assume that the block length L is long enough for equation (4.17) to hold, and that $\mathbf{H}$ does not change over each symbol-block. Now, we have an expression for the capacity that includes propagation channel properties and mutual coupling effects by having a block of received data with no further parameters required.

The mean capacity of a 3×3 MIMO system versus the real and imaginary parts of the terminal impedance loads, is shown in Figure 4.3 for the following scenarios: (i) using (4.9) when the actual channel matrix $\mathbf{H}_{mc}$ in known , and (ii) using (4.18) and the estimated covariance matrix per block. The results are averaged over 100 channel realisations for a block length of $L = 1000$ symbols, SNR $= 10$ dB, and $d = 0.05\lambda$. The noise power is assumed to be $\sigma_n^2 = -20$ dB for the simulation results. Although there is a large bias between the capacity values for known channel matrix and the estimated covariance matrix, we see that the choice of load impedances to maximise the capacity for both approaches are roughly the same. Therefore, we can use this method to find the optimum load impedance which maximises the actual capacity. We

[1]This estimation is valid when we have a white additive noise at the receiver

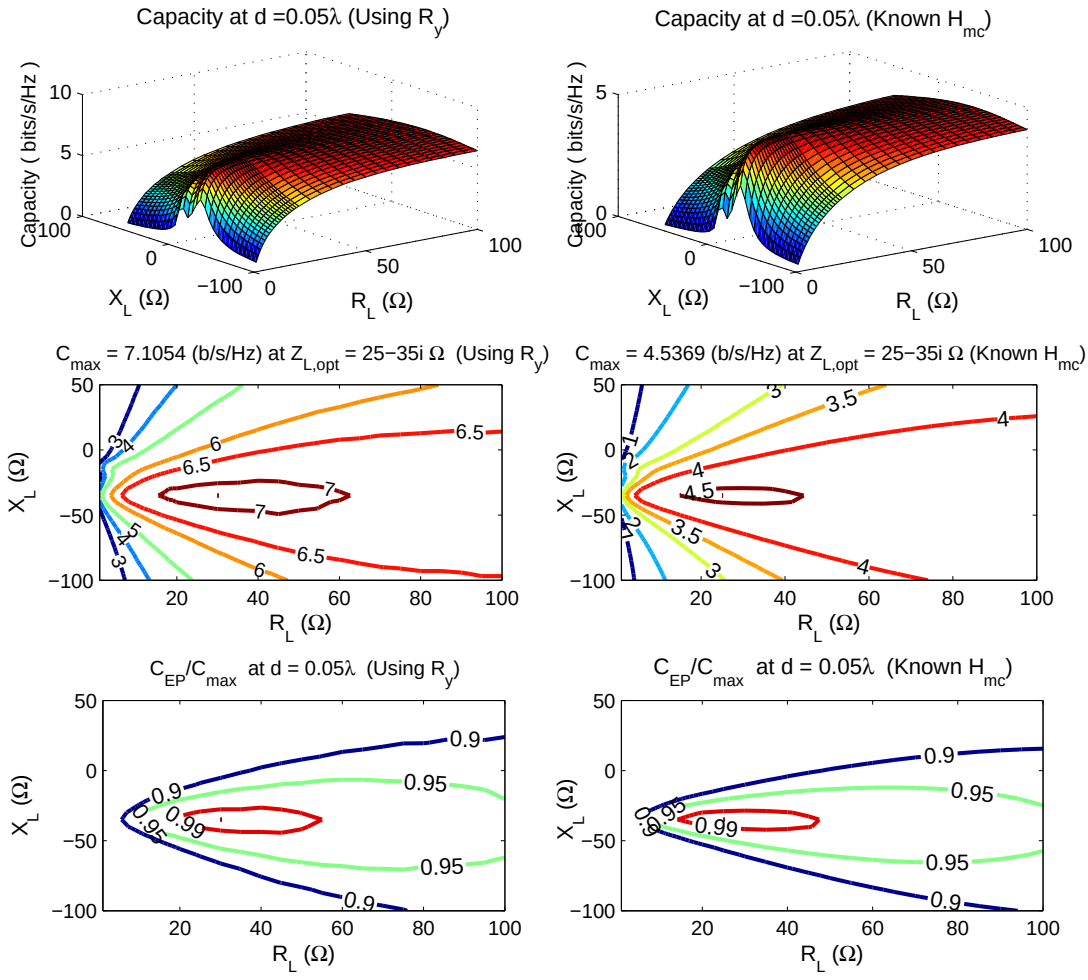

Figure 4.3: *Mean capacity of a* 3×3 *MIMO system using the covariance matrix estimate* $\hat{\mathbf{R}}_y$ *and the actual channel matrix* $\mathbf{H}_{mc}$ *over* 100 *channel realisations, with the symbol-block length of* $L = 1000$ *symbols, SNR* $= 10$*dB, and the element spacing* $d = 0.05\lambda$.

further investigate this approach by calculating the singular values of the covariance matrix estimate $\hat{\mathbf{R}}_\mathbf{y}$ and $\mathbf{H}_{mc}\mathbf{H}_{mc}^H$ as shown in Figure 4.4 versus the real and imaginary parts of $z_L = r_L + jx_L$. It confirms that such estimation method can be used to track the behaviour of the actual propagation scenario.

Looking back to Section 3.4.3, and assuming $\mathbf{y}[k]$ is the received voltage vector across the resistive parts of the receive antenna terminal loads, the received power for ith antenna can be

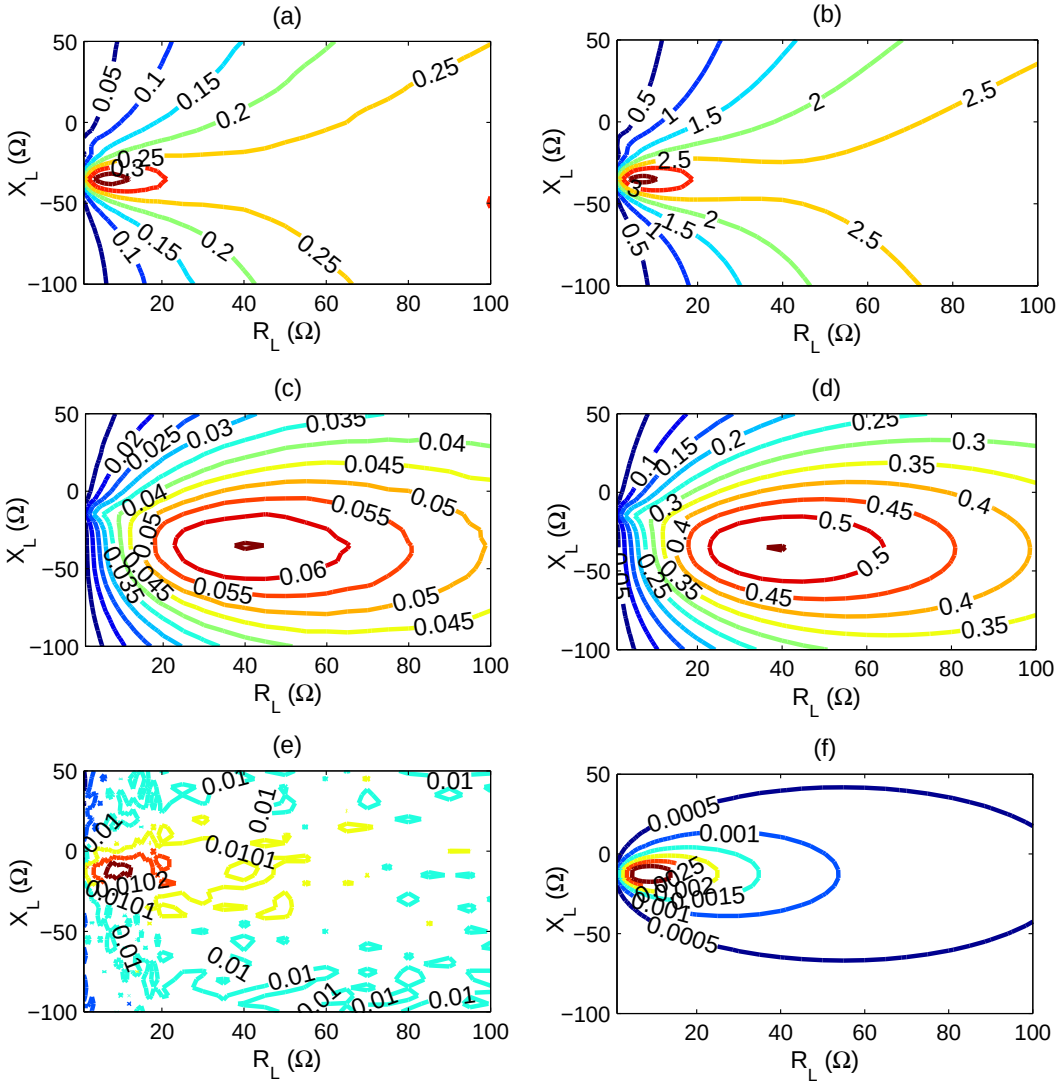

Figure 4.4: *Averaged singular values of the covariance matrix estimate* $\hat{\mathbf{R}}_y$*, and* $(\mathbf{H}_{mc}\mathbf{H}_{mc}^H)$ *for a* 3×3 *MIMO system with the symbol-block length of* $L = 1000$ *symbols, over* 100 *channel realisations. Singular values are in descending order so that* $(\sigma_1 > \sigma_2 > \sigma_3)$ *for: (a) averaged* σ_1 *of* $\hat{\mathbf{R}}_y$*, (b) averaged* σ_1 *of* $(\mathbf{H}_{mc}\mathbf{H}_{mc}^H)$*, (c) averaged* σ_2 *of* $\hat{\mathbf{R}}_y$*, (d) averaged* σ_2 *of* $(\mathbf{H}_{mc}\mathbf{H}_{mc}^H)$*, (e) averaged* σ_3 *of* $\hat{\mathbf{R}}_y$*, (f) averaged* $(\mathbf{H}_{mc}\mathbf{H}_{mc}^H)$*.*

written as

$$P_{r,i} = \left(\frac{1}{P_0}\right) E\left\{\frac{y_i[k]y_i^*[k]}{r_{L,i}}\right\}, \qquad i = 1, \cdots, M \tag{4.19}$$

where $(\cdot)^*$ denotes conjugate operator, $r_{L,i}$ represents the real part of the load impedance $z_{L,i}$ for antenna i, and P_0 is the power received by a conjugate matched isolated antenna which is used to normalise the MIMO received power. Assuming identical load impedances, the *total mean received power* can be expressed as

$$P_r = \left(\frac{1}{P_0}\right) E\left\{\frac{1}{r_L}\mathbf{y}[k]\mathbf{y}^H[k]\right\} \tag{4.20}$$

Similar to the estimation procedure for the capacity, we can estimate the total received power from the following expression

$$\hat{P}_r = \frac{1}{P_0}\left(\frac{1}{Lr_L}\sum_{k=k_0}^{k_0+L-1}\mathbf{y}[k]\mathbf{y}^H[k]\right). \tag{4.21}$$

The total mean received power using the covariance matrix estimate $\hat{\mathbf{R}}_{\mathbf{y}}$, versus the real and imaginary parts of z_L for the previous scenario is shown in Figure 4.5. We see that there are choices of z_L that maximise the received power. Therefore, the adaptive impedance matching technique can also be applied to improve the received power in the presence of mutual coupling effects.

4.6 Optimisation Techniques

In this chapter, we examine *Gradient-ascent, Newton-Raphson,* and *random search* techniques to determine the vector $\Delta\mathbf{z}$ for the *identical* loading. The results can easily be extended to the *non-identical* impedance termination. We shall now discuss these three methods in turn.

4.6.1 Gradient ascent method

Suppose the function f, representing the desired performance metric, is differentiable with respect to the variables r_L and x_L. Using the Gradient ascent method [77], we can find a

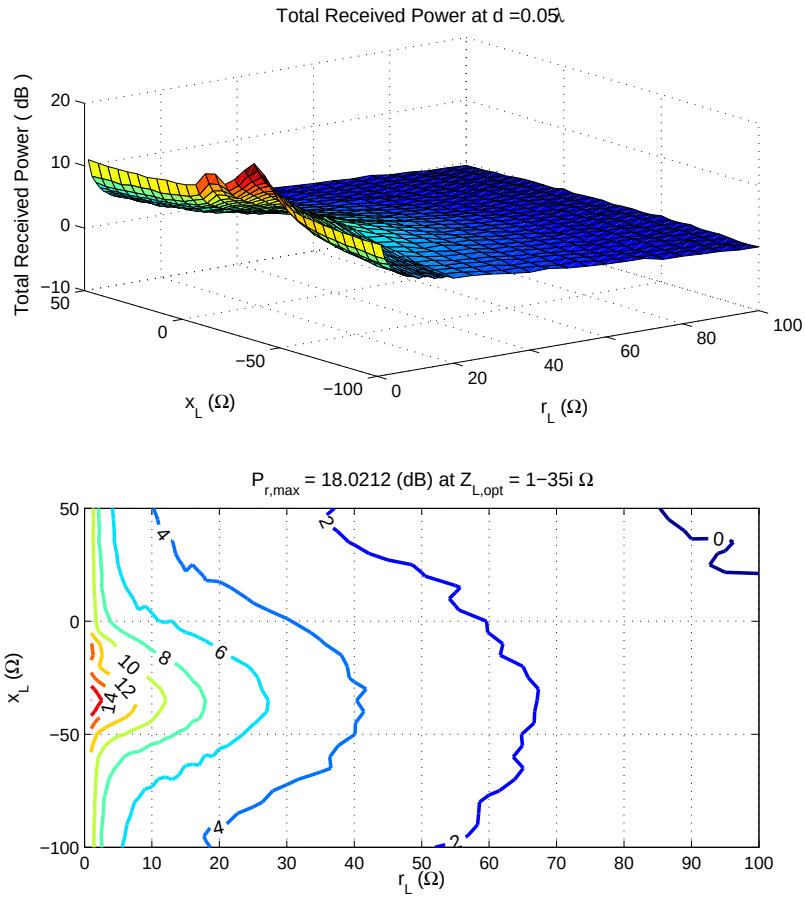

Figure 4.5: *Total received power in dB calculated using the covariance matrix estimate* $\hat{\mathbf{R}}_y$ *over* 1000 *channel realisations, with the symbol-block length of* $L = 1000$ *symbols, SNR* $= 10$ *dB, the element spacing* $d = 0.05\lambda$*,* $P_0 = 1$*, and* $\sigma_n^2 = 1$*.*

solution for (4.6) by substituting $\Delta\mathbf{z} = \nabla f(\mathbf{z})$ into (4.7) as follows

$$\mathbf{z}^{(m+1)} = \mathbf{z}^{(m)} + \alpha^{(m)} \nabla f(\mathbf{z}^{(m)}) \tag{4.22}$$

where $\mathbf{z}^{(m)} = [r_L^{(m)}, x_L^{(m)}]^T$ is the value of the vector of variables at iteration number m, and $\alpha^{(m)} > 0$ here is called step size. The term $\nabla f(\mathbf{z}^{(m)})$ represents the gradient of f with respect to the entries of $\mathbf{z}$ at iteration m, given by

$$\nabla f(r_L, x_L) = \left[\frac{\partial f}{\partial r_L}, \frac{\partial f}{\partial x_L} \right]^T. \tag{4.23}$$

As stated previously, usually no parameter is known for practical systems except the received signals, and the termination impedance network (which can be controlled by the optimisation algorithm). Therefore the gradient term at (4.22) has to be estimated.

One way of calculating the gradient is to use the following forward differences [80]

$$\frac{\partial f}{\partial r_L} \approx \frac{f(r_L + \Delta r, x_L) - f(r_L, x_L)}{\Delta r} \tag{4.24}$$

$$\frac{\partial f}{\partial x_L} \approx \frac{f(r_L, x_L + \Delta x) - f(r_L, x_L)}{\Delta x}. \tag{4.25}$$

This means for each estimation value of ∇f, we need three channel estimates. Such an estimation approach is more suitable for optimising the received power. To examine the Gradient-based methods for the capacity, we rewrite the instant capacity and change the notation of the argument of $\log_2 \det$ function as follows

$$C_{inst}(r_L, x_L) = \log_2 \det(\mathbf{I}_M + \frac{\rho}{N} \mathbf{H}_{mc} \mathbf{H}_{mc}^H) \tag{4.26a}$$

$$= \log_2 \det(\mathbf{I} + \mathbf{A}\mathbf{A}^H) \tag{4.26b}$$

$$= \log_2 \det(\mathbf{Y}). \tag{4.26c}$$

Since $\log(\cdot)$ is a monotonically increasing function, we consider $f(r_L, x_L) = \det(\mathbf{Y})$ and maximise it with respect to r_L and x_L. Using the following rule of matrix algebra [81]

$$\frac{\partial \det(\mathbf{Y})}{\partial t} = \det(\mathbf{Y}) \operatorname{Tr}\left[\mathbf{Y}^{-1} \frac{\partial \mathbf{Y}}{\partial t} \right] \tag{4.27}$$

we have

$$\nabla f = \begin{bmatrix} \dfrac{\partial f}{\partial r_L} \\ \dfrac{\partial f}{\partial x_L} \end{bmatrix} = \begin{bmatrix} \det(\mathbf{Y}) \operatorname{Tr}\left[\mathbf{Y}^{-1}\dfrac{\partial \mathbf{Y}}{\partial r_L}\right] \\ \det(\mathbf{Y}) \operatorname{Tr}\left[\mathbf{Y}^{-1}\dfrac{\partial \mathbf{Y}}{\partial x_L}\right] \end{bmatrix} \tag{4.28}$$

where

$$\frac{\partial \mathbf{Y}}{\partial r_L} = \frac{\partial}{\partial r_L}\left(\mathbf{A}\mathbf{A}^H\right) = \left(\frac{\partial \mathbf{A}}{\partial r_L}\right)\mathbf{A}^H + \mathbf{A}\left(\frac{\partial \mathbf{A}}{\partial r_L}\right)^H \tag{4.29}$$

$$\frac{\partial \mathbf{Y}}{\partial x_L} = \frac{\partial}{\partial x_L}\left(\mathbf{A}\mathbf{A}^H\right) = \left(\frac{\partial \mathbf{A}}{\partial x_L}\right)\mathbf{A}^H + \mathbf{A}\left(\frac{\partial \mathbf{A}}{\partial x_L}\right)^H. \tag{4.30}$$

Now we can estimate $\partial\mathbf{A}/\partial r_L$ and $\partial\mathbf{A}/\partial x_L$ terms from (4.24) and (4.25), where

$$\mathbf{A} = \sqrt{\rho/N}\mathbf{H}_{mc}. \tag{4.31}$$

According to the above equations, to calculate an estimate of $\nabla f(r_L, x_L)$, at least three channel estimates corresponding to the load impedances $z_{L1} = r_L + jx_L$, $z_{L2} = (r_L + \Delta r) + jx_L$, and $z_{L3} = r_L + j(x_L + \Delta x)$ are required. We numerically examined the Gradient-based method for the capacity of a 3×3 MIMO system with different Δr and Δx values. This method can converge to the optimum load impedance if we choose a proper step size $\alpha^{(m)}$ for each channel realisation. Furthermore, convergence rate of the Gradient-based method depends on the quantisation level of $\mathbf{z}^{(m)}$.

4.6.2 Newton-Raphson method

In this subsection, we present the Newton-Raphson method to solve the optimisation problem (4.6). Assume that f is at least twice differentiable with respect to the real and imaginary parts of the termination impedances. Then $\Delta\mathbf{z}$ from (4.7) for the Newton-Raphson method is defined as [77]

$$\Delta\mathbf{z} = [\nabla^2 f(\mathbf{z})]^{-1}\nabla f(\mathbf{z}) \tag{4.32}$$

where $\nabla^2 f$ denotes the Hessian matrix of f whose entry (i, j) is given by $[\nabla^2 f(\mathbf{z})]_{ij} = \partial^2 f/\partial z_i \partial z_j$ when it exists [80]. Substituting (4.32) and $\alpha^{(m)} = 1$ for the pure Newton-Raphson method into (4.7), we obtain

$$\mathbf{z}^{(m+1)} = \mathbf{z}^{(m)} + [\nabla^2 f(\mathbf{z}^{(m)})]^{-1}\nabla f(\mathbf{z}^{(m)}). \tag{4.33}$$

As mentioned earlier, the function f is unknown for practical systems. Therefore, we need to estimate $\Delta\mathbf{z}$ from the knowledge of the received signals and termination network. Assuming the identical loading case, the gradient term for $f(r_L, x_L)$ could be estimated from (4.24) and (4.25). Furthermore, the Hessian matrix $\nabla^2 f$ can be estimated by applying the partial derivative approximations from equations (4.34)-(4.37).

$$\frac{\partial^2 f}{\partial r_L^2} \approx \frac{f(r_L + 2\Delta r, x_L) - 2f(r_L + \Delta r, x_L) + f(r_L, x_L)}{\Delta r^2}, \tag{4.34}$$

$$\frac{\partial^2 f}{\partial x_L^2} \approx \frac{f(r_L, x_L + 2\Delta x) - 2f(r_L, x_L + \Delta x) + f(r_L, x_L)}{\Delta x^2}, \tag{4.35}$$

$$\frac{\partial^2 f}{\partial r_L \partial x_L} \approx \frac{f(r_L + \Delta r, x_L + \Delta x) - f(r_L + \Delta r, x_L) - f(r_L, x_L + \Delta x) + f(r_L, x_L)}{\Delta r \Delta x} \tag{4.36}$$

$$\frac{\partial^2 f}{\partial x_L \partial r_L} = \frac{\partial^2 f}{\partial r_L \partial x_L}. \tag{4.37}$$

Therefore, for each estimate of the Hessian matrix $\nabla^2 f$, six estimate values of f and at least six channel estimates corresponding to the following load impedances: $z_{L1} = r_L + jx_L$, $z_{L2} = (r_L + \Delta r) + jx_L$, $z_{L3} = (r_L + 2\Delta r) + jx_L$, $z_{L4} = r_L + j(x_L + \Delta x)$, $z_{L5} = r_L + j(x_L + 2\Delta x)$, and , $z_{L6} = (r_L + \Delta r) + j(x_L + \Delta x)$ are required. We numerically evaluated the Newton-Raphson method for a 3×3 MIMO system. This method failed to converge for all possible conditions we applied to the numerical study. It might be due to complexity of the second order derivative approximations.

4.6.3 Random Search method

In this subsection, we explain how the adaptive algorithm can use a random search (motivated by random phase selection [82] and random walk [83] algorithms) for the optimum load impedance. Assuming an identical loading network, and describing the receive array load network (4.5) as $\mathbf{Z}_L = z_L^{(m+1)}\mathbf{I}_M$ at iteration $(m+1)$, the impedance load $z_L^{(m+1)}$ is obtained from the following equation:

$$z_L^{(m+1)} = z_{opt}^{(m)} + \Delta z^{(m)}, (m = 0, 1, \cdots, N_s - 1) \tag{4.38}$$

where $z_{opt}^{(m)}$ is the optimum load at mth iteration (it can be initialised by $z_{opt}^{(0)} = Z_0$), the non-zero scalar $\Delta z^{(m)}$ denotes a complex step size randomly selected from the set $\{\pm\Delta r, \pm j\Delta x, (\pm\Delta r \pm$

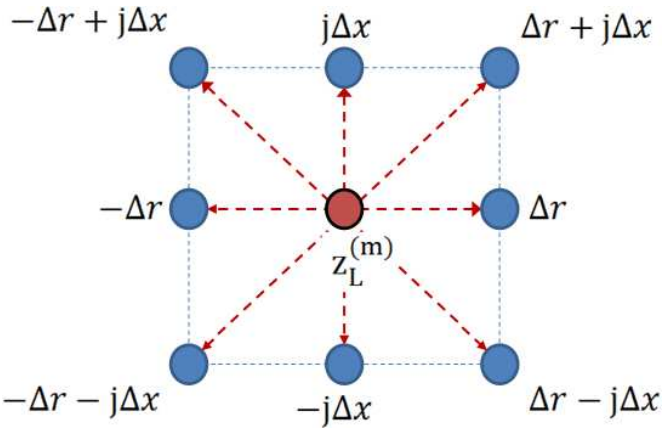

Figure 4.6: *Complex step size $\Delta z^{(m)}$ at iteration m is selected randomly from the set $\{\pm\Delta r, \pm j\Delta x, (\pm\Delta r \pm j\Delta x)\}$ with an equal probability.*

$j\Delta x)\}$ with an equal probability, and N_s is the number of load network variations. An overview of the choice of step size $\Delta z^{(m)}$ at iteration m is shown in Figure 4.6. In practice, N_s can be estimated from the experimental data, or in a similar way the algorithm can stop after having no change in the optimal load network for a specific number of iterations while a small step size is used.

At each iteration $(m+1)$, the capacity or received power is calculated (or estimated from the knowledge of the received signals) and compared to the previous value corresponds to $z_{opt}^{(m)}$. The impedance which corresponds to the higher capacity/received power is held as the optimum load $z_{opt}^{(m+1)}$ for the $(m+1)$th iteration. Fig. 4.7 illustrates the flowchart of the proposed algorithm for identical loading.

4.7 Simulation Results

To investigate the proposed adaptive matching algorithm, some simulations for a 3×3 MIMO system of half-wavelength dipoles with identical loads at antenna spacing $d = 0.05\lambda$ is carried out. We optimize the mean capacity under different propagation environments: 2D uniform, and 2D Laplacian defined by the mean ϕ_0 and the standard deviation σ of the distribution, for two SNR values of 5 and 20 dB at the receiver. We assume the transmit antennas to be separated far enough (negligible mutual coupling effect at the transmit side) and to be self-impedance conjugate matched. The mean capacity is calculated using (4.9) for both non-adaptive and adaptive matching methods. The received signal vector $\mathbf{y}$ is calculated from (4.1) by generating a com-

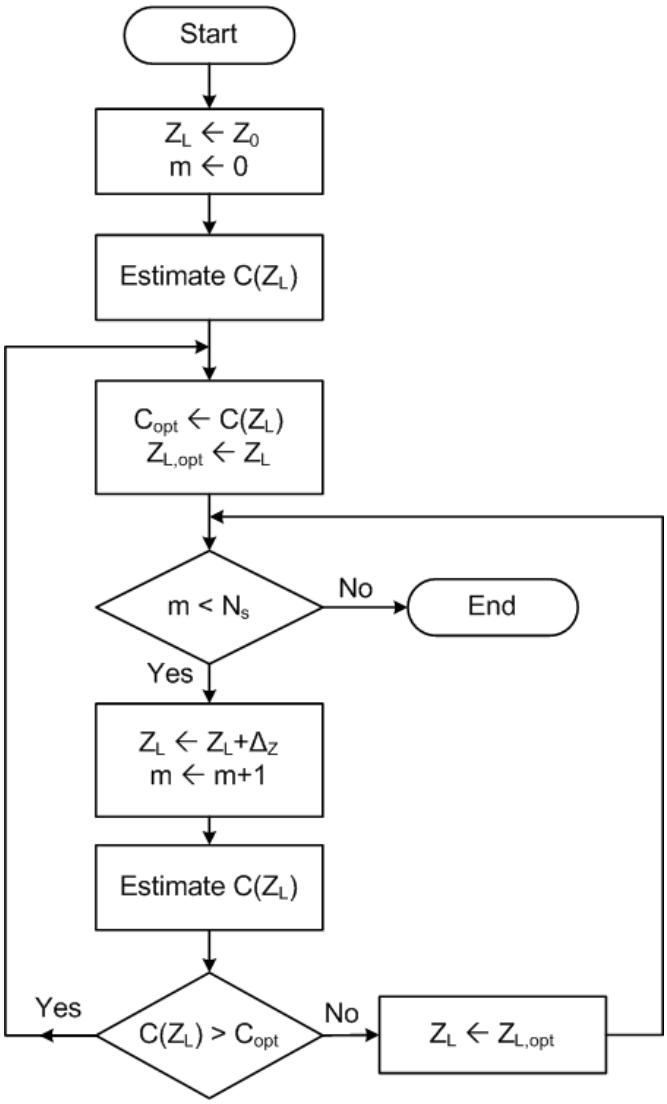

Figure 4.7: *Flowchart of the proposed adaptive termination approach.*

Capacity (bits/s/Hz)	Uniform	Laplacian ($0°$, $40°$)	Laplacian ($90°$, $67°$)
SNR $= 5$ dB, $z_L = 50\Omega$	2.20	1.87	2.10
SNR $= 5$ dB, optimum z_L	2.58	2.18	2.61
SNR $= 20$ dB, $z_L = 50\Omega$	9.83	8.92	8.98
SNR $= 20$ dB, optimum z_L	10.51	9.56	9.61
Optimum $z_L(\Omega)$	Uniform	($0°$, $40°$)	($90°$, $67°$)
SNR $= 5$ dB	$14 - j34$	$98 - j54$	$9 - j34$
SNR $= 20$ dB	$32 - j39$	$44 - j33$	$30 - j37$

Table 4.1: *Optimized mean capacity and the corresponding load impedances $z_L(\Omega)$ for the uniform and Laplacian (ϕ_0,σ) scattering distributions.*

plex Gaussian transmit signal $\mathbf{x}$ with zero-mean and $\sigma_x^2 = \text{SNR} = \{5, 20 \text{ dB}\}$ variance, and the channel matrix $\mathbf{H}_{mc}$ is given by (3.58). The matrix $\mathbf{H}_w$ entries are complex Gaussian random variables of zero-mean and average power of unity, $\mathbf{\Psi}_T$ and $\mathbf{\Psi}_R$ are the spatial correlation matrices at the transmit and receive ends, respectively. Furthermore, we assume $\mathbf{\Psi}_T = \mathbf{I}$, data block length $L = 2000$.

Figure 4.8 shows contour plots of the mean capacity versus the real and imaginary parts of $z_L = r_L + jx_L$ where $r_L \in (0, 100]\Omega$ and $x_L \in [-100, 50]\Omega$, for different propagation scenarios: uniform (a)-(b), and Laplacian with $(\phi_0, \sigma) = (0°, 40°)$ for (c)-(d), and $(90°, 67°)$ for (e)-(f). We note that the magnitudes of the correlation coefficient for these two set of Laplacian parameters are equal. The received SNR $= 5$ dB for the left column (subfigures (a),(c),(e)) and 20 dB for (b),(d) and (f) is considered. It can be seen that the mean capacity at any case can be maximized by selecting a proper load z_L (black square marked points). Maximum values of the mean capacity and the corresponding terminal loads (optimum z_L) are shown in Table 4.1. The mean capacity values corresponding to the characteristic impedance match ($z_L = 50\Omega$) are also shown to evaluate the performance of the impedance matching approach. We can see that at least 17% capacity improvement for SNR = 5 dB can be achieved. This improvement for SNR = 20 dB is about 7%. A brief look at the table reveals that the optimum load depends on different factors of the propagation environment. Therefore, existence of an adaptive matching approach would be necessary in practice.

We first investigate using the Gradient algorithm for the adaptive impedance matching technique. Figure 4.9 shows the convergence behaviour of this method for one channel realisation applying different values of the step size α. Since the mutual coupling model in our problem is unknown, we can not separate the channel matrix $\mathbf{H}$ from the total channel matrix $\mathbf{H}_{mc}$ which

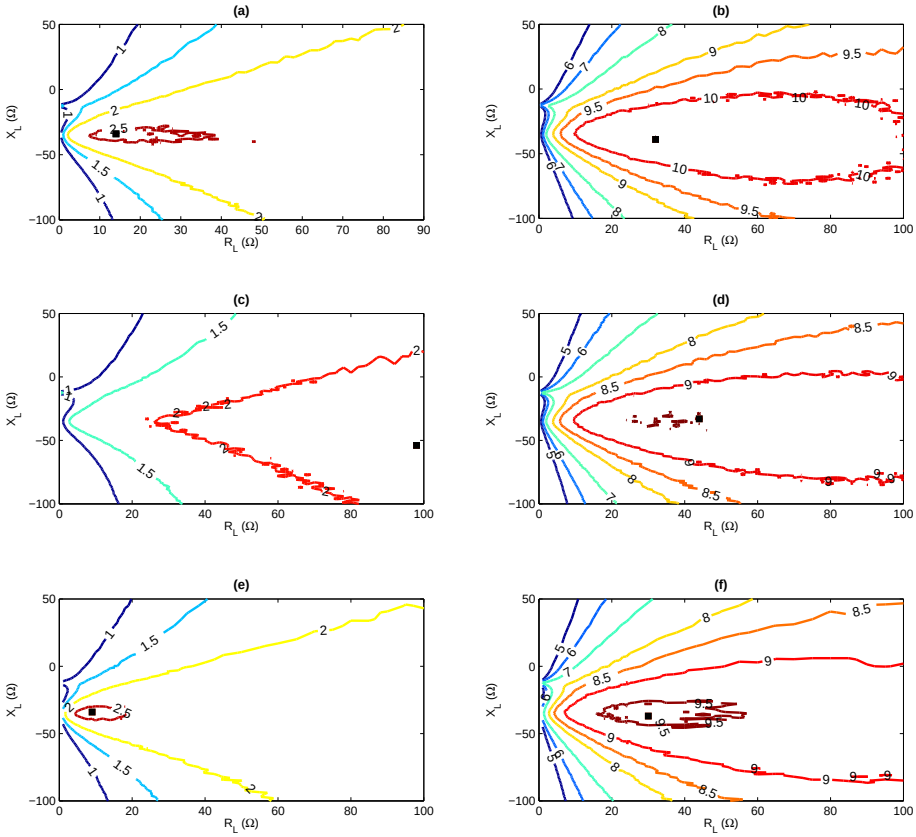

Figure 4.8: *Mean capacity versus real and imaginary parts of the antenna load impedance Z_L for uniform ((a) and (b)) and Laplacian distributions with $(\phi_0, \sigma) = (0°, 40°)$ at (c)-(d), and $(90°, 67°)$ at (e)-(f). Signal to noise ratio 5 dB for (a),(c),(e) and 20 dB for (b),(d) and (f) is considered. The optimum loads which maximise the mean capacity are marked by black squares for all cases.*

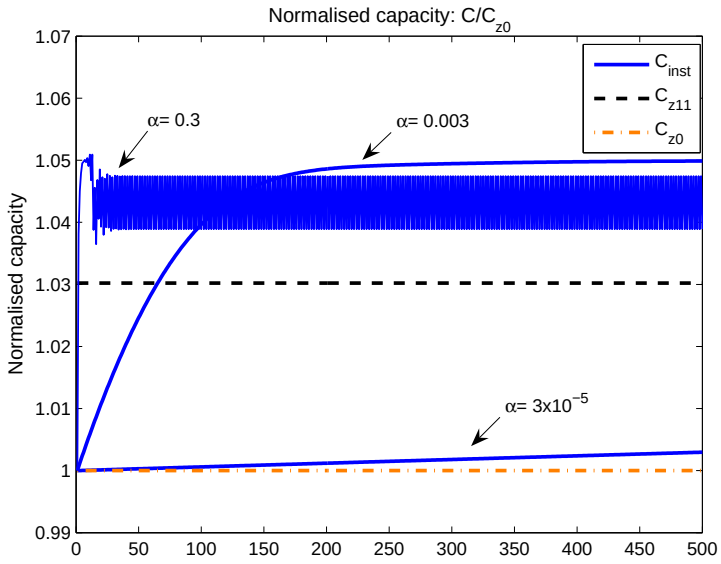

Figure 4.9: *Normalised capacity of one channel realisation using the Gradient-based adaptive identical impedance matching technique for different step size values.*

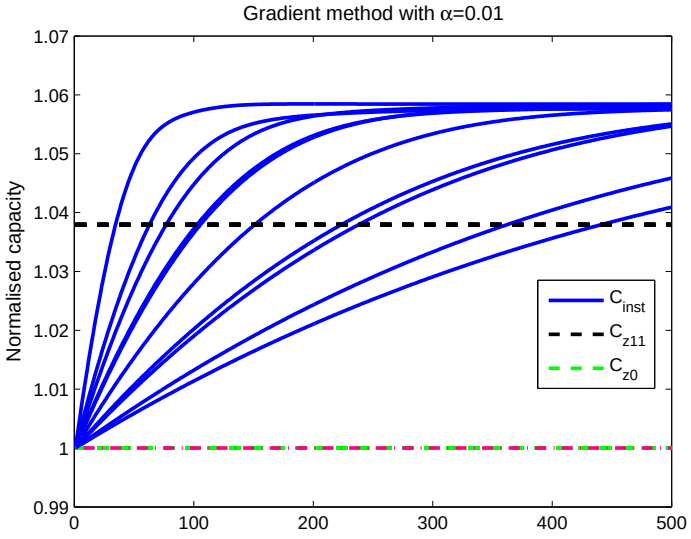

Figure 4.10: *Normalised capacity values for 10 channel realisations using the adaptive impedance matching by applying Gradient algorithm with the step size* $\alpha = 0.01$.

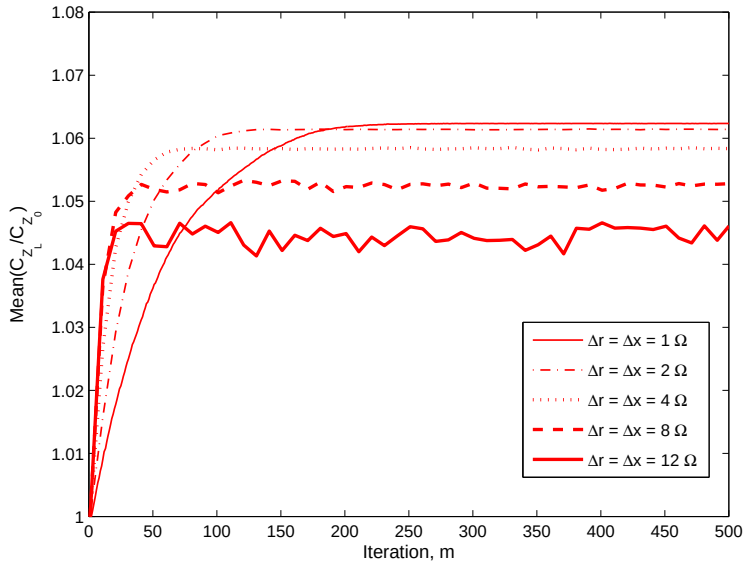

Figure 4.11: *Normalised mean capacity versus the iteration number m for adaptive identical impedance matching approach using random search algorithm for different values of $\Delta r = \Delta x$. The channel is known to the receiver.*

includes the mutual coupling effects and can be measured/estimated from the received signals (refer to (4.2)). However, assuming known $\mathbf{H}$ we applied the following normalisation

$$\mathbf{H} = \sqrt{NM}\frac{\mathbf{H}}{||\mathbf{H}||_F} \tag{4.39}$$

to further investigate the Gradient-based adaptive impedance match. As we see from Figure 4.10, even for normalised $\mathbf{H}$, we still need to adjust the step size α for each channel matrix using the Gradient-based method. In addition to the above issue, convergence of this method is affected by the quantisation error of the load impedance. We recall that for identical impedance loads, at each iteration we need at least 3 channel estimates.

Alternatively, we use the random search algorithm for the adaptive (identical) impedance matching technique. Such an algorithm can converge to the optimum load for each channel realisation. Figure 4.11 shows the normalised mean capacity for 200 channel realisations for adaptive identical impedance matching using random search algorithm. In this work, we consider several values for the step sizes $\Delta r, \Delta x$ from the range of $1\Omega - 12\Omega$. Larger values of Δr and Δx result in a faster convergence but lower steady-state performance compared to the smaller step sizes. So to obtain improved performance, the algorithm can start with a large step size and then

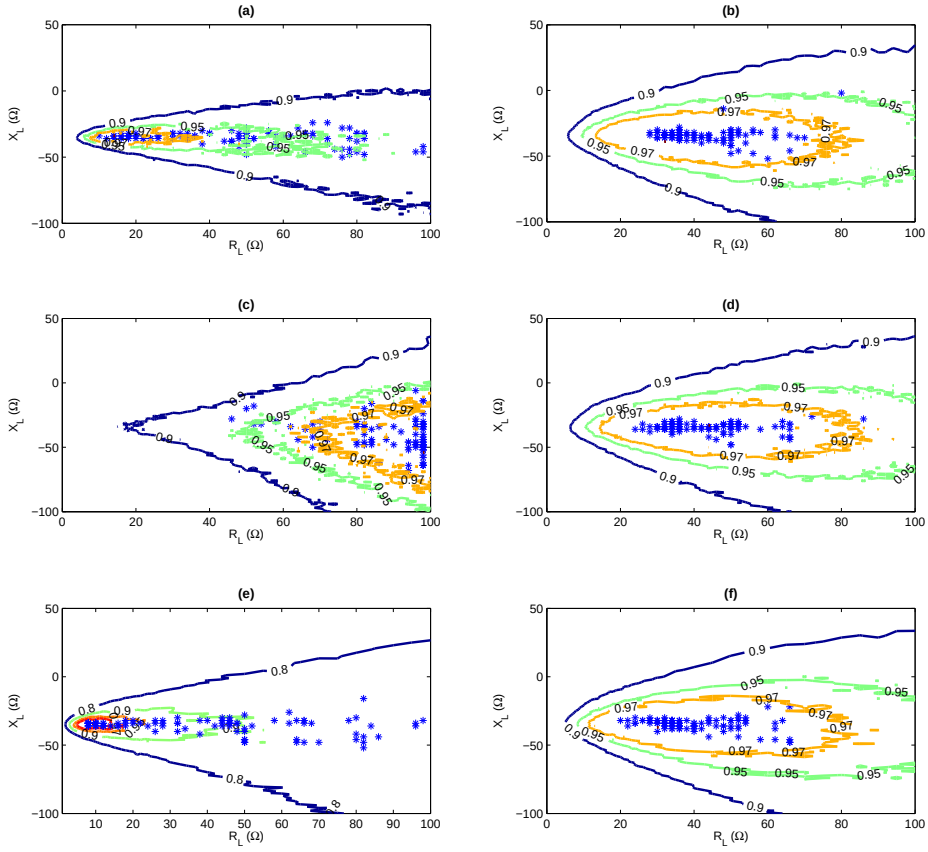

Figure 4.12: *Adaptive matching results for 100 runs (asterisk marked points) with initial load $Z_0 = 50\Omega$ and normalized mean capacity contour for uniform ((a) and (b)) and Laplacian distributions with $(\phi_0, \sigma) = (0°, 40°)$ at (c)-(d), and $(90°, 67°)$ at (e)-(f). $SNR = 5$ dB for (a),(c),(e) and 20 dB for (b),(d) and (f) is considered.*

decrease the step size after having a completed specific number of load variations. Referring back to section 4.6.3, the random search algorithm requires only one channel estimate at each step.

The results of 100 Monte Carlo runs of the adaptive matching algorithm with initial load $z_0 = 50\Omega$ and 50 steps per execution, are shown with asterisk marked points in Figure 4.12. Additionally, the mean capacity contours normalized to their corresponding maximum values are plotted to evaluate the adaptive algorithm results. We observe that the adaptive algorithm has found an optimum load which gives a mean capacity higher than 97% of the maximum mean capacity value at Table 4.1 for SNR $= 20$ dB. For the lower SNR case, the algorithm still goes to the area of 97% and 95% of the maximum C_{mean} for propagation scenario (c), and (a) respectively. It means we have more than 16% capacity improvement for (c), and (a) . However, this improvement is about 7% for (f). This performance could be improved by trying different initial load impedances or longer block lengths L.

As it is shown in the simulation results, the proposed adaptive matching algorithm can be used to improve the compact MIMO performance by choosing a proper antenna load impedance based on the received signals. This algorithm does not require any knowledge of the channel or mutual coupling model which are practical issues for previous studies. So, it could be a practical solution to deal with mutual coupling effects in compact MIMO systems.

4.8 Conclusion

In this chapter we proposed the idea of adaptive impedance match for compensating the performance degradation of compact MIMO systems due to the mutual coupling. Although some studies have suggested impedance matching networks to counteract the mutual coupling effects, they can not detect and compensate the time variations of the propagation channel and the mutual coupling. Simulation results show that a capacity improvement of at least 7% can be achieved for all propagation scenarios.

In order to implement the adaptive impedance match, we reviewed some estimation methods for the received power and the capacity. Then we examined three optimisation techniques: Gradient-ascent, Newton-Raphson, and random-search. We observed that random search technique can achieve the optimum load for different propagation scenarios.

Chapter 5
Adaptive Non-identical Impedance Matching Network

5.1 Introduction

In Chapter 4, we investigated the idea of *adaptive impedance matching network* for a MIMO system equipped with a coupled receive array terminated with *identical* impedance loads. We examined three optimisation techniques: *Gradient-based*, *Newton-Raphson*, and *random-search* in order to tune terminal loads iteratively. We found the random-search to be a simple method converging to the optimum load impedance which maximises the performance metric (the mean capacity or the received power), while other approaches were not able to find the optimum load.

In this chapter, we extend the adaptive matching technique to the *non-identical* case in which all impedance loads are tuned individually. We evaluate the performance of adaptive identical and non-identical matching, by comparing their results to the corresponding conventional terminations such as: the characteristic impedance match and the self-impedance conjugate match. We consider quasi-static, and (slow and fast) fading channel models in our investigation.

This chapter is organised as follows. Section 5.2 introduces the model of fading channels for our investigation. Then Section 5.3 describes the non-identical adaptive match in addition to some conventional matching networks such as: characteristic impedance match and self-impedance conjugate match. Next, the performance of both adaptive identical and non-identical impedance matching techniques are investigated in Section 5.4 by comparing the capacity of such techniques with the conventional methods for a 3×3 MIMO system with strong mutual coupling ($d = 0.05\lambda$) at the receiver. The effects of channel fading and channel estimation errors are also considered in our investigation. Finally, this chapter is concluded in Section 5.5.

5.2 System Model

In this chapter, we consider the *adaptive non-identical impedance matching* technique in addition to the *identical* case. In order to investigate the matching performance of both adaptive matching techniques, we include the fast-fading channel model and the channel estimation error into our simulations. We remind the discrete-time baseband input-output relationship described in Section 4.3 as follows

$$\mathbf{y}[k] = \mathbf{H}_{mc}[k]\mathbf{x}[k] + \mathbf{n}[k] \tag{5.1}$$

To describe the time-variation of the channel, we use a Gauss-Markov process model [84] given by

$$\mathbf{H}[k+1] = \sqrt{1-\epsilon}\mathbf{H}[k] + \sqrt{\epsilon}\mathbf{W}[k] \tag{5.2}$$

where $\mathbf{W}[k] \in \mathbb{C}^{M\times M}$ includes complex Gaussian entries with zero-mean and unit-variance. The entries of $\mathbf{W}$ are independent across rows, columns and time indices k. The parameter $\epsilon \in \mathbb{R}, 0 \leq \epsilon \leq 1$ is introduced to control the coherence time of the channel. In [84], some practical ranges for ϵ have been calculated by fitting the above Gauss-Markov model into real systems measurements. For instance

- $3\times 10^{-7} \leq \epsilon \leq 10^{-4}$, for a slow-fading indoor environment with mobile speed 1-5 km/h and carrier frequencies from 800 MHz to 5 GHz.
- $10^{-4} \leq \epsilon \leq 1.8 \times 10^{-3}$, for a slow-fading outdoor environment with mobile speeds of the order of 5 km/h and carrier frequencies from 800 MHz to 5 GHz.
- $\epsilon = 1.8 \times 10^{-2}$, for a fast-fading outdoor environment with mobile speed 50 km/h and carrier frequency 5 GHz.

We consider $\epsilon = 0$ for time invariant or quasi-static, and $\epsilon = 1.8 \times 10^{-3}$ and 1.8×10^{-2} for slow and fast fading channels respectively. We assume that time invariant channel model is described by (3.58).

5.2.1 Channel Estimation

Some channel estimation approaches are discussed in Chapter 4. Here, we rather assume that an estimated channel matrix $\hat{\mathbf{H}}_{mc}[k]$ is available. Considering the channel estimation error, we

can write [85]

$$\mathbf{H}_{mc}[k] = \hat{\mathbf{H}}_{mc}[k] + \mathbf{E}[k] \tag{5.3}$$

where $\mathbf{E}[k]$ is the channel estimation error matrix, whose entries are zero-mean complex Gaussian random variables with variance σ_E^2. For a system with a known channel estimate $\hat{\mathbf{H}}_{mc}$ and a known estimate variance σ_E^2, a lower bound of (4.9) is given by [85]

$$C_{lower} = E_{\mathbf{H}} \left\{ \log_2 \left| \mathbf{I}_M + \frac{1}{1+\sigma_E^2 P_T} \frac{\rho}{N} \hat{\mathbf{H}}_{mc} \hat{\mathbf{H}}_{mc}^H \right| \right\}. \tag{5.4}$$

Throughout this work, we assume that each block includes some training-symbols and at least one channel estimate is obtained by the receiver per symbol-block from the knowledge of transmitted training symbols.

5.3 Impedance Matching Strategies

Here, we extend the proposed adaptive matching technique in Chapter 4 to non-identical case in which all impedance loads are tuned individually. We note that the proposed adaptive match (using either identical or non-identical impedances) only relies on knowledge of the received signals and a training-based channel estimate $\hat{\mathbf{H}}_{mc}$ per symbol-block. We compare the performance of adaptive matching networks to the conventional terminations such as: characteristic impedance match, and self-impedance conjugate match. It is followed by an investigation to the effect of different practical issues such as estimation error, and time-variation of the channel matrix on the matching performance.

5.3.1 Characteristic Impedance Match

All receive antennas are terminated in a characteristic impedance z_0. Therefore, the receive load network $\mathbf{Z}_L$ at (3.58) is set to $z_0\mathbf{I}_M$. This means we have no matching network for this case.

5.3.2 Self-Impedance Conjugate Match

In this termination case, each receive antenna is terminated in the conjugate of its self-impedance. In other words, $\mathbf{Z}_L = \mathrm{diag}(\mathbf{Z}_R^*)$. This termination would result in maximum power transfer to

the load network when there is no mutual coupling between array elements [37].

5.3.3 Adaptive Impedance Match

The previous terminations in subsections 5.3.1 and 5.3.2 do not consider the mutual coupling effects. Here, we extend the proposed adaptive matching technique using random search algorithm described in Chapter 4 to a more general form in which all load impedances are individually tuned. We call this extended form as *adaptive non-identical impedance match*. Inserting diagonal matrix $\mathbf{Z}_L$ from (4.5) into the iterative equation for random search method in (4.38), we obtain

$$\begin{pmatrix} z_{L1}^{(m+1)} & 0 & \cdots & 0 \\ 0 & z_{L2}^{(m+1)} & \cdots & 0 \\ \vdots & \vdots & \ddots & \vdots \\ 0 & 0 & \cdots & z_{LM}^{(m+1)} \end{pmatrix} = \begin{pmatrix} z_{opt1}^{(m)} & 0 & \cdots & 0 \\ 0 & z_{opt2}^{(m)} & \cdots & 0 \\ \vdots & \vdots & \ddots & \vdots \\ 0 & 0 & \cdots & z_{optM}^{(m)} \end{pmatrix} + \begin{pmatrix} \Delta z_1^{(m)} & 0 & \cdots & 0 \\ 0 & \Delta z_2^{(m)} & \cdots & 0 \\ \vdots & \vdots & \ddots & \vdots \\ 0 & 0 & \cdots & \Delta z_M^{(m)} \end{pmatrix} \tag{5.5}$$

where $z_{Li}^{(m+1)}$, $(i = 1, \cdots, M)$, are the selected terminal impedances at $(m+1)$th iteration, $z_{opt,i}^{(m)}$, $(i = 1, \cdots, M)$ are the optimum loads for the mth iteration, and $\Delta z_i^{(m)}$, $(i = 1, \cdots, M)$ are independent random complex step sizes at mth iteration. Each step size $\Delta z_i^{(m)}$, similar to what explained in section 4.6.3, is selected randomly from the set $\{\pm\Delta r, \pm j\Delta x, (\pm\Delta r \pm j\Delta x)\}$ with an equal selection probability. Let us summarise the algorithm to optimise the capacity C as follows.

1. Initialise the array termination load $z_L^{(0)} = z_0$ (or $\mathbf{Z}_L = z_0\mathbf{I}_M$);
2. Estimate the corresponding C from (4.9) for known channel or (5.4) for estimated channel;
3. Set $C_{opt} = C$, and $z_{opt} = z_L^{(0)}$ (or $\mathbf{Z}_{opt} = \mathbf{Z}_L^{(0)}$ for non-identical loading);
4. Calculate the next termination for the following symbol-block from (4.38) or (5.5);
5. Estimate the corresponding C from (4.9) or (5.4);
6. If ($C > C_{opt}$) then ($z_{opt} = z_L$, and $C_{opt} = C$); otherwise $z_L = z_{opt}$ and go back to step 4.

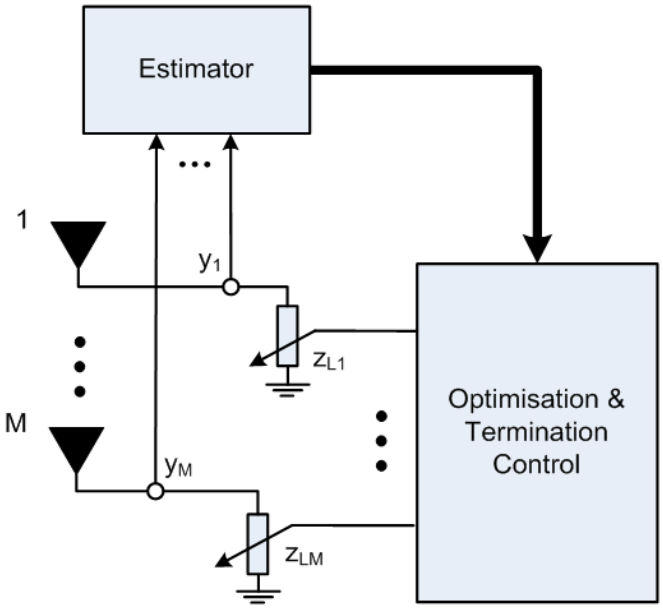

Figure 5.1: *Schematic diagram of the adaptive impedance matching techniques for a compact MIMO system.*

A simplified schematic diagram of the proposed method is shown in Figure 5.1. This method comprises two major parts. One is an estimator which provides instances of the channel matrix $\mathbf{H}_{mc}$ (or the statistical moments of the channel) including the actual effects of the mutual coupling and the time-varying propagation channel. The other part is an adaptive matching network controller which selects the loads to counteract the performance degradation due to the mutual coupling and/or changes of the channel, based on the performance metric estimates (capacity or received power).

This algorithm can also be applied to maximise the received power P_r by substituting P_r from (4.20) or (4.21) for C, and $P_{r,opt}$ for C_{opt}. However, most commonly it is of interest to increase the data rate and the capacity of MIMO wireless systems rather than the received power.

5.4 Investigation of the Adaptive Matching Techniques

In this section we provide a numerical study to evaluate the matching performance of the proposed adaptive termination approach for a 3×3 MIMO system with a coupled receive array. Here, we consider MIMO capacity optimisation, but the result can similarly be extended to the received power as well. We assume linear arrays of identical half-wavelength dipoles are ap-

plied for both transmit and receive sides. The receive array antenna element spacing is assumed to be $d = 0.05\lambda$, where λ is the wavelength, and the transmit antennas are considered to be placed far enough such that we neglect the mutual coupling effect at the transmit side. *Mutual coupling impedances* for the receive array are calculated using the electromotive force (EMF) method [31]. Following our assumptions in sections 4.2 and 5.2, we apply the channel model of (3.58) including a time-variant term $\mathbf{H}_w[k]$, under different scattering distributions: 2D uniform, and a truncated 2D Laplacian defined by the mean angle of incidence $\bar{\phi}$ and an angular spread of 40° for a signal-to-noise-ratio (SNR) 20dB at the receiver. In the following subsections, we consider (i) perfect channel state information (CSI) at the receiver for quasi-static channels, and (ii) imperfect CSI at the receiver for fading channels to investigate the effect of channel estimation error on the performance.

5.4.1 Perfect CSI at the receiver

Let us begin with a simple case that the channel matrix is perfectly known at the receiver. We generate 200 random time-invariant channel realisations assuming a uniform scattering distribution such that the entries of the receive spatial correlation matrix $\mathbf{\Psi}_R$ are given by

$$\Psi_{R,ii} = 1 \qquad (i = 1, 2, \cdots, M) \tag{5.6a}$$

$$\Psi_{R,ij} = J_0\left(\frac{2\pi d}{\lambda}\right) \qquad (i \neq j), (i, j = 1, 2, \cdots, M). \tag{5.6b}$$

Figure 5.2 illustrates the average capacity as a function of real and imaginary parts of the antenna load for a non-adaptive identical impedance match. It shows three different terminating cases of self-impedance match (marked by a square), $z_0 = 50\Omega$ match (marked by a triangle), and the numerically optimum match (marked by a circle) and the corresponding average capacity values. We observe that the average capacity has a maximum for a specific identical termination called the optimum load [6, 7]. The optimal load can be extended to the non-identical case as well [74]. Although these papers revealed the relevance of compact MIMO capacity/received power to the termination, they require prior knowledge of the propagation channel and the mutual coupling model in order to perform a numerical search over all possible termination loads for the optimal load. Furthermore, these studies perform the optimisation process over the mean values of the performance metric(s) with respect to the termination load(s), *whereas our proposed adaptive techniques seek the optimum load network for each channel*

realisation.

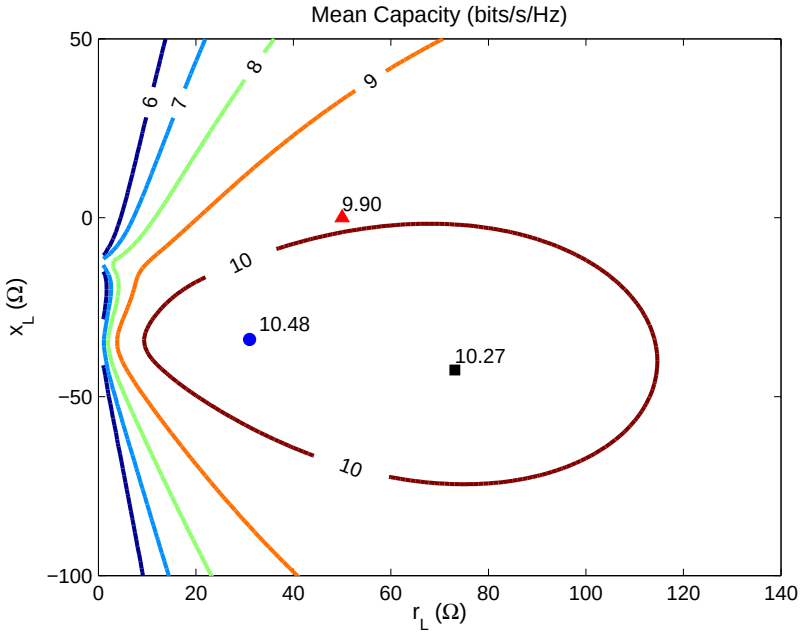

Figure 5.2: *Contour plot of the mean capacity versus real and imaginary parts of the antenna load impedance z_L for uniform scattering distribution at the receiver. Three points are marked for: self-impedance match z_{11}^* (square), $z_0 = 50\Omega$ (triangle), and optimum load z_{opt} (circle) for the identical loading.*

Now, we apply the adaptive uncoupled terminations for the assumed propagation channel scenario. We investigate the effect of having different values of step size Δz by choosing fixed $\Delta r = \Delta x$ values from the set $\{1, 2, 4, 8, 12\}\Omega$. At each iteration, the algorithm applies an estimate of the channel matrix including the realistic mutual coupling effects and selected antenna loads. This is provided from the received signal and knowledge of the training signals. Convergence results of the normalised mean capacity for adaptive identical and non-identical terminations versus the number of changes of the termination network (mth iteration) are illustrated in Figure 5.3. The most significant feature for both termination cases is that applying a smaller step size leads to a higher steady-state performance but requires a longer convergence time. Assuming the same step size for both termination cases, the adaptive identical termination rises sharply and reaches its steady- state about five to ten times faster than the non-identical termination. However, as depicted in Figure 5.3, the adaptive non-identical termination can achieve significantly higher steady state capacity performance albeit with a slower convergence time, for all step sizes except for the case with $\Delta r = \Delta x = 12\Omega$.

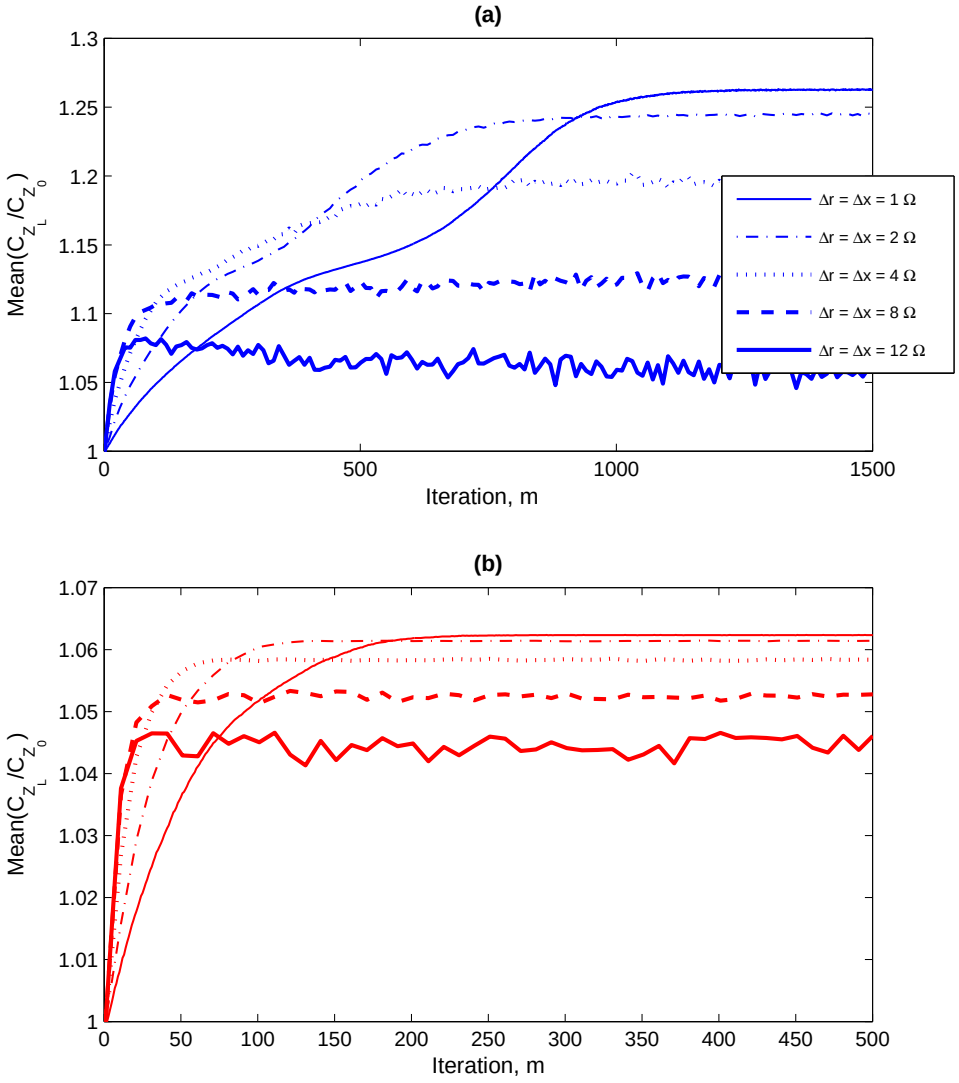

Figure 5.3: *Normalised mean capacity versus iteration number for the adaptive (a) non-identical, and (b) identical uncoupled terminations considering $\Delta r = \Delta x$ values from the set $\{1, 2, 4, 8, 12\}(\Omega)$. We note that part (b) matches Figure 4.11.*

In Figure 5.4, the mean capacity of the system is shown for four different matching networks: adaptive non-identical, adaptive identical, self-impedance conjugate, and $z_0 = 50\Omega$ matched termination networks. Steady state values of the mean capacity for all termination strategies are shown on the right hand side of the figure. In order to achieve a higher steady-state performance in a shorter convergence time, the adaptive algorithm applies a variable step size for both termination cases according to the results reported in Figure 5.3. Therefore, initially $\Delta r = \Delta x$ is assumed to be 8Ω for both termination cases and then reduced to 4Ω, 2Ω, and 1Ω at iterations 100, 400, and 1000 for the non-identical case, and at iterations 30, 80, and 200 for the identical case respectively. As we see, it takes a longer time for the adaptive non-identical impedance matching technique to converge to its steady state value in comparison to adaptive identical matching algorithm and non-adaptive termination scenarios. However, even after a few iterations, the adaptive non-identical matching algorithm can achieve higher capacity improvement.

Any change in the propagation channel or mutual coupling would result in a new optimal $\mathbf{Z}_L$ which may change with time. In order to track these possible changes, the algorithm can also decide to update the selected optimum values of $C_{opt}^{(m)}, \mathbf{Z}_{opt}^{(m)}$ and to increase the step size, whenever $(C^{(m)} - C^{(m-1)})$ is not positive or $C_{opt}^{(m)}$ is not changed for a large number of steps. These occurrences may indicate that the optimal $\mathbf{Z}_L$ has changed and the receiver should find the new best solution.

As we observe from Figure 5.4, both adaptive terminations find an optimum load network which results in a higher mean capacity than the conventional terminations. The adaptive identical case reaches to its steady state performance just after 85 iterations while for the non-identical case it takes about 1000 iterations to achieve to a point above 99% of the steady-state. However, the latter case achieves about 2 (bits/s/Hz) higher capacity gain in the expense of a longer convergence time.

Unlike earlier studies, the adaptive termination algorithm performs the optimisation process over the capacity instances rather than the mean capacity. For further investigation of the adaptive algorithm behaviour, percentage histogram plots of the normalised capacity instances $C/C(z_0)$, and the real and imaginary parts of the termination loads for both adaptive termination cases at iteration number 3000 are shown in Figure 5.5. The y-axes are relative frequencies for the total of 200 channel realisations. Figure 5.5a shows that the capacity instances are improved for both adaptive terminations compared to the conventional $z_0 = 50\Omega$ match by at least 20% for the non-identical case and by 5% for the identical loading case. As can be seen from

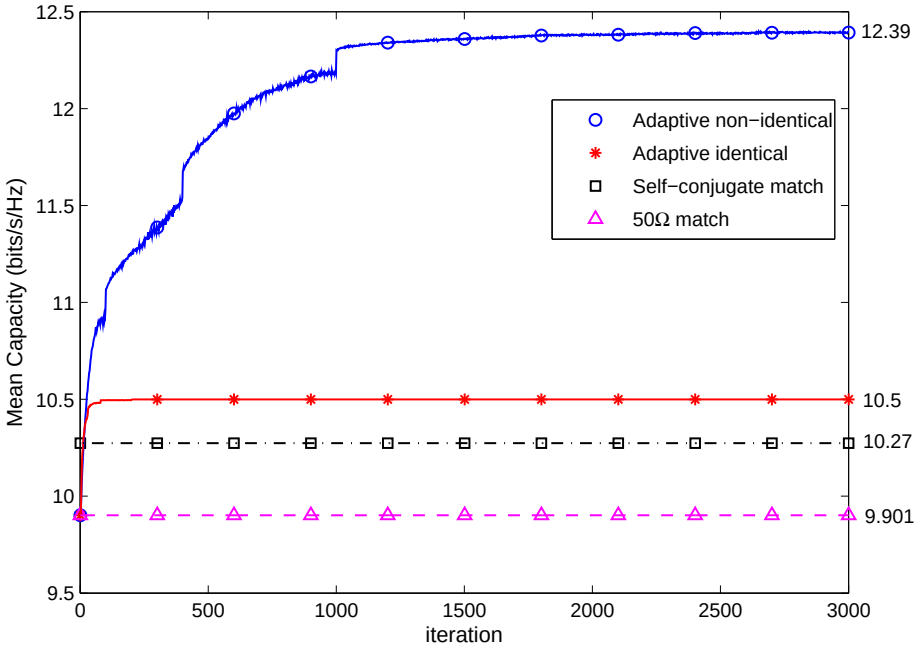

Figure 5.4: *Mean capacity of a* 3×3 *MIMO system for the following matching conditions: adaptive non-identical, adaptive identical, self-impedance conjugate, and* $z_0 = 50\Omega$ *matched termination networks. The element separation for the receiver is* $d = 0.05\lambda$.

the results in Figure 5.5b and 5.5c, more than 75% of the channel realisations are optimised by selecting a non-identical terminal network as $\mathbf{Z}_L = \mathrm{diag}(6-j35, 1+j1, 6-j35)\Omega$, and about 50% of them by having an identical network equals to $\mathbf{Z}_L = (32-j35)\mathbf{I}_{3\times 3}\Omega$. The antenna pattern of the array elements for the above optimal load networks are plotted in Figure 5.6 with $\phi = 0^\circ$ as the array broadside. The results confirm the beamforming behaviour [9, 74] and decoupling effect of the antennas by having optimal uncoupled terminations, which is more effective for the non-identical match.

Furthermore, we examine the eigenvalues of $\mathbf{H}_{mc}\mathbf{H}_{mc}^H$ using the above terminations in addition to the case with no mutual coupling as shown in Figure 5.7. The figure clearly shows that the non-identical termination tends to improve stronger eigenvalues to achieve higher capacity, while the identical match has a similar trend for all eigenvalues.

Since the 3rd eigenvalue of the channel in Figure 5.7 is small in value, and the impedance load of the middle receive antenna for the adaptive non-identical match is small, one may argue that the middle receive antenna does not affect the performance. In other words, the middle antenna can be removed from the system with no change to the performance. This is similar to antenna selection for the receive array in the presence of mutual coupling in [86] when there is no impedance matching solution. To investigate this issue, we simulate the performance of a 3×2 MIMO considering the same propagation scenario as the above, except the element spacing between the receive antennas which is doubled here, i.e. 0.1λ. Figure 5.8 shows the mean capacity of this system over 200 channel realisations using the following matching networks: adaptive non-identical match, adaptive identical match, self-conjugate match and $z_0 = 50\Omega$ match. We see that removing the middle receive antenna does not change the performance improvement of the adaptive identical match (about 6% above the capacity for $z_0 = 50\Omega$), while it reduces the performance of the adaptive non-identical match. To further the investigation, the element patterns for both adaptive matching networks is shown in Figure 5.9. Both identical and non-identical match result in the same optimum loads and consequently similar antenna pattern for such a receiver with two antennas. Comparing Figures 5.6 and 5.9 reveals the impact of the middle antenna (which is terminated in a small load impedance, i.e. roughly short circuited) on antennas 1 and 3 such that the performance is improved significantly. It can be interpreted as a beamforming process which antenna currents are sufficiently weighted by employing proper impedance loads.

To complete our investigation in this subsection, we plot the mean capacity of the assumed

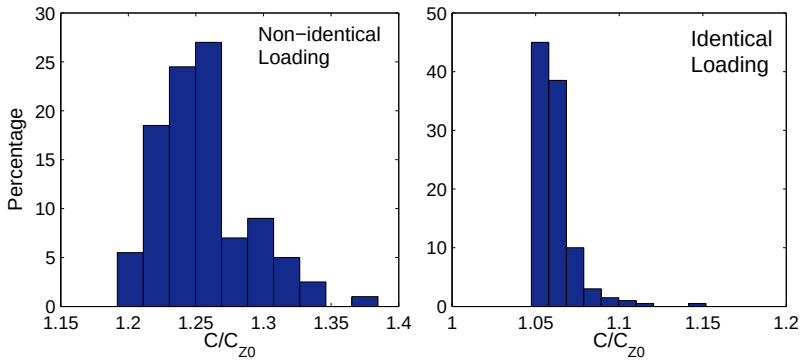

(a) C/C_{Z_0} instances

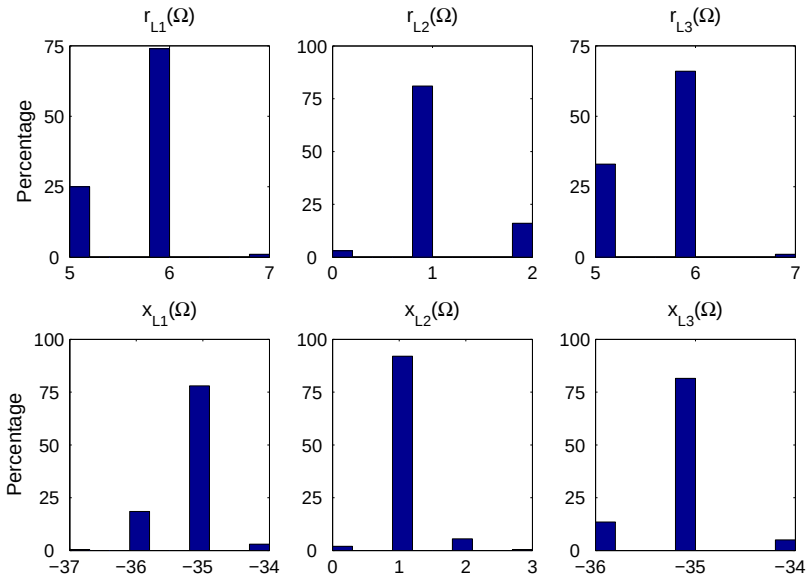

(b) Non-identical Loads: $z_{Li} = r_{Li} + jx_{Li}$, $(i = 1, 2, 3)$

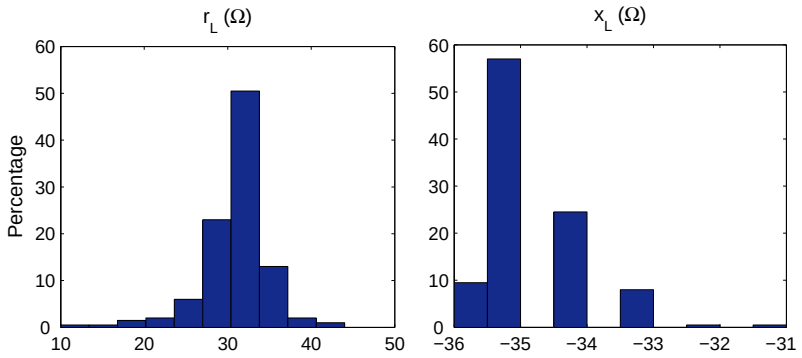

(c) Identical Loads: $z_{Li} = r_L + jx_L$, $(i = 1, 2, 3)$

Figure 5.5: *Histogram plots of (a) C/C_{Z_0} instances for both adaptive termination cases, and the real and imaginary parts of the termination loads for (b) non-identical, and (c) identical terminations at iteration number 3000.*

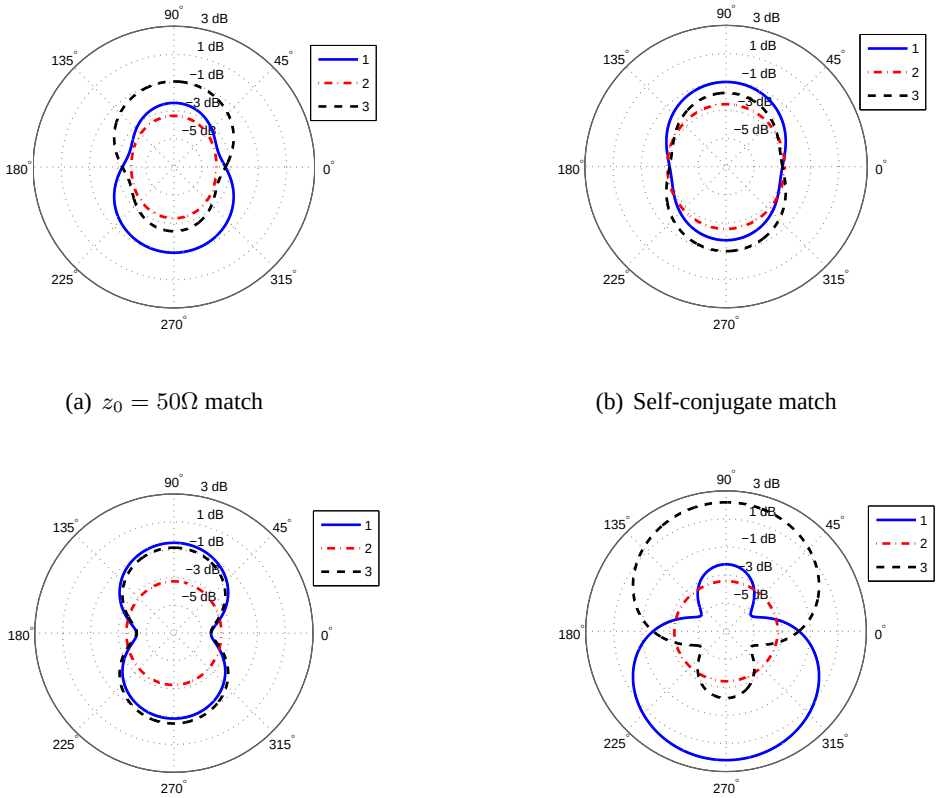

(a) $z_0 = 50\Omega$ match

(b) Self-conjugate match

(c) Adaptive identical match

(d) Adaptive non-identical match

Figure 5.6: *Antenna patterns for the adaptive non-identical, adaptive identical, self-impedance conjugate, and $z_0 = 50\Omega$ matched termination networks. Zero degrees corresponds to the array broadside (Refer back to Figure 3.11).*

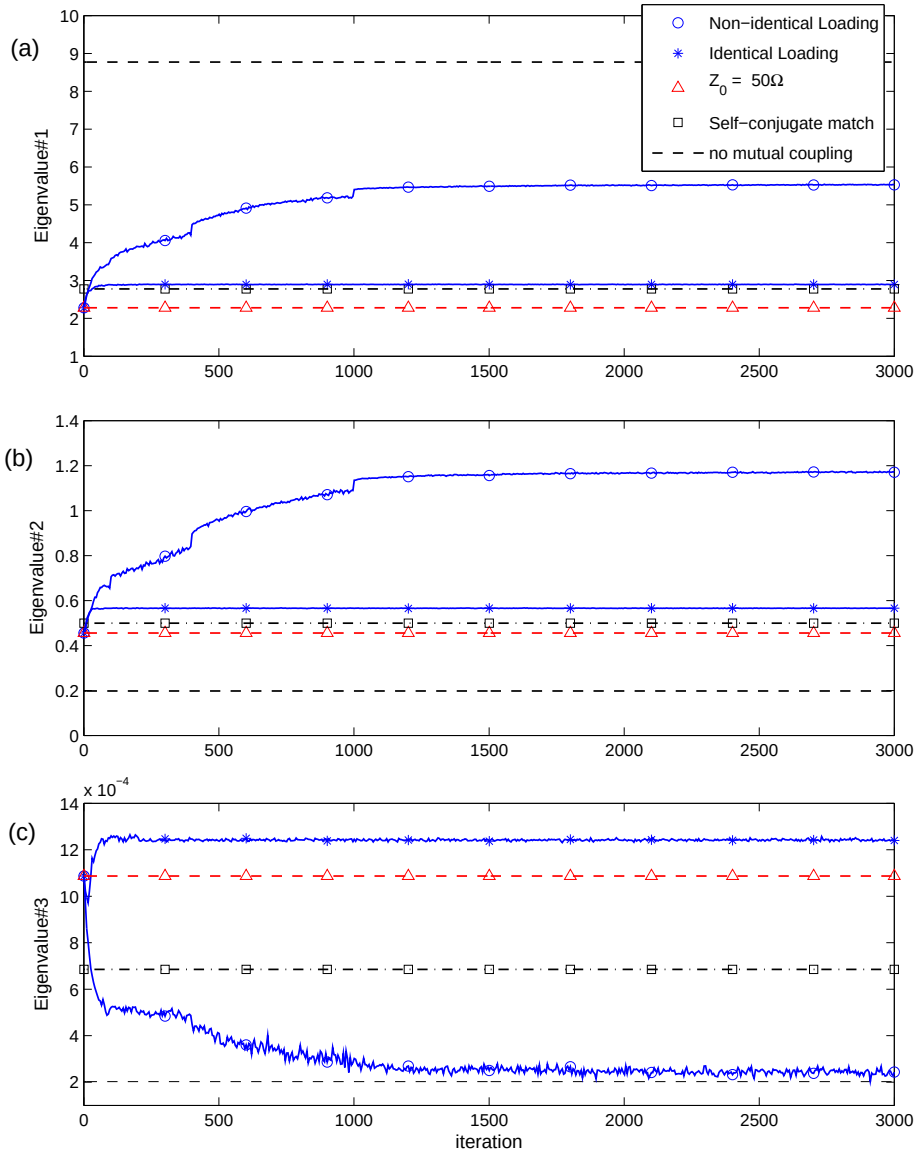

Figure 5.7: *Mean eigenvalues of ($\mathbf{H}_{mc}\mathbf{H}_{mc}^{H}$) for different antenna terminations, and averaged over 200 channel realisations, versus iteration number. The eigenvalues are in an ascending order as follows: (a) the largest eigenvalue, (b) the second largest eigenvalue, and (c) the smallest eigenvalue.*

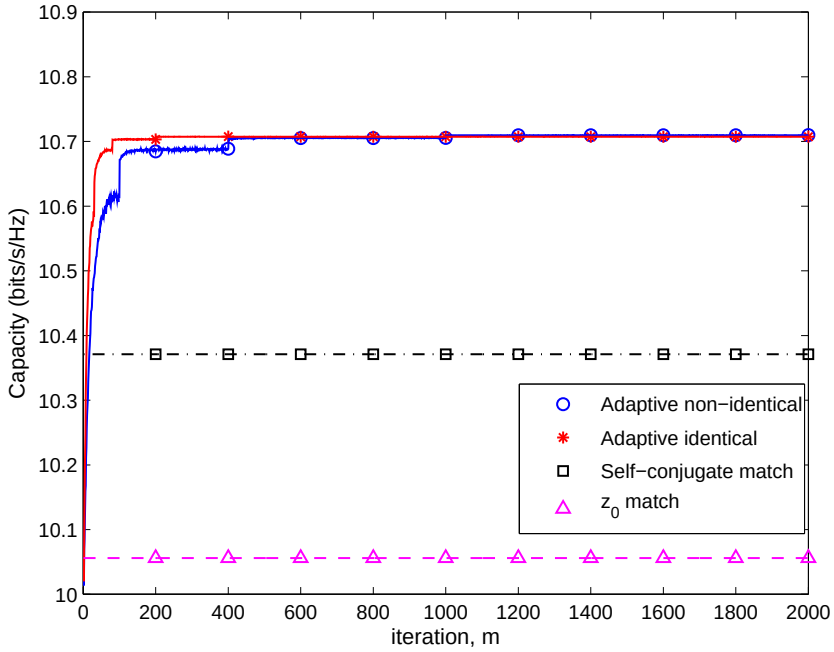

Figure 5.8: *Mean capacity of a* 3×2 *MIMO with the element spacing of* $d = 0.1\lambda$ *at the receiver, for the following matching conditions: adaptive non-identical, adaptive identical, self-impedance conjugate, and* $z_0 = 50\Omega$ *matched termination networks.*

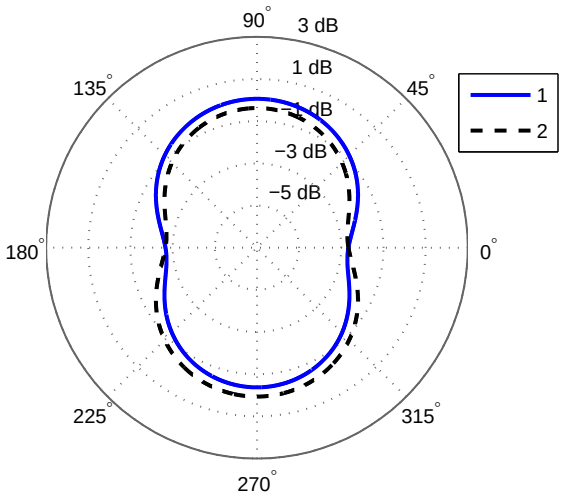

Figure 5.9: *Element pattern of the receive antennas with* $d = 0.1\lambda$ *for the assumed* 3×2 *MIMO using the adaptive impedance matching techniques. Results for the non-identical and identical matching scenarios are similar .*

3×3 MIMO system at iteration number 4000 for the above terminations versus antenna element spacing in Figure 5.10, under the following scattering distributions: (a) uniform, (b) Laplacian centred at $\bar{\phi} = 0°$ (broadside), and (c) Laplacian with $\bar{\phi} = 90°$ (endfire). We observe that for the element spacing larger than 0.3λ, both uncoupled terminations provide roughly the same capacity improvement for all propagation scenarios. For $d < 0.2\lambda$, the non-identical termination gives a much higher performance improvement but at the cost of a longer convergence time.

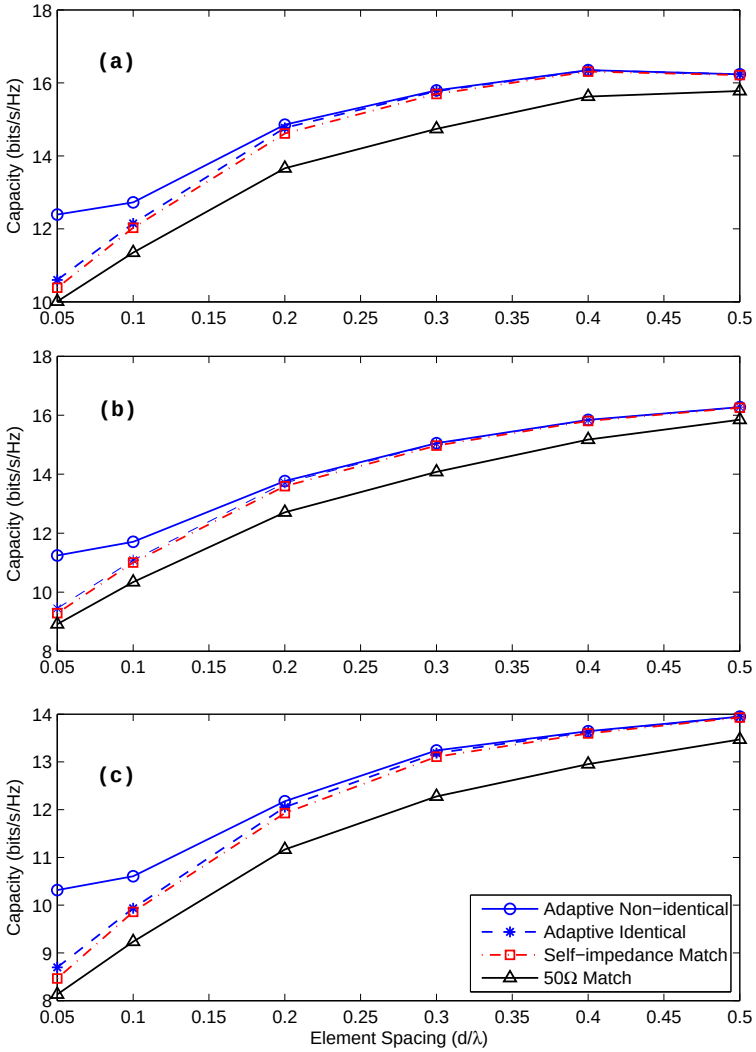

Figure 5.10: *Mean capacity as a function of element spacing for different matching methods and three different propagation scenarios: (a) Uniform, (b) Laplacian ($\phi = 0°, \sigma = 40°$), and (c) Laplacian($\phi = 90°, \sigma = 40°$).*

5.4.2 Imperfect CSI at the receiver: channel estimation error

We extend our investigation to the case that the channel matrix is unknown for the receiver and it has to be estimated. We assume a training-based estimation approach is applied and the channel estimate $\hat{\mathbf{H}}_{mc}$ is provided with an estimation error variance σ_E^2. The algorithm decides to select the termination load(s) based on the capacity estimates calculated from the knowledge of $\hat{\mathbf{H}}_{mc}$, either by applying (5.4) for block-flat fading channels or directly substituting $\hat{\mathbf{H}}_{mc}$ into (4.9). In order to assess the performance of the algorithm, we calculate and plot the actual capacity corresponds to the selected terminal network at each iteration. We include Doppler effects and time-variations of the channel by applying Gauss-Markov channel model described in Section 5.2.

We consider the block data transmission with a block length of $L = 100$ symbols, including $L_p = 18$ training symbols per block which are split into 6 groups among the block. For each block, a channel estimate $\hat{\mathbf{H}}_{mc}$ is obtained by averaging the channel estimates from sub-blocks, where each sub-block channel estimate has an estimation error σ_E^2. We also assume a uniform scattering distribution at the receiver. To investigate the effect of time-variations of the channel, we use the Gauss-Markov channel model with $\epsilon = 1.8 \times 10^{-3}$, and 1.8×10^{-2} for the slow- and fast-fading scenarios, respectively.

The mean value of the normalised capacity instances for the adaptive and non-adaptive uncoupled terminations are depicted in Figure 5.11 for slow-fading with solid lines and fast-fading scenario with dashed lines. Capacity instances for all termination cases have been normalised to the corresponding instances for the 50Ω match. Mean capacity values for the adaptive terminations are plotted for three different iterations $m = 100, 500$, and 2000, in order to evaluate the convergence behaviour of these termination cases. We observe that for both slow and fast fading scenarios, better channel estimates (i.e., lower σ_E^2) result in larger capacity improvements.

Furthermore, we can see that the adaptive identical termination achieves a slightly better performance than the self-conjugate match for both fading scenarios after sufficient iterations. It is noted that the self-conjugate match requires the knowledge of the diagonal elements of the receive array impedance matrix $\mathbf{Z}_R$, whereas the adaptive identical method presented in this chapter does not. In comparison, the non-identical termination provides larger capacity improvements even for less accurate channel estimation scenarios (i.e. larger σ_E^2). We recall that self-impedances of coupled antennas are different than the case when they are isolated[4, 7],

and that measuring these impedances is difficult in practice. We also note that practical antenna arrays and consequently their impedance matrices may not be Toeplitz in structure. The adaptive non-identical termination would be a reliable solution to optimise the performance for these corresponding scenarios.

5.5 Conclusion

In this chapter, we extended the adaptive matching technique to a non-identical matching solution in which all terminal load impedances are tuned individually to find the optimum impedance network. The performance of the adaptive matching networks are compared with the conventional termination scenarios such as: characteristic impedance match, and self-impedance conjugate match. Simulation results for a 3×3 MIMO system under different propagation scenarios show that both *identical* and *non-identical* adaptive impedance matching networks are capable of optimising the performance in the presence of strong mutual coupling and time variations of the channel. The adaptive non-identical match gives a significant improvement in the mean capacity (more than 20% compared to non-adaptive terminations for 0.05λ element separation) at the expense of a longer convergence time compared to the identical match. The adaptive non-identical approach can also be suggested as a reliable solution for non-symmetric arrays whose antenna elements or array parameters may vary along the array.

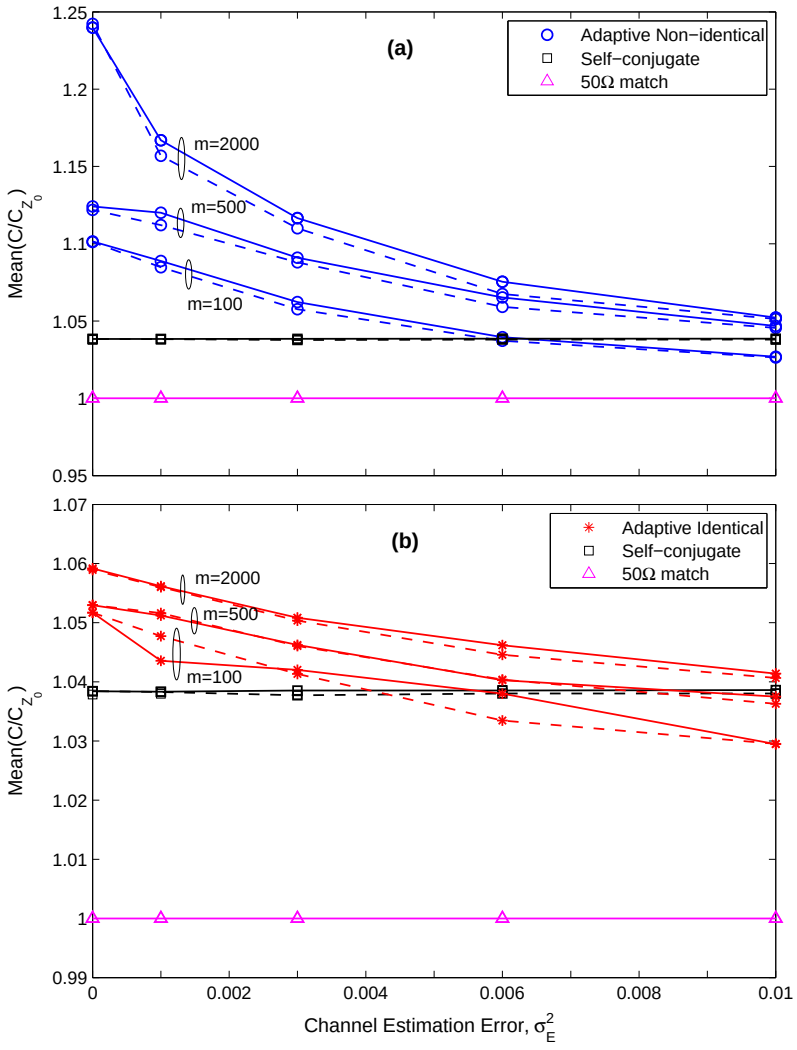

Figure 5.11: *Mean value of the normalised capacity instances $C/C(Z_0)$ as a function of estimation error σ_E^2, applying adaptive (a) identical, and (b) non-identical terminations for slow-fading and fast-fading scenarios at iterations $m = 100, 500, 2000$.*

Chapter 6
Conclusions

In this thesis, the impact of mutual coupling on the performance of compact MIMO systems is studied. The use of uncoupled antenna impedance matching techniques is examined as a solution to counteract the mutual coupling effect on the performance. Existing impedance matching approaches are shown to be dependent on the mutual coupling model and on the channel matrix. However, existing techniques are not able to adapt to changes of the channel matrix and there is no mathematical mutual coupling model in general for coupled arrays. Therefore, we propose an *adaptive impedance matching* technique which optimises the received power or the capacity of compact MIMO systems. The proposed technique uses the channel estimate (obtained from the knowledge of received signals, and training sequences) to take account of mutual coupling. The performance of the proposed technique is proved by simulation results for a 3×3 MIMO system under different propagation scenarios. In this chapter, we summarise the key findings of the thesis and suggest some future works.

6.1 Conclusions Summary

Using MIMO technology for small size wireless devices is restricted by limits on the achievable antenna element separation. Element spacings less than one half-wavelength lead to mutual coupling which degrades the performance of compact MIMO systems. Existing studies have presented an antenna impedance matching approach to compensate the impact of mutual coupling effects on the performance of compact MIMO systems. These studies require knowledge of the mutual coupling model and the channel matrix to find an optimum load impedance network which maximises the performance metric (either the received power or the capacity) [5, 40]. The values of these load impedances are found to be dependent on the proportion of the mutual coupling and on the entries of the channel matrix [7, 38, 40, 74]. However, these studies use a mutual coupling model based on the open-circuit voltages which is only valid for specific types of antennas such as half-wavelength dipoles. Furthermore, existing studies are not capable of adapting to changes of the channel matrix.

In Chapter 3, two mutual coupling models: the conventional open-circuit based, and the receiving mutual impedance methods are studied by using the electromagnetic simulation software FEKO. The existing definitions of the coupling matrix to model the mutual coupling are also compared, and their relations are clarified. Using the antenna impedance matching technique to compensate the mutual coupling effects on the signal correlation, the received power, and the capacity is examined for both open-circuit and receiving mutual impedance models for half-wavelength dipoles. Simulation results show that the latter method is not suitable for finding the optimum load impedances to optimise the received power or the channel capacity. We found no explicit mutual coupling model to be accurate in general, and separable from the channel matrix, to use for our purpose of impedance matching for coupled arrays.

We proposed the *adaptive impedance matching* technique in Chapter 4. This technique uses the received signals, the voltages across the resistive parts of the terminal load impedances, to find the total effect of the channel matrix and the mutual coupling, and to evaluate any performance improvement due to impedance matching. It tunes the antenna load impedances according to an optimisation technique and examine the performance improvement using the received signals. In order to implement the idea of the adaptive impedance matching solution, several estimation approaches for the capacity and the received power are discussed, and optimisation techniques such as: Gradient-based, Newton-Raphson, and random search methods are examined for *identical* load impedance scenario. We found the random search method to be simple and robust for our scenarios.

In Chapter 5, we extended the adaptive impedance matching technique to *non-identical* load impedances. The matching performance of both the identical and non-identical adaptive matching approaches are examined and compared to conventional termination approaches: the characteristic impedance match, and the self-impedance conjugate match. The effect of different conditions in the propagation environment such as slow and fast fading channels, and channel estimation error are included in our investigation. Simulation results for the capacity of a 3×3 MIMO system of half-wavelength dipoles proved that both the identical and non-identical adaptive matching approaches can improve the performance in the presence of a strong mutual coupling effect (element separation of 0.05λ at the receiver) and fast time variations of the channel. We found that the adaptive non-identical match can give a significant capacity improvement (more than 20% to the conventional terminations for 0.05λ element separation)

Previous studies on non-adaptive impedance matching networks, showed that the performance

of such approaches are very sensitive to the array geometry and the antenna element structure [38, 74]. However, our proposed techniques can be adapted to the actual conditions of the propagation environment and the array structure (the mutual coupling, and the channel matrix), and optimise the performance.

6.2 Future Work

During the time of writing this thesis, we found some commercial products [87, 88] which use the adaptive impedance matching approach for a single antenna. However, no such product or paper found for MIMO systems, except a patent [89] proposed by Lau and Andersen who introduced the idea of using the uncoupled impedance matching networks [5, 40]. Although, this patent introduces several possible ideas to have an adaptive impedance match, no practical approach is examined. Therefore, the use of the proposed adaptive impedance matching approaches can be a promising solution for small devices in wireless mobile communication industry.

Here are some extensions to this thesis for future works:

- The proposed adaptive impedance matching techniques can be investigated for planar array structures. Although a simple circular array is studied in [74] for non-adaptive impedance match, it would be more useful to examine the adaptive match for different planar array geometries. It would benefit the coming wireless systems which are faced with a rising demand for higher data rates, by using more antennas.

- The performance of the adaptive matching approaches can be examined for more general cases in which the antennas are not identical, and the array parameters such as impedance matrix are non-symmetric. We suggest the use of the adaptive non-identical impedance match for such scenarios.

- Due to the limit of mutual coupling modelling and a non-separable channel model for MIMO configurations larger than 3×3, it would be beneficial to construct a prototype to validate the performance of the proposed adaptive match using empirical measurement results.

Appendix A
Publications

The author of this thesis has the following publications:

- R. Mohammadkhani, J. S. Thompson, “MIMO capacity improvement in the presence of antenna mutual coupling”, *18th Iranian Conference on Electrical Engineering (ICEE)*, pp. 167-171, Isfahan, Iran, May 2010.
- R. Mohammadkhani, J. S. Thompson, “Adaptive matching for compact MIMO systems”, *7th International Symposium on Wireless Communication Systems (ISWCS)*, pp.107 -111, York, UK, September 2010.
- R. Mohammadkhani, J. S. Thompson, “Adaptive Uncoupled Termination for Coupled Arrays in MIMO Systems”, *IEEE Transactions on Antennas and Propagation*, paper under revision in preparation for second round review.

Appendix B
Mutual Impedance of Thin Wire Dipoles

As mentioned in Chapter 3, the mutual impedances between two antennas using open-circuit voltages, can be expressed as follows:

$$z_{21} = \left.\frac{V_2}{I_1}\right|_{I_2=0} = \frac{V_{oc,2}}{I_1} \tag{B.1a}$$

$$z_{12} = \left.\frac{V_1}{I_2}\right|_{I_1=0} = \frac{V_{oc,1}}{I_2} \tag{B.1b}$$

For identical antennas due to the reciprocity theorem, $z_{21} = z_{12}$. Assuming a linear array of two identical thin wire dipoles, placed in a side-by-side configuration and separated by a distance of d, the real and imaginary parts of the mutual impedance $z_{21} = r_{21} + jx_{21}$ using the classical induced electromagnetic force (EMF) method are given by [31, 56]:

$$r_{21} = 30[2C_i(u_0) - C_i(u_1) - C_i(u_2)] \tag{B.2a}$$

$$x_{21} = -30\left[2S_i(u_0) - S_i(u_1) - S_i(u_2)\right] \tag{B.2b}$$

where $C_i(u)$ and $S_i(u)$ are the cosine and sine integrals defined as:

$$C_i(u) = \int_{\infty}^{u} \frac{\cos(x)}{x} dx \tag{B.3a}$$

$$S_i(u) = \int_{0}^{u} \frac{\sin(x)}{x} dx \tag{B.3b}$$

and

$$u_0 = kd \tag{B.4a}$$

$$u_1 = k(\sqrt{d^2 + l^2} + l) \tag{B.4b}$$

$$u_2 = k(\sqrt{d^2 + l^2} - l) \tag{B.4c}$$

References

[1] A. Paulraj, D. Gore, R. Nabar, and H. Bolcskei, "An overview of MIMO communications - a key to gigabit wireless," Proceedings of the IEEE, vol. 92, pp. 198–218, Feb 2004.

[2] I. E. Telatar, "Capacity of multi-antenna gaussian channels," European Transactions on Telecommunications, vol. 10, pp. 585–595, 1999.

[3] G. J. Foschini and M. J. Gans, "On limits of wireless communications in a fading environment when using multiple antennas," Wireless Personal Communications, vol. 6, pp. 311–335, 1998.

[4] J. W. Wallace and M. A. Jensen, "Mutual coupling in MIMO wireless systems: a rigorous network theory analysis," IEEE Transactions on Wireless Communications, vol. 3, pp. 1317–1325, July 2004.

[5] J. B. Andersen and B. K. Lau, "On closely coupled dipoles in a random field," IEEE Antennas and Wireless Propagation Letters,, vol. 5, pp. 73–75, Dec. 2006.

[6] B. K. Lau, J. Andersen, A. Molisch, and G. Kristensson, "Antenna matching for capacity maximization in compact mimo systems," ISWCS '06. 3rd International Symposium on Wireless Communication Systems,, pp. 253–257, Sep. 2006.

[7] Y. Fei, Y. Fan, J. S. Thompson, and B. K. Lau, "Optimal single-port matching impedance for capacity maximization in compact MIMO arrays," IEEE Transactions on Antennas and Propagations, vol. 56, pp. 3566–3575, Nov. 2008.

[8] M. A. Jensen and B. Booth, "Optimal uncoupled impedance matching for coupled MIMO arrays," in First European Conference on Antennas and Propagation (EuCAP), pp. 1 –4, Nov. 2006.

[9] M. Jensen and B. K. Lau, "Uncoupled matching for active and passive impedances of coupled arrays in MIMO systems," IEEE Transactions on Antennas and Propagation, vol. 58, pp. 3336 –3343, Oct. 2010.

[10] FEKO. [Online]: http://www.feko.info/.

[11] E. Biglieri, R. Calderbank, A. Constantinides, A. Goldsmith, A. Paulraj, and H. V. Poor, MIMO Wireless Communications. New York, NY, USA: Cambridge University Press, 2007.

[12] A. F. Molisch, Wireless Communications. John Wiley & Sons, 2005.

[13] A. Goldsmith, Wireless Communications. New York, NY, USA: Cambridge University Press, 2005.

[14] Y. S. Cho, J. K. Kim, W. Y. Yang, and C. G. Kang, MIMO-OFDM Wireless Communications with MATLAB. John Wiley & Sons, 2010.

[15] D. Gesbert, M. Shafi, D. Shiu, P. J. Smith, and A. Naguib, "From theory to practice: an overview of MIMO space-time coded wireless systems," IEEE Journal on Selected Areas in Communications,, vol. 21, no. 3, pp. 281–302, 2003.

[16] M. A. Jensen and J. W. Wallace, "A review of antennas and propagation for MIMO wireless communications," IEEE Transactions on Antennas and Propagation, vol. 52, pp. 2810–2824, Nov. 2004.

[17] A. F. Molisch and et al., "MIMO antennas, propagation channels, and their impact on system design," ISWC, 2007.

[18] P. Almers, E. Bonek, and et al., "Survey of channel and radio propagation models for wireless MIMO systems," EURASIP Journal on Wireless Communications and Networking, vol. 2007, 2007.

[19] J. Kermoal, L. Schumacher, K. Pedersen, P. Mogensen, and F. Frederiksen, "A stochastic MIMO radio channel model with experimental validation," IEEE Journal on Selected Areas in Communications,, vol. 20, pp. 1211–1226, Aug. 2002.

[20] D. Chizhik, J. Ling, P. Wolniansky, R. Valenzuela, N. Costa, and K. Huber, "Multiple-input-multiple-output measurements and modeling in manhattan," IEEE Journal on Selected Areas in Communications,, vol. 21, pp. 321–331, Apr 2003.

[21] J. W. Wallace and M. A. Jensen, "Termination-dependent diversity performance of coupled antennas: network theory analysis," IEEE Transactions on Antennas and Propagation, vol. 52, pp. 98–105, Jan. 2004.

[22] R. Janaswamy, "Effect of element mutual coupling on the capacity of fixed length linear arrays," IEEE Antennas and Wireless Propagation Letters,, vol. 1, pp. 157–160, 2002.

[23] B. Clerckx, D. Vanhoenacker-Janvier, C. Oestges, and L. Vandendorpe, "Mutual coupling effects on the channel capacity and the space-time processing of mimo communication systems," IEEE International Conference on Communications, vol. 4, pp. 2638–2642 vol.4, May 2003.

[24] A. A. Abouda, Characterization of MIMO Channel Capacity in Urban Microcellular Environment. PhD thesis, Helsinkin University of Technology, 2007.

[25] H. Shin and J. H. Lee, "Capacity of multiple-antenna fading channels: spatial fading correlation, double scattering, and keyhole," IEEE Transactions on Information Theory,, vol. 49, pp. 2636–2647, Oct. 2003.

[26] C. Waldschmidt, J. Hagen, and W. Wiesbeck, "Influence and modelling of mutual coupling in MIMO and diversity systems," IEEE Antennas and Propagation Society International Symposium,, vol. 3, pp. 190–193, 2002.

[27] O. Oyman, R. Nabar, H. Bolcskei, and A. Paulraj, "Characterizing the statistical properties of mutual information in MIMO channels," IEEE Transactions on Signal Processing,, vol. 51, pp. 2784–2795, Nov 2003.

[28] H. Ozcelik, M. Herdin, W. Weichselberger, J. Wallace, and E. Bonek, "Deficiencies of 'kronecker' MIMO radio channel model," Electronics Letters, vol. 39, pp. 1209–1210, Aug. 2003.

[29] T. Svantesson and J. Wallace, "Tests for assessing multivariate normality and the covariance structure of MIMO data," Acoustics, Speech, and Signal Processing, 2003. Proceedings. (ICASSP '03). 2003 IEEE International Conference on, vol. 4, pp. IV–656–9 vol.4, Apr 2003.

[30] A. Goldsmith, S. Jafar, N. Jindal, and S. Vishwanath, "Capacity limits of MIMO channels," IEEE Journal on Selected Areas in Communications,, vol. 21, pp. 684–702, June 2003.

[31] C. A. Balanis, Antenna Theory: Analysis and Design. John Wiley & Sonc, Inc., 2nd edition ed., 1997.

[32] W. L. Stutzman and G. A. Thiele, Antenna Theory and Design. John Wiley & Sonc, Inc., 1998.

[33] M. K. Ozdemir, E. Arvas, and H. Arslan, "Dynamics of spatial correlation and implications on mimo systems," IEEE Communications Magazine, vol. 42, pp. S14 – S19, June 2004.

[34] X. Li and Z. Nie, "Mutual coupling effects on the performance of MIMO wireless channels," IEEE Antennas and Wireless Propagation Letters,, vol. 3, pp. 344–347, 2004.

[35] P.-S. Kildal and K. Rosengren, "Electromagnetic analysis of effective and apparent diversity gain of two parallel dipoles," IEEE Antennas and Wireless Propagation Letters, vol. 2, pp. 9–13, 2003.

[36] T. Svantesson and A. Ranheim, "Mutual coupling effects on the capacity of multielement antenna systems," Proc. IEEE Int. Conf. Acoustics, Speach, and Signal Processing, vol. 4, pp. 2485–2488, 2001.

[37] B. K. Lau, J. B. Andersen, G. Kristensson, and A. F. Molisch, "Impact of matching network on bandwidth of compact antenna arrays," IEEE Transactions on Antennas and Propagation, vol. 54, pp. 3225–3238, Nov. 2006.

[38] Y. Fei, Compact MIMO Terminals with Matching Networks. PhD thesis, The University of Edinburgh, 2008.

[39] J. Andersen and H. Rasmussen, "Decoupling and descattering networks for antennas," IEEE Transactions on Antennas and Propagation, vol. 24, pp. 841 – 846, Nov. 1976.

[40] B. K. Lau and J. B. Andersen, "On closely coupled dipoles with load matching in a random field," IEEE 17th International Symposium on Personal, Indoor and Mobile Radio Communications,, pp. 1–5, Sep. 2006.

[41] S. Pan, S. Durrani, and M. Bialkowski, "MIMO capacity for spatial channel model scenarios," IEEE Conference, pp. 25–29, 2007.

[42] I. Gupta and A. Ksienski, "Effect of mutual coupling on the performance of adaptive arrays," IEEE Transactions on Antennas and Propagation, vol. 31, pp. 785–791, Sep 1983.

[43] K. Lo and T. Vu, "Simple s-parameter model for receiving antenna array," Electronics Letters, vol. 24, pp. 1264 –1266, Sep. 1988.

[44] T. Su and H. Ling, "On modeling mutual coupling in antenna arrays using the coupling matrix," Microwave and Optical Technology Letters, vol. 28, pp. 231–237, 2001.

[45] K. Pasala and E. Friel, "Mutual coupling effects and their reduction in wideband direction of arrival estimation," IEEE Transactions on Aerospace and Electronic Systems, vol. 30, pp. 1116 –1122, Oct 1994.

[46] R. Adve and T. Sarkar, "Compensation for the effects of mutual coupling on direct data domain adaptive algorithms," IEEE Transactions on Antennas and Propagation, vol. 48, pp. 86 –94, Jan 2000.

[47] H. Hui, "Improved compensation for the mutual coupling effect in a dipole array for direction finding," IEEE Transactions on Antennas and Propagation, vol. 51, pp. 2498–2503, Sep 2003.

[48] H. Hui, "Compensating for the mutual coupling effect in direction finding based on a new calculation method for mutual impedance," IEEE Antennas and Wireless Propagation Letters, vol. 2, pp. 26 – 29, 2003.

[49] A. Kerkhoff and H. Ling, "A simplified method for reducing mutual coupling effects in low frequency radio telescope phased arrays," IEEE Transactions on Antennas and Propagation, vol. 59, pp. 1838 –1845, June 2011.

[50] B. Friedlander and A. Weiss, "Direction finding in the presence of mutual coupling," IEEE Transactions on Antennas and Propagation, vol. 39, pp. 273 –284, Mar. 1991.

[51] D. Kelley and W. Stutzman, "Array antenna pattern modeling methods that include mutual coupling effects," IEEE Transactions on Antennas and Propagation, vol. 41, pp. 1625 – 1632, Dec. 1993.

[52] K. Dandekar, H. Ling, and G. Xu, "Effect of mutual coupling on direction finding in smart antenna applications," Electronics Letters, vol. 36, pp. 1889 –1891, Oct 2000.

[53] C. Lau, R. Adve, and T. Sarkar, "Minimum norm mutual coupling compensation with applications in direction of arrival estimation," IEEE Transactions on Antennas and Propagation, vol. 52, pp. 2034 – 2041, Aug. 2004.

[54] H. T. Hui, "Decoupling methods for the mutual coupling effect in antenna arrays: a review," Recent Patents on Engineering, vol. 1, pp. 187–193, 2007.

[55] H. T. Hui, "A new definition of mutual impedance for application in dipole receiving antenna arrays," IEEE Antennas and Wireless Propagation Letters, vol. 3, pp. 364–367, 2004.

[56] S. J. Orfanidis, Electromagnetic Waves and Antenna. 2010.

[57] T. Svantesson, "The effects of mutual coupling using a linear array of thin dipoles of finite length," in Ninth IEEE SP Workshop on Statistical Signal and Array Processing, pp. 232 –235, Sep 1998.

[58] B. Clerckx, C. Craeye, D. Vanhoenacker-Janvier, and C. Oestges, "Impact of antenna coupling on 2 2 MIMO communications," IEEE Transactions on Vehicular Technology,, vol. 56, pp. 1009–1018, May 2007.

[59] H. T. Hui, H. P. Low, T. T. Zhang, and Y. L. Lu, "Receiving mutual impedance between two normal mode helical antennas (NMHAs)," IEEE Antennas and Propagation Magazine, vol. 48, no. 4, pp. 92–96, 2006.

[60] H. T. Hui, W. T. O. Yong, and K. B. Toh, "Signal correlation between two normal-mode helical antennas for diversity reception in a multipath environment," IEEE Transactions on Antennas and Propagation, vol. 52, pp. 572–577, Feb. 2004.

[61] P.-S. Kildal and K. Rosengren, "Correlation and capacity of MIMO systems and mutual coupling, radiation efficiency, and diversity gain of their antennas: simulations and measurements in a reverberation chamber," IEEE Communications Magazine, vol. 42, pp. 104–112, Dec. 2004.

[62] Z. Huang, C. Balanis, and C. Birtcher, "Mutual coupling compensation in ucas: Simulations and experiment," IEEE Transactions on Antennas and Propagation, vol. 54, pp. 3082 –3086, Nov. 2006.

[63] H. L. V. Trees, Optimum Array Processing (Detection, Estimation, and Modulation Theory, Part IV). John Wiley & Sons, 2002.

[64] A. Gera, "A simplified computational procedure for the analysis of planar arrays," IEEE Transactions on Antennas and Propagation, vol. 32, pp. 647 – 651, Jun 1984.

[65] P. Leather and D. Parsons, "Antenna diversity for UHF handportable radio," Electronics Letters, vol. 39, pp. 946 – 948, Jun. 2003.

[66] S. Blanch, J. Romeu, and I. Corbella, "Exact representation of antenna system diversity performance from input parameter description," Electronics Letters, vol. 39, pp. 705 – 707, May 2003.

[67] S. Dossche, S. Blanch, and J. Romeu, "Optimum antenna matching to minimise signal correlation on a two-port antenna diversity system," Electronics Letters, vol. 40, pp. 1164–1165, Sep. 2004.

[68] A. Forenza, D. Love, and R. Heath, "Simplified spatial correlation models for clustered mimo channels with different array configurations," IEEE Transactions on Vehicular Technology, vol. 56, pp. 1924 –1934, July 2007.

[69] J. Fuhl, A. Molisch, and E. Bonek, "Unified channel model for mobile radio systems with smart antennas," IEE Proceedings, vol. 145, pp. 32–41, Feb 1998.

[70] L. Schumacher, K. Pedersen, and P. Mogensen, "From antenna spacings to theoretical capacities - guidelines for simulating MIMO systems," The 13th IEEE International Symposium on Personal, Indoor and Mobile Radio Communications, vol. 2, pp. 587–592 vol.2, Sept. 2002.

[71] H. T. Hui, "Reply to comment on 'signal correlation between two normal-mode helical antennas for diversity reception in a multipath environment'," IEEE Transactions on Antennas and Propagation, vol. 53, no. 8, pp. 2777–2777, 2005.

[72] S. Lu, H. Hui, and M. Bialkowski, "Optimizing mimo channel capacities under the influence of antenna mutual coupling," Antennas and Wireless Propagation Letters, IEEE, vol. 7, pp. 287 –290, 2008.

[73] R. Mohammadkhani and J. Thompson, "Adaptive matching for compact MIMO systems," in 7th International Symposium on Wireless Communication Systems (ISWCS), pp. 107 –111, Sept. 2010.

[74] R. Tian and B. K. Lau, "Uncoupled antenna matching for performance optimization in compact MIMO systems using unbalanced load impedance," IEEE Vehicular Technology Conference (VTC Spring 2008), Singapore, pp. 299–303, May 2008.

[75] W. F. Tsen and H.-J. Li, "Uncoupled impedance matching for capacity maximization of compact MIMO arrays," IEEE Antennas and Wireless Propagation Letters, vol. 8, pp. 1295 –1298, 2009.

[76] M. K. Ozdemir, H. Arslan, and E. Arvas, "A mutual coupling model for MIMO systems," in IEEE Topical Conference on Wireless Communication Technology, pp. 306 – 307, Oct. 2003.

[77] S. Boyd and L. Vandenberghe, Convex Optimization. Cambridge University Press, 2009.

[78] Y. Li, "Optimum training sequences for OFDM systems with multiple transmit antennas," in IEEE Global Telecommunications Conference, 2000. GLOBECOM '00., vol. 3, pp. 1478 –1482 vol.3, 2000.

[79] M. Biguesh and A. Gershman, "Training-based MIMO channel estimation: a study of estimator tradeoffs and optimal training signals," IEEE Transactions on Signal Processing, vol. 54, pp. 884 – 893, Mar. 2006.

[80] C. T. Kelley, Iterative Methods for Optimization. Society for Industrial and Applied Mathematics (SIAM), 1999.

[81] K. B. Petersen and M. S. Pedersen, The Matrix Cookbook. Technical University of Denmark, Oct 2008. Version 20081110.

[82] R. Mudumbai, D. Brown, U. Madhow, and H. Poor, "Distributed transmit beamforming: challenges and recent progress," IEEE Communications Magazine, vol. 47, pp. 102 –110, Feb. 2009.

[83] D. Aldous and J. Fill, Reversible Markov Chains and Random Walks on Graphs. (Monograph in preparation.) [Online]. Available: http://stat-www.berkeley.edu/users/aldous/RWG/book.html.

[84] R. Etkin and D. Tse, "Degrees of freedom in some underspread MIMO fading channels," IEEE Transactions on Information Theory, vol. 52, pp. 1576 – 1608, Apr. 2006.

[85] T. Yoo and A. Goldsmith, “Capacity and power allocation for fading MIMO channels with channel estimation error,” IEEE Transactions on Information Theory, vol. 52, pp. 2203 – 2214, May. 2006.

[86] D. Lu, D. So, and A. Brown, “Receive antenna selection scheme for v-blast with mutual coupling in correlated channels,” in IEEE 19th International Symposium on Personal, Indoor and Mobile Radio Communications, 2008. PIMRC 2008., pp. 1 –5, Sep. 2008.

[87] Paratek Microwave, Inc., http://www.paratek.com/aimm.html, Adaptive Impedance Matching Module (AIMM).

[88] I. Ida, J. Takada, A. Honda, and Y. Oishi, “Experimental results of the adaptive impedance matching system,” COST 273 TD(04)187, 2004.

[89] B. K. Lau and J. B. Andersen, “Antenna system and method for operating an antenna system,” U.S. Patent 2010/0201598 A1, Aug. 2010.